Hydrogel electrolytes for aqueous zinc metal batteries

Yixuan Zhao

A thesis submitted in fulfilment of the requirements for the degree of

Master of Philosophy

Faculty of Engineering

School of Chemical and Biomolecular Engineering

The University of Sydney

2026

Statement of originality

I declare that this thesis is an original work of scholarship undertaken by me.

This thesis includes material prepared for publication. Such material is entirely my own work and is presented here prior to/independent of formal publication.

This thesis is not submitted for any other degree or award.

Sept 22, 2025

Abstract

Aqueous zinc-ion batteries (AZIBs) are promising for next-generation energy storage due to their safety, low cost, and sustainability, but they remain limited by water-driven instability, sluggish Zn^{2+} desolvation, parasitic reactions, and dendritic deposition. This thesis develops a progressive electrolyte design based on hydrophilic, hydrophobic, and amphiphilic hydrogel frameworks, combining molecular water regulation with interfacial chemical engineering to achieve dendrite-free cycling and long-term stability.

In Chapter 1, the functions and limitations of hydrophilic hydrogels are systematically examined. Hydrophilic networks immobilize water, provide ion-conduction channels, and homogenize Zn^{2+} flux, suppressing dendritic growth and reducing side reactions. However, their water-rich microenvironments sustain proton activity and corrosion, revealing a trade-off between ionic conductivity and interfacial stability. To overcome these constraints, the chapter discusses the advantages of incorporating hydrophobic domains that by reducing free-water activity, restructuring Zn^{2+} solvation, and stabilizing interfacial reactions, hydrophobic or amphiphilic hydrogels are introduced as a more effective design strategy for durable aqueous zinc-ion batteries.

Chapter 2 proposed a hydrophobic-spacer engineering strategy, in which fluorinated methacrylate monomers are incorporated into zwitterionic hydrogel networks to construct controlled amphiphilic microdomains. Spectroscopic and thermal analyses reveal that these domains suppress free water activity and reorganize hydrogen-bonding into polymer/ion-associated states, lowering water reactivity and widening the electrochemical stability window. Molecular dynamics simulations confirm that hydrophobic segments weaken zwitterion self-association, redistribute Zn^{2+} solvation from water-dominated to polymer/anion-assisted configurations, and accelerate ion diffusion. Electrochemical measurements demonstrate improved Zn^{2+} transference numbers, reduced interfacial charge-transfer barriers, and extended symmetric-cell cycling lifetimes exceeding 2500 h without dendritic failure.

In Chapter 3, the thesis concludes with a forward-looking outlook. Hydrophobic-spacer engineering is identified as a paradigm shift from passive water immobilization to active interfacial design, and future work should focus on scalable synthesis, in situ polymerization, and sustainable biopolymer networks to advance AZIBs toward practical applications.

This work demonstrates a paradigm shift from passive water immobilization to active interfacial chemical engineering.

Key words: Aqueous zinc-ion batteries, Hydrophobic, Zwitterionic polymer, Zn^{2+} transport

Acknowledgments

I would like to extend my sincere gratitude to all the teachers, colleagues, and friends who have supported and accompanied me during my master's studies.

Firstly, I am deeply grateful to Dr. Zengxia Pei for his constant support, patient guidance, and invaluable encouragement throughout my postgraduate journey. He not only taught me how to become an independent researcher but also helped me develop critical thinking skills that will benefit me in both academic and personal life. At the beginning, when I felt lost, he provided me with academic direction and patiently answered my questions. Later, when the academic pressure grew heavier, he acted as a mentor in life as well, offering thoughtful advice and helping me consider different paths for my future.

I would also like to sincerely thank Mr. Zhe Gong for his generous experimental guidance and unfailing assistance during my research. Without his support, the completion of my experiments would not have been possible. As a senior colleague, he was always patient with my carelessness, never losing his temper, and instead became both a dependable mentor and a good friend. My heartfelt thanks also go to my dear friend, Miss Mengwei Cao, for her encouragement and companionship. She has always supported me in pursuing my academic path and, as a true friend, has never brought me negative emotions and only positive energy and strength to carry on.

Finally, I owe my deepest gratitude to my family for their endless love, understanding, and support. Becoming part of this research group and meeting so many wonderful people has been one of the most rewarding and unforgettable experiences of my postgraduate life.

Statement of use of generative artificial intelligence

During the preparation of this thesis, the author used [ChatGPT (OpenAI)] only for limited text-enhancement purposes, including paraphrasing for clarity, improving sentence structure, correcting grammar and spelling, refining academic tone. All AI-assisted changes were reviewed by the author for accuracy and bias. The author remains fully responsible for the content and confirms compliance with the University of Sydney Generative AI Guide for Researchers.

Sept 22, 2025

Table of contents

List of Figure

Chapter 1: Introduction

1.1 The promise and challenges of aqueous zinc-ion batteries

Although rechargeable lithium-ion batteries (LIBs) have been widely studied, their development has been constrained to some extent by safety concerns and resource scarcity. Compared with existing LIBs, aqueous batteries (ABs) have significant competitive advantages due to their environmental friendliness, low cost, and intrinsic safety. In addition, aqueous electrolytes have the characteristics of high ionic conductivity and high-power density, making them particularly suitable for flexible devices and other fields[1-3].

However, aqueous batteries face a fundamental challenge stemming from their solvents: the electrochemical stability window (ESW) of water is very narrow, theoretically only 1.23 V. When the battery operates outside this voltage range, parasitic side reactions (hydrogen evolution reaction and oxygen evolution reaction) are triggered, resulting in electrolyte consumption, gas generation, and reduced Coulombic efficiency[4]. While researchers have proposed coping strategies such as "salt-in-water" electrolytes[1; 5] and new electrode materials[2; 6], inherent stability limitations, especially instability at the electrode-electrolyte interface, remain a key obstacle to the commercial development of aqueous batteries.

Among the many aqueous batteries, aqueous zinc-based batteries (ZABs), especially zinc-ion batteries (ZIBs), have attracted much attention due to their abundant zinc resources, high safety and excellent theoretical capacity. The global reserves of zinc are as high as 1.9 billion tons, which ensures its low-cost advantage[7]. Zinc has a suitable redox potential and a high theoretical capacity of 820 mAh g^{-1}.[8]. Compared with other metal ions, Zn/Zn^{2+} has excellent reversibility in aqueous media, proving that zinc-ion batteries have great development potential.[1].

At the same time, the development of zinc-ion batteries is still full of challenges. One of the core issues is the formation of zinc dendrites[1]. During the battery cycle, zinc ions are prone to form diameters due to their unique deposition morphology, and dendrites are the main cause of short circuits, capacity decay and battery failure. Especially at high current density, zinc ions are more likely to be unevenly deposited, leading to uncontrolled growth of zinc dendrites.[2]. Another core issue is that the electrochemical stability window of aqueous batteries is relatively narrow, and water often produces hydrogen evolution (HER) during battery operation. Some

progress has been made in the design of interfaces using artificial interface layer optimization [7], but the long-term stability and reversibility of aqueous battery cycles and the problem of how to solve the dissolution of positive electrode materials still exist.[6].

To fully realize the necessity of designing advanced electrolytes, we must deeply understand the inherent limitations of traditional liquid electrolytes, as electrolytes play a decisive role in the performance, safety and life of batteries.

A fundamental constraint is the narrow electrochemical stability window (ESW). For aqueous systems, the water decomposition reaction (HER/OER) thermodynamically limits the ESW to approximately 1.23 V, which hinders the application of high-voltage cathode materials and thus limits the energy density of the battery[9-11]. Similarly, in lithium battery systems, the oxidation limit of traditional carbonate electrolytes is approximately 4.3-4.5 V, which is insufficient for next-generation high-voltage cathode materials[12-14].

Interfacial kinetics and stability issues are common. In ZIBs, Zn^{2+} ions form a strong hydrated shell, which leads to sluggish desolvation kinetics at the interface, hindering the transport of Zn^{2+} and exacerbating uneven deposition[15]. The resulting solid electrolyte interface (SEI) is often inhomogeneous and chemically unstable, especially under long-term cycling or high voltage conditions[14; 16; 17]. In aqueous ZIBs, this instability leads to electrode passivation through the deposition of insoluble byproducts like ZHS ($Zn_4SO_4(OH)_6$-xH_2O), resulting in higher impedance[10; 15; 17; 18].

Conventional electrolytes face operational and safety concerns. Compared to aqueous electrolytes, organic electrolytes are flammable and volatile, making them less safe. They can even decompose and produce toxic HF gas.[11; 15; 17; 18]. While aqueous electrolytes are safe, if water evaporation and gas evolution cannot be guaranteed, the entire battery still faces electrolyte loss or unstable operation. Cold weather applications and dendrite growth are particularly problematic. Postal electrolytes increase viscosity and even solidify in cold weather, leading to failure, while water-based electrolytes freeze at low temperatures, losing conductivity and severely inhibiting reaction kinetics.[11-13]. Furthermore, both systems face severe dendrite growth issues.[15].

In summary, both aqueous and nonaqueous batteries still face fundamental challenges including limited electrochemical stability, dendrite growth, sluggish ion transport and interfacial instability, which restrict their practical development. These unresolved issues highlight the necessity of advanced electrolyte strategies. Hydrogel electrolytes have recently

attracted increasing attention as they provide distinctive advantages in regulating water activity, stabilizing interfaces and improving safety, offering new opportunities for the next stage of aqueous zinc-ion battery research.

1.2 Development and design of hydrophilic hydrogel electrolytes

Hydrogel electrolytes offer a novel solution to the side reactions and dendrites that occur during long-term cycling in aqueous zinc-ion batteries. The hydrogel polymer network provides mechanical strength, enabling it to replace glass fiber separators and reduce battery weight, while maintaining minimal loss of ionic conductivity due to its hydrophilic nature. These advantages have made hydrogel electrolytes a new hotspot for flexible energy storage.

1.2.1 Ion transport enhancement mechanisms

One of the core mechanisms of hydrogel electrolytes in aqueous zinc-ion batteries (AZIBs) is the construction of ion channels, which immobilize anions and accelerate Zn^{2+} migration. This rapid ion transport is fundamental to fast charging, improved energy density, and stable operation under extreme conditions.

To achieve this goal, polymer networks are engineered with customized functional groups to create directional and efficient transport channels. For example, hierarchical PVA/PAA/Zn hydrogels employ directional pores to promote Zn^{2+} diffusion and inhibit uneven deposition[19]. In dual-network hydrogels, zwitterionic groups (-COOH and -SO_3H) provide electrostatic interactions and reversible hydrogen bonds, establishing independent migration pathways for cations and anions[20]. This design enhances Zn^{2+} transport and maintains stability over a wide pH range. Furthermore, the Zn^{2+} solvation shell was tuned by introducing sulfonate and imidazole groups into the zwitterionic gel; these functional groups partially replaced water molecules, lowered the desolvation barrier, and deposited Zn^{2+} onto the (002) plane, favoring dendrite-free growth[21].

Another effective approach involves enhancing Zn^{2+} transference numbers and tuning solvation structures via zwitterionic monomers. As shown in Figure 1, SBMA units are built into the polymer network to create clear ion channels, The negative charge of the sulfonic acid group can attract Zn^{2+} and guide its movement, while the ammonium group can capture the larger -OTF^- anion and fix it. This separation of transport routes promotes rapid zinc migration,

delivering an ultrahigh Zn^{2+} transference number of 0.84 and ionic conductivity above 30 $mS \cdot cm^{-1}$[22]. Polymeric zwitterions he zwitterionic chains bond with water molecules, lowering their activity and reducing side reactions.

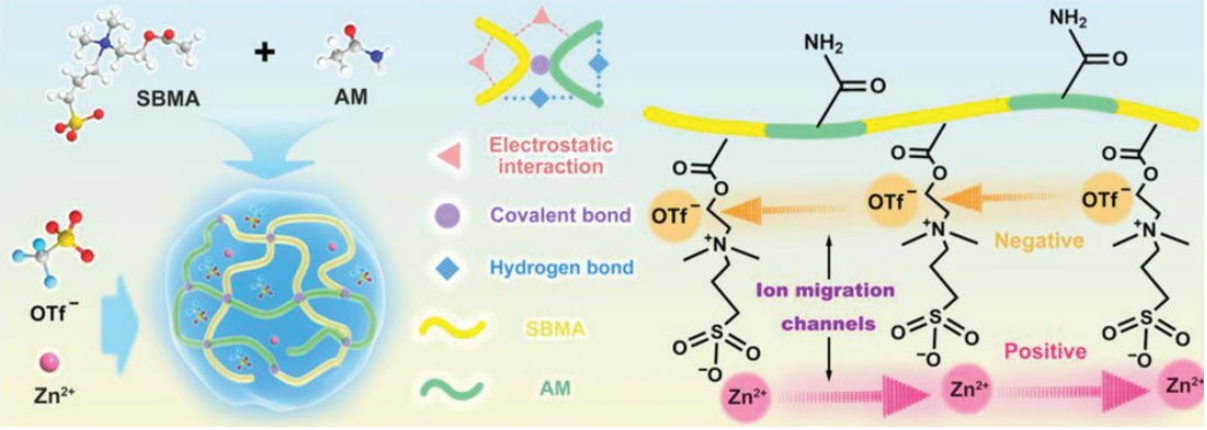

Figure 1. Schematic diagram of ion channel construction using zwitterion addition. [22] Copyright 2022, Advanced Energy Materials.

In addition to solvent engineering, designing single-ion conducting architectures that direct Zn^{2+} migration has become an increasingly attractive strategy. Within these systems—such as pseudo-polyrotaxane hydrogels or macrocyclic assemblies, the movement of anions is deliberately restricted through steric confinement or hydrogen-bond interactions. By limiting anionic mobility, Zn^{2+} can migrate with reduced interference, resulting in markedly elevated transference numbers[23].

Among zwitterionic strategies, the incorporation of L-carnitine (CN) into hydrogel electrolytes stands out. The carboxyl groups of CN coordinate with Zn^{2+}, while electrostatic interactions at the electrode/electrolyte interface generate water-deficient, ion-selective layers. This configuration not only mitigates side reactions and dendrite proliferation but also promotes the formation of discrete Zn^{2+} exclusive transport pathways, enabling transference numbers up to 0.847 and providing superior resistance against corrosion and self-discharge[24]. Likewise, immobilizing anions through polyelectrolyte backbones or covalently crosslinked frameworks, as demonstrated by Peng et al.[24] enables directional ion transport, alleviates concentration polarization, and enhances long-term cycling stability. Such synergy of solvation structure tuning and single-ion transport control holds immense promise for the development of hydrogel electrolytes tailored for fast, durable, and dendrite-free operation in aqueous zinc-ion batteries. Chelation-assisted conduction channels further enrich this design paradigm. Hydrogels based on tannic acid-sodium alginate (TA-SA) employ dense phenolic hydroxyl and carboxyl groups

to coordinate Zn^{2+}, thereby constructing confined tunnels that promote uniform nucleation and hinder dendritic propagation, exhibit an impressive ionic conductivity and transference number[25].

Zwitterionic polymeric frameworks also represent a powerful design platform. A polyzwitterionic hydrogel electrolyte (PZHE) synthesized from SBMA and AA via nanoreinforced self-catalytic gelation demonstrates not only robust interfacial adhesion but also excellent low-temperature tolerance, maintaining stable operation down to -60 °C. Within this system, zwitterionic and carboxyl functionalities coordinate Zn^{2+} while immobilizing water, ensuring homogeneous ion distribution in-plane and suppressing parasitic processes, even under mechanical deformation[26]. Similarly, sulfobetaine-functionalized cellulose hydrogels establish three-dimensional interconnected ionic pathways, allowing for uniform Zn^{2+} migration. These systems achieve a Zn^{2+} transference number of approximately 0.656, ionic conductivity of ~2.46 $S \cdot m^{-1}$, and extended cycle lifetimes with suppressed dendrite formation[27]. Moreover, hybrid cellulose-CMC hydrogels enhance dendrite resistance by generating dense hydrogen-bond networks with limited free-water content. This confined structure accelerates Zn^{2+} desolvation and channels ionic flux through nanocellulose tunnels, thereby enabling smooth Zn deposition and effectively mitigating parasitic side reactions, even under high current densities[28].

In summary, the rational design of hydrogel electrolytes, achieved through structural confinement, enhanced Zn^{2+} transference numbers, and interface-specific functionalization, has been shown to effectively suppress dendrite formation and stabilize metal-electrolyte interfaces. Approaches such as introducing anionic or zwitterionic groups, constructing hierarchical porous networks, and exploiting ion-polymer coordination collectively ensure uniform Zn^{2+} flux, mitigate parasitic side reactions, and enable long-term cycling stability. These advances provide a solid basis for developing durable and high-performance aqueous Zn-based energy storage systems.

1.2.2 Dendrite Suppression and Interface Stabilization

Zinc dendrite growth is widely recognized as the dominant failure mechanism in aqueous zinc-ion batteries (AZIBs), severely compromising both cycling stability and device safety. In recent years, functional hydrogel electrolytes have demonstrated unique advantages in stabilizing the Zn anode interface, primarily through their ability to modulate electric field distribution,

regulate solvation behavior, and control deposition dynamics. A particularly effective approach is the incorporation of anionic functional groups, such as sulfonate ($-SO_3^-$) and carboxylate ($-COO^-$), into polymer backbones. These functional moieties exhibit strong coordination with Zn^{2+} ions, thereby directing their deposition preferentially onto the thermodynamically stable (002) crystal plane and effectively suppressing dendritic nucleation at the electrode surface.

In one representative implementation, sulfonate-modified covalent organic frameworks (COF-BSO_3Zn) dispersed throughout a PAM hydrogel create well-ordered, confined ion-transport channels. These pathways accelerate Zn^{2+} migration and endow the composite with both high ionic conductivity and a high Zn^{2+} transference number, indicative of strong cation selectivity. As a result, the COF-BSO_3Zn/PAM electrolyte delivers uniform Zn plating/stripping over prolonged cycling, effectively curbing dendritic growth and sustaining long-term electrochemical stability[29].

Hydrogel electrolytes designed since the Hofmeister effect, particularly those incorporating chaotropic anions such as ClO_4^-, can establish ternary hydrogen-bond networks involving water molecules and polymer chains. This structural regulation lowers the freezing point, reduces the proportion of free water, and improves interfacial uniformity at the Zn electrode. Benefiting from these effects, such hydrogels enable highly reversible Zn plating/stripping for more than 1200 hours and maintain stable electrochemical performance even at -30 °C, underscoring the synergistic role of chaotropic-ion coordination and tailored polymer frameworks[30]. Another representative class involves thermoregulatory hydrogel electrolytes (TRHEs), which incorporate phase-change materials such as polyethylene glycol (PEG). These systems possess the capacity for self-adaptive heat absorption during sudden thermal fluctuations, thereby preventing thermal runaway. In addition to thermal regulation, well-organized ion transport channels and strong hydrogen bonding in TRHEs help Zn^{2+} spread evenly. This uniform distribution limits dendrite growth and reduces corrosion at both room temperature and high temperature. As a result, the electrode surface remains stable during cycling.[31].

These findings show that functional hydrogel electrolytes form a flexible and effective platform for dendrite control. Different strategies have been explored, including anionic or zwitterionic modification, tuning water activity, and introducing thermal-responsive structures. Each method helps balance Zn^{2+} movement and direct smooth deposition, which supports long-term and efficient battery operation.

Maintaining a stable local pH and reducing parasitic reactions are essential for long-term

cycling stability in aqueous zinc-ion batteries. Side processes such as hydrogen evolution and zinc corrosion can severely weaken electrochemical performance. As highlighted in Figure 2, zinc-based batteries face hydrogen evolution under acidic conditions and form byproducts such as Zn $(OH)_2$ or zinc oxysalts in alkaline media. These competing reactions reduce Coulombic efficiency, increase interfacial impedance, and accelerate electrode degradation. Consequently, neutral or mildly acidic electrolytes are considered more favorable for achieving stable cycling behavior. Hydrogel electrolytes provide unique chemical and physical pathways to regulate water activity, buffer local pH fluctuations, and suppress parasitic reactions, thereby offering a promising strategy to realize durable and reliable zinc-based energy storage systems.

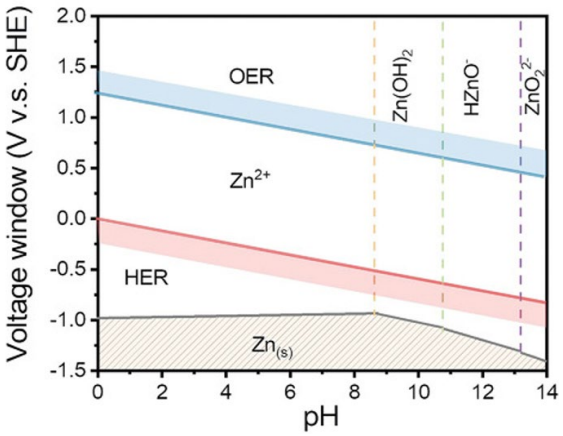

Figure 2. The Pourbaix diagram of Zn anodes in aqueous solution. [27]

A key strategy is to restrict free water, which is the main driver of hydrogen evolution and zinc corrosion. By constructing a strong hydrogen bond network to fix water near polar groups, the molecular mobility is reduced, the reactivity is reduced, and thus the gas formation and surface pitting are inhibited[32]. By introducing polar cosolvents such as glycerol or dimethyl sulfoxide (DMSO), the local water structure can be reorganized, the water-polymer interaction is enhanced, the water-water interaction is weakened, the microviscosity is increased, the electrochemical stability window is widened, and the frequency of side reactions is reduced[33]. Hydrophilic crosslinkers, including polyacrylamide, polyacrylic acid, and polyvinyl alcohol, can provide dense coordination sites to confine water within the network. Inside, the trapped water exchanges more slowly and participates in fewer interfacial reactions, resulting in more uniform zinc plating and stripping and fewer corrosion products[34; 35]. Through these methods, the goal of suppressing free water, stabilizing the interface, and limiting parasitic pathways can be achieved without affecting ion transport.

By introducing functional groups such as $-NH_2$, -OH, and $-COO^-$ into the hydrogel backbone,

the deposition of Zn^{2+} can be stabilized by coordinating and moderating interfacial pH fluctuations. These groups can form a stable coordination shell within the hydrogel backbone, reducing proton activity and inhibiting HER[27; 36]. Natural polymer hydrogels such as alginate and xanthan gum are rich in these pendant groups, which can significantly improve the deposition morphology of Zn [25; 37].

Zwitterionic and polyacidic hydrogels can build artificial solid electrolyte interphase (SEI)-like barriers on the zinc surface, preventing direct contact with water and thereby suppressing HER and corrosion[36]. At a more advanced stage, sulfonate-modified covalent organic frameworks (COFs) or ligands with electron-dense groups have been employed to regulate water distribution and homogenize interfacial electric fields, further restraining HER and achieving stable Zn plating/stripping over thousands of cycles[34].

Taken together, hydrogel electrolytes couple water-state control, Zn^{2+} coordination, and interfacial shielding to regulate pH, suppress parasitic reactions, and improve the longevity and safety of AZIBs.

1.2.3 Mechanical Adaptability and Self-Healing Properties

Mechanical adaptability is essential for hydrogel electrolytes in flexible and wearable batteries, and self-healing supports reusability and long-term durability under repeated damage. To meet these needs, researchers design double network hydrogels that combine ionic and covalent crosslinks to deliver high toughness with reversible repair. Many systems stretch well beyond 1000% and heal on their own within minutes at room temperature without external triggers[38; 39]. Dynamic interactions, including hydrogen bonds, Schiff base linkages, and ionic associations such as coordination between metals and ligands, add resilience and reversibility during repeated deformation[40; 41]. Certain designs even sustain multiple healing cycles while retaining stable electrochemical performance[42; 43].

Adhesive moieties such as catechol, amine, and charged groups are often added to ensure intimate contact between the hydrogel and the current collector. This improves interfacial ion transport and strengthens mechanical robustness[26; 42; 44]. Flexible zinc batteries using these electrolytes can retain more than 90% of their capacity during folding, twisting, or cutting. The mechanical strength of a hydrogel works hand in hand with its electrochemical behavior, and this link is an important path toward making aqueous zinc-ion batteries both long-lasting and suitable for wearable use.

1.3 Progress in electrolyte design from hydrophilic to amphiphilic interfaces

A key direction in recent research is to boost environmental adaptability, especially at low temperatures, while at the same time reducing side reactions. One common strategy is to adjust how water behaves inside hydrogels. For example, Huang et al.[30] created a CSAM-C hydrogel that could run stably at −30 °C by using ClO_4^- ions to break hydrogen-bond networks. Pushing this boundary further, Zhu et al.[33] added ethylene glycol to make a hydrogel that worked down to −60 °C. More recently, Shi et al.[45] reported a $Zn(BF_4)_2$-based system that stayed reliable even at −70 °C. These approaches inherently suppress HER by lowering the activity of free water. An illustrative example is the “lean-water” strategy, such as the zwitterionic gel (ZIG) containing only 20 wt% water, reported by Zhang et al.[46] which maintains ionic conductivity while effectively minimizing parasitic reactions.

The versatility of hydrogels is further reflected in their integration with multifunctional and sustainable frameworks. For instance, Yang et al.[47; 48] engineered advanced cation-conducting and dual-layer hydrogels to simultaneously regulate Zn^{2+} deposition and polyiodide crossover in high-performance Zn-I_2 batteries. Meanwhile, mechanical resilience and sustainability have also received strong emphasis. Chen et al.[49] designed a PAM-Hbimcp-Zn hydrogel displaying outstanding anti-fatigue properties and ultrahigh toughness. On the sustainability side, natural polymers have been adopted to construct environmentally benign electrolytes. Illustrating a shift toward a circular economy, Lu et al.[50] developed a degradable and recyclable chitosan-polyaspartic acid hydrogel, exemplifying how performance and ecological goals can be jointly addressed.

In summary, extensive research on hydrogel electrolytes, spanning structural design, functional group tuning, environmental adaptation, and biological integration, demonstrates their enormous potential. These diverse and highly successful strategies, however, share a common operational principle: they are all sophisticated attempts to manage and control the behavior of water within a fundamentally hydrophilic system. Despite effectively reducing "free water" activity, tuning solvation shells, and guiding ion flux, the electrode-electrolyte interface remains intrinsically "wet." This persistent, direct hydrophilic contact, even if mitigated, is the ultimate source of residual side reactions like HER and long-term corrosion, which still impose a ceiling on the ultimate lifespan and energy density of aqueous batteries.

This body of work, while impressive, reveals an inherent limitation of purely hydrophilic systems. Although these strategies effectively modulate bulk water activity and ion solvation,

they are constrained by the intrinsically hydrophilic nature of the polymer matrix, which permits a persistent presence of water molecules at the critical electrode-electrolyte interphase. This underscores the need for a conceptual evolution in electrolyte design: from the global management of water throughout the bulk electrolyte to the deliberate reconstruction of the interfacial microenvironment. Such a strategy does not abandon the principle of water regulation but rather refines it by incorporating hydrophobic or amphiphilic domains directly into the hydrogel architecture. These domains are designed to preferentially orient at the electrode surface, displacing reactive water molecules and fundamentally altering the local solvation shell of Zn^{2+} to create a more stable, less corrosive interphase. This refined approach provides a compelling rationale for exploring the next generation of materials.

1.4 Hydrophobic/amphiphilic hydrogel electrolytes

1.4.1 The rationale for hydrophobic/amphiphilic hydrogel electrolytes

Traditional hydrogels, hydrophilic polymer networks with soft, tissue-like mechanics and exceptionally high water content, have long been valued for biomedical uses such as drug delivery, tissue engineering, and advanced wound dressings owing to their biocompatibility and facile preparation[51; 52]. Their practical utility under load bearing, mechanically dynamic, or long-term operating conditions remains constrained by intrinsic limitations that arise from network architecture and water-polymer interactions. Conventional gels are typically brittle, exhibiting low tensile strength and limited toughness because their static networks lack efficient energy dissipation pathways. They fracture readily under stretching, bending, or compression, which compromises durability in devices that experience repeated deformation[53-55]. Environmental instability further narrows their applicability: highly hydrophilic matrices undergo uncontrolled swelling in aqueous media, which causes dimensional drift, loss of interfacial conformity, and deterioration of functional properties, while dehydrating rapidly in air, which leads to shrinkage, embrittlement, and loss of function[56; 57]. At interfaces, a strongly bound hydration layer impedes intimate contact with diverse substrates, yielding weak adhesion on wet or underwater surfaces and complicating integration into soft bioelectronics and energy systems[58; 59]. These challenges have driven strong efforts to design hydrogels that can self-heal, be injected, stick well under water, and

still offer conductivity and responsiveness to external signals. The goal is to keep them soft and flexible while not losing stability [60]. As shown in Figure 3, a self-assembled micellar strategy can create nanoscale hydrophobic domains and physical crosslinks in water, offering a clear pathway to stronger and more adaptive hydrogel electrolytes.

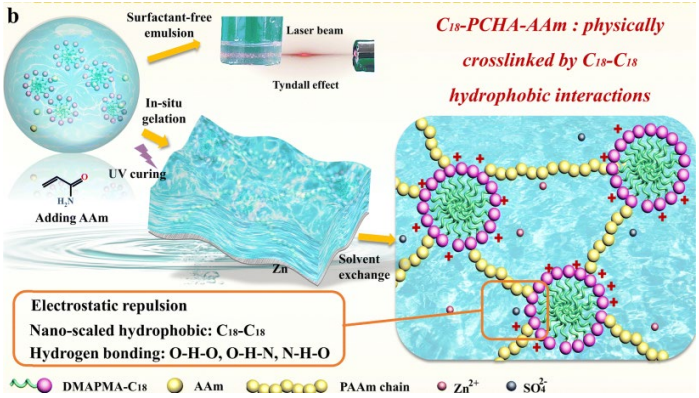

Figure 3. Self-assembled micellar strategy that creates nanoscale hydrophobic domains and physical crosslinks in water.[61] Copyright 2024, Energy & Environmental Science.

A growing approach is to add hydrophobic segments into mainly hydrophilic networks. This idea often comes from natural elastomers, where hydrophobic parts and crosslinking points work together to give toughness and recovery[52; 62-64]. By embedding alkyl or fluorinated groups, the system takes advantage of the hydrophobic effect in water. Nonpolar units gather together, forming reversible junctions that act like physical crosslinks. These links can break under stress and then rebuild when the stress is gone [65; 66].

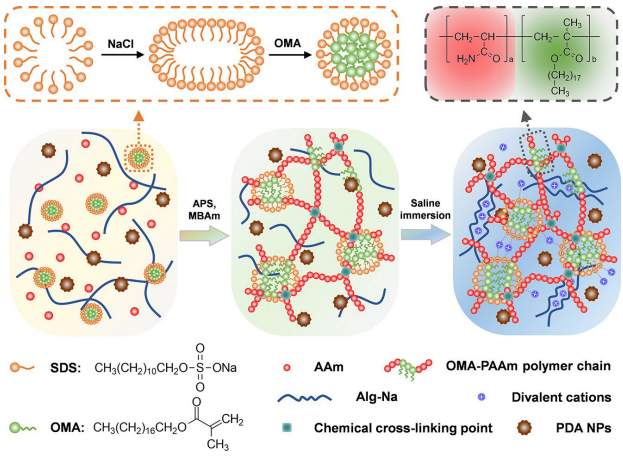

Figure 4. Surfactant micelle templates that packages hydrophobics into micellar monomers and supports wet adhesion and energy dissipation.[58] Copyright 2021, ACS Applied Bio Materials.

Figure 4 shows a micelle method, in this approach surfactant micelles wrap nonpolar molecules

and help them disperse in water. Once incorporated into the polymer framework, these micellar domains act as dynamic crosslinking points. They strengthen the network, guide ion transport, and improve interfacial adhesion, giving the hydrogel both mechanical stability and electrochemical functionality. When the material is stretched or pressed, the hydrophobic domains act as sacrificial bonds. They break first and release energy, so the stress does not fall on the covalent chains. This gives the hydrogel higher toughness, better resistance to fatigue, and strong recovery. Once the load is removed, the hydrophobic parts come back together on their own, allowing the network to heal repeatedly over many cycles[53; 62; 65; 67]. At the continuum scale, the same hydrophobic domains help to constrain water uptake, reducing volumetric swelling and preserving dimensional stability in geometrically confined or patterned constructs[68]. At interfaces, they partially disrupt hydration layers and strengthen interfacial interactions, thereby improving adhesion on wet or underwater substrates and sustaining device coupling under physiological or humid environments[69]. Because hydrophobic associations can be tuned in density and strength, they also serve as design handles for introducing stimuli responsiveness, hierarchical microstructures, and composite architectures that integrate fillers, ionic conductors, or functional nanoparticles without compromising softness[70; 71].

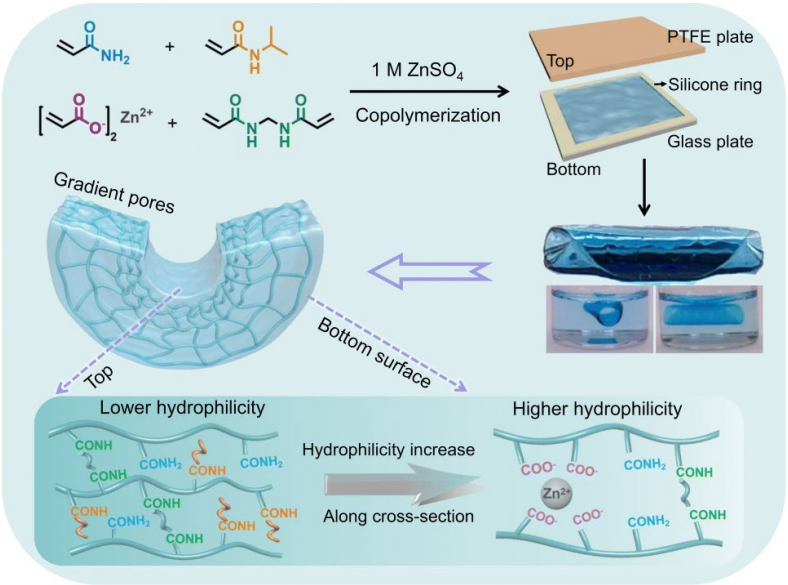

Figure 5. Direct copolymerization of hydrophilic and hydrophobic monomers to form continuous ion pathways with embedded hydrophobic regulators[72]. Copyright 2024, Energy & Environmental Science.

The direct polymerization method provides a straightforward way to integrate functional groups into hydrogel networks. Monomers and crosslinkers polymerize in the presence of zinc salts, producing a structure with gradient pores and spatially varied hydrophilicity. As shown

in Figure 5, the top and bottom surfaces differ in hydrophilic character, creating asymmetric ion transport pathways. This gradient design not only improves electrolyte wettability and ion conduction but also stabilizes zinc deposition, offering a simple yet effective strategy for building advanced hydrogel electrolytes.

The incorporation of hydrophobic monomers into hydrogel electrolytes can be achieved through three approaches: self-assembly of micellar domains, micelle-assisted monomer solubilization, and direct copolymerization of hydrophilic and hydrophobic units. Spontaneous aggregation of micelles can generate nanoscale hydrophobic clusters that act as dynamic physical crosslinkers, dissipating energy under stress and reforming upon unloading, thereby imparting toughness and self-healing properties. In a second strategy, micelles encapsulate otherwise water-insoluble monomers, enabling their uniform dispersion and subsequent polymerization within a hydrophilic matrix; the resulting micellar domains not only strengthen the network but also facilitate interfacial regulation and wet adhesion. A third strategy achieves molecular-level integration through direct copolymerization of polar and nonpolar monomers, creating a framework with continuous ion transport pathways interspersed with localized hydrophobic modulators that regulate water activity and Zn^{2+} solvation.

Despite differences in implementation, these approaches share a unifying principle: hydrophobic domains serve both as physical crosslinks in the bulk and as interfacial modifiers at the electrode surface. Through this dual role, they enhance mechanical robustness, suppress excessive expansion, and establish a waterproof interface that stabilizes zinc plating/stripping, thus providing a versatile design toolkit for next-generation amphiphilic hydrogel electrolytes.

1.4.2 Hydrophobic design in amphiphilic hydrogel electrolytes

Amphiphilic hydrogel electrolytes can be understood as interfacial microenvironment designs that exploit the hydrophobic effect on the Zn surface while maintaining liquid-like ion transport in the bulk. Incorporation of nonpolar segments into the hydrogel network drives their enrichment at the electrode, where they assemble into a nanometric, water-repelling barrier. This interfacial layer separates bulk water from active metal yet remains permeable to charge carriers, creating a local “water-poor” environment that suppresses hydrogen evolution, alkaline corrosion, and basic zinc sulfate formation without significantly hindering Zn^{2+} transport when thin and dynamic[73]. In the bulk, water activity can be regulated through specific coordination and hydrogen-bond reorganization, reducing the reactivity of free and

solvating water, expanding the electrochemical stability window, and enabling stable operation across a wide temperature range. Thus, bulk regulation complements interfacial hydrophobization[74]. True amphiphilicity requires balance at the molecular level: hydrophilic segments ensure salt uptake and continuous Zn^{2+} transport, while hydrophobic domains concentrate at interfaces to block water-driven side reactions and promote partial desolvation prior to reduction. This balance is realized through several strategies with distinct advantages and application ranges.

One approach is additive engineering. Small molecules or amphiphiles are introduced either to reconstruct the solvation shell or to assemble at the electrode surface. In hydrogels, additives that coordinate or hydrogen-bond can reorganize the water network and participate in Zn^{2+} solvation, lowering water activity and limiting proton availability. For example, glucose in PAM/$Zn(ClO_4)_2$ hydrogels strengthens water-water covalency, suppresses hydrogen evolution, and maintains ionic conductivity across wide temperature ranges[74]. At the Zn surface, amphiphiles such as dodecanoic acid form ultrathin monolayers with carboxylate heads bound to Zn and hydrocarbon tails oriented outward. These films block interfacial water, lower HER currents, resist passivation, and sustain long-term cycling, serving as prototypical interfacial hydrophobes that integrate naturally with hydrogel matrices. More broadly, diverse additives regulate solvation, adsorption, and interfacial energy, providing a versatile toolkit for amphiphilic systems[24; 75].

Copolymer and interpenetrating-network designs covalently link hydrophilic and hydrophobic components, or combine soft and rigid networks, thereby coupling liquid-like conduction with structural stability. Double-network and polyelectrolyte architectures improve modulus, homogenize Zn^{2+} flux, and limit swelling, which are prerequisites for stable plating and stripping at practical current densities[24]. Polyanionic hydrogels further exemplify this principle: dense sulfonate and amide groups establish rapid Zn^{2+} channels, enhance the transference number, and suppress anion back-diffusion, reducing space-charge accumulation and guiding uniform deposition, while the hydrophilic-hydrophobic balance regulates water uptake and durability[76].

Functional-monomer strategies embed well-defined coordination motifs that simultaneously tune Zn^{2+} solvation and strengthen mechanics. Benzo-15-crown-5-acrylamide, with its macrocyclic cavity, selectively coordinates Zn^{2+} to reconstruct the solvation shell, while the rigid benzene ring stabilizes conformation and increases strength. The resulting hydrogels

exhibit high conductivity and elevated transference numbers, enabling uniform Zn deposition without reliance on fragile additive-heavy systems[77]. In situ interfacial self-assembly provides another route. Molecules such as lauric acid spontaneously adsorb on Zn and organize into ultrathin hydrophobic coatings. These layers remain ion-permeable, inhibit hydrogen evolution and corrosion, promote smooth nucleation, and lower hysteresis during extended cycling[73].

Collectively, these strategies represent a shift from passively restricting water to actively regulating its chemistry and spatial distribution. Hydrophobic domains reduce water activity and facilitate desolvation, while hydrophilic networks preserve conductivity and adhesion. Well-designed amphiphilic systems thus achieve liquid-like ion transport in the bulk and solid-like interfacial stability, overcoming the limitations of purely hydrophilic or purely hydrophobic gels.

1.5 Hydrophobic design in hydrogel electrolytes

1.5.1 Water activity regulation

The electrochemical stability window (ESW) sets the working voltage and energy density of aqueous zinc batteries. In water-based electrolytes, it is limited by water splitting, with oxygen evolution at high potential and hydrogen evolution at low potential. Amphiphilic hydrogels expand this window by lowering water activity in the bulk and blocking water access at the interface, while still supporting fast ion transport. Reported systems reach ESWs close to 3.0 V, and in optimized cases up to 3.3 V, even with high water content such as 68 wt%[78; 79]. The next section explains how these materials achieve this through hydrogen-bond restructuring and interfacial hydrophobization.

From a thermodynamic view, the main task is to raise the barrier for water decomposition. This is done by strengthening noncovalent interactions that hold water molecules more tightly and reduce their reactivity. Amphiphilic hydrogels use polar groups on hydrophilic backbones, such as amides in polyacrylamide, and may also include small molecules that act as strong hydrogen-bond donors or acceptors. These groups create stronger polymer-water and additive-water bonds than those in the native water-water network, shifting water from a free, active state to a bound, ice-like state. Spectroscopic signatures include a blue shift and sharpening of the H-O stretching band, indicating reinforcement of the hydrogen-bond network and a decrease in

the fraction of highly mobile water[74; 79; 80]. The same restructuring is captured calorimetrically. Differential scanning calorimetry reveals that, relative to conventional hydrogels, amphiphilic networks reduce the mass fraction of free water while increasing the fraction of nonfreezable bound water that is essentially inert during electrochemical operation, with representative values showing a decrease of free water from about 1.232 mg mg^{-1} to about 0.15 mg mg^{-1} and a concomitant increase of bound water from about 0.129 mg mg^{-1} to above 0.4 mg mg^{-1}[32]. Because cleaving these strengthened hydrogen bonds requires more energy, the thermodynamic thresholds for hydrogen and oxygen evolution shift to more negative and more positive potentials, respectively, and the cathodic and anodic limits of the ESW separate accordingly [74; 79].

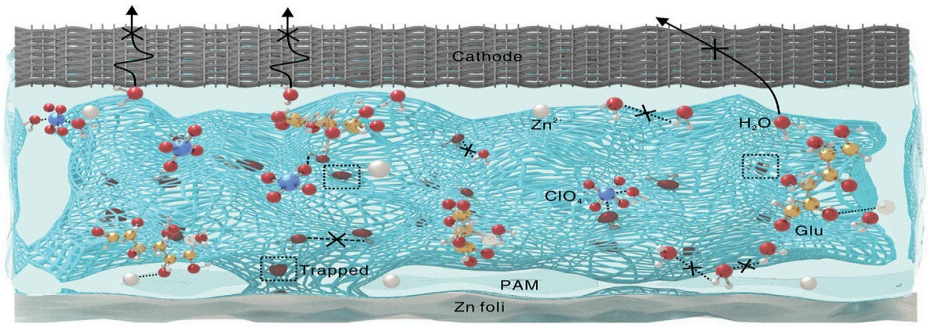

Figure 6. PAM traps/disrupts bulk water, ClO_4^- forms tight anion-water associations and Zn^{2+}-Glu coordination expels interfacial solvation water and releases ClO_4^- to bind more water.[74] Copyright 2024, Advanced Energy Materials.

On the kinetic side amphiphilic hydrogels create a physical barrier that impedes the delivery of water to the reactive metal surface. Hydrophobic domains format or enrich near the interface and present a water-repelling layer that is thin and ion permeable. Typical contributors include relatively rigid or less polar segments within the network and hydrophobic side chains that orient outward at the boundary. The barrier reduces the arrival rate of water to the electrode, moderates interfacial proton availability, and facilitates partial desolvation of Zn^{2+} prior to charge transfer. Even when water splitting remains thermodynamically allowed, the reduced interfacial concentration of labile water suppresses the kinetics of the hydrogen and oxygen evolution reactions. The same hydrophobic elements also constrain water uptake at the device scale, thereby stabilizing dimensions, preserving contact, and smoothing concentration and potential gradients during plating and stripping[74; 80; 81]. These effects act without materially penalizing ionic conductivity because the hydrophobic structures are discontinuous in the bulk and the hydrophilic matrix supplies continuous pathways for Zn^{2+} transport[74].

The synergy between bulk thermodynamic suppression and interfacial kinetic hindrance produces an ESW expansion that exceeds either strategy alone. Stronger polymer-water interactions lower water activity throughout the hydrogel, as evidenced by vibrational shifts and DSC-derived water-state fractions[32; 74; 79] , while the interfacial hydrophobic layer selectively excludes the remaining free water from the electrode and limits its participation in parasitic reactions[74; 80; 81]. As a result, hydrogen evolution, oxygen evolution, and corrosion are simultaneously suppressed, and the electrolyte remains operative at high water content with a widened window that supports high voltage charging and discharging. This multilayer regulation, realized within a single amphiphilic network, establishes water-activity control as the central molecular mechanism by which amphiphilic hydrogels achieve a broadened and practically useful ESW for aqueous zinc batteries.

1.5.2 Ion solvation and transport kinetics

Hydrophobic and amphiphilic hydrogels not only control the state of water but also reshape the Zn^{2+} solvation environment, which improves ion transport and desolvation. In liquid electrolytes, Zn^{2+} usually exists as $[Zn(H_2O)_6]^{2+}$, a stable octahedral complex. Removing this hydration shell at the electrode surface requires high energy, leading to slow charge transfer and unwanted side reactions[82; 83]. By contrast, gel electrolytes provide ion-conducting channels formed by functional groups like carbonyls, sulfonates, or ether linkages. These groups coordinate with Zn^{2+}, partially replace water in the solvation sheath, and create new complexes such as $[Zn(Polymer)(H2O)_{6-x}]^{2+}$[84-86]. As shown in Figure 7, this channel-guided solvation environment reduces free water activity, ensures efficient Zn^{2+} migration, and supports dendrite-free deposition.

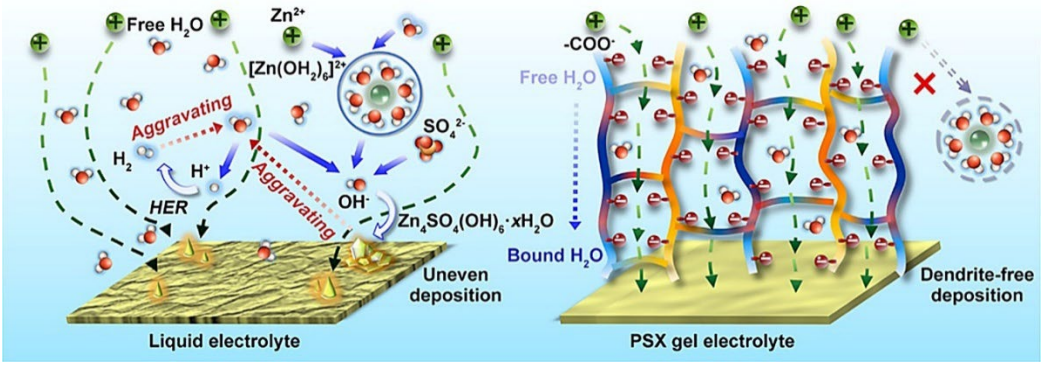

Figure 7. Schematic illustration of the Zn deposition behavior and interfacial reactions in liquid and PSX gel electrolyte.[86] Copyright 2022, Energy Storage Materials.

This solvation-shell reconstruction directly reduces the desolvation energy barrier at the electrode interface. Both experimental measurements and theoretical calculations confirm that hydrophobic hydrogels dramatically lower the activation energy for Zn^{2+} desolvation—for instance, from 15.36 kJ mol^{-1} in a standard PAM hydrogel to only 3.16 kJ mol^{-1}[86], or from 62.31 kJ mol^{-1} in aqueous ZnSO4 solution to 36.42 kJ mol^{-1}[87]. Lowering this barrier allows Zn^{2+} ions to more readily shed coordinated water and participate in electrode reactions, significantly accelerating interfacial kinetics and reducing the likelihood of side reactions[76; 86; 87]. In addition to solvation regulation, ionic functional groups along the polymer backbone play a decisive role in guiding ion transport. Polyanionic chains containing $-COO^-$ or $-SO_3^-$ moieties provide directional electrostatic "ion highways" for Zn^{2+} migration while simultaneously repelling co-charged SO_4^{2-} anions. This selectivity increases the Zn^{2+} transference number ($t_{Zn^{2+}}$) to exceptionally high values, reaching 0.8 to 0.912[61; 82; 88]. Similarly, polycationic backbones can immobilize SO_4^{2-} anions through strong electrostatic interactions, also achieving elevated $t_{Zn^{2+}}$ values around 0.85[89]. A high transference number is critical for suppressing concentration polarization, maintaining uniform ion flux, and establishing the conditions necessary for dendrite-free Zn deposition[82; 89].

In summary, hydrophobic/amphiphilic hydrogels optimize Zn^{2+} electrochemistry by reconstructing the solvation sheath, lowering the desolvation barrier, and enabling selective ion transport, collectively accelerating reaction kinetics and ensuring uniform, dendrite-free deposition.

1.5.3 Zinc anode deposition

Through the synergistic regulation of water activity and ion transport dynamics, hydrophobic and amphiphilic hydrogels ultimately promote highly uniform, compact, and dendrite-free zinc deposition at the electrode interface. This desirable outcome is realized through the cooperation of multiple interrelated mechanisms. First, the hydrogel-electrolyte interface can direct the preferential orientation of zinc crystal growth. Numerous studies have confirmed that deposition along the thermodynamically stable (002) basal planes produces flat and dense layers, whereas deposition along the metastable (101) planes tends to generate needle-like dendrites that compromise performance[87; 89; 90]. Certain functional moieties on polymer chains, particularly polycationic groups, display lower adsorption energies on the Zn (002) surface. This selective interaction retards the growth rate of the (002) facets, and according to the

Bravais law of crystal growth, the planes with the slowest growth eventually dominate the exposed surface. As a result, deposition is guided toward the Zn (002) orientation, yielding smoother and more compact electrode surfaces[87; 89].

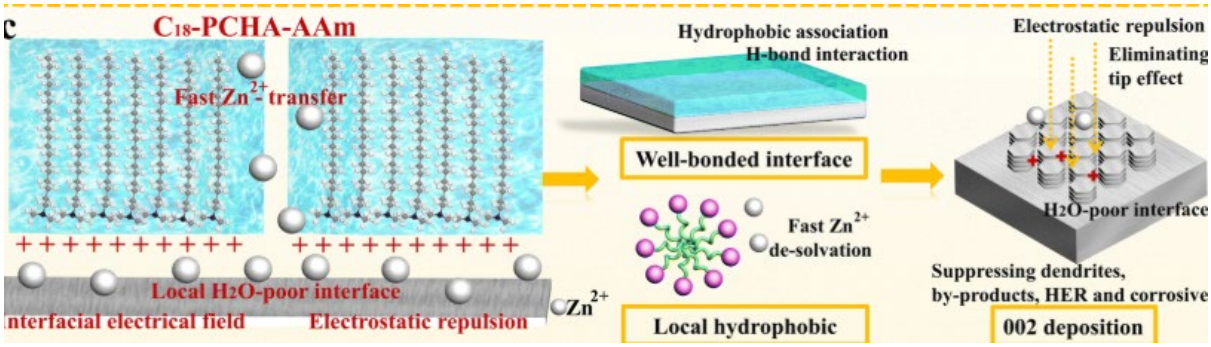

Figure 8. Schematic depictions for the C18-PCHA-AAm hydrogel electrolyte and the corresponding Zn deposition behavior regulation.[61] Copyright 2024, Energy & Environmental Science.

Second, the hydrogel's internal network—especially when enriched with charged polymer backbones—effectively homogenizes the interfacial electric field and ion flux distribution[86; 89]. Polycationic chains generate electrostatic repulsion toward incoming Zn^{2+} ions, establishing a shielding effect that suppresses the so-called "tip effect." This prevents the localized concentration of current and ions at protruding sites on the electrode, ensuring that nucleation events occur more evenly across the surface[79]. When coupled with the intrinsically high Zn^{2+} transference number achieved in such hydrogels, Zn^{2+} ions are delivered to the anode in a gradual and spatially uniform manner. This regulated ion transport eliminates the kinetic driving forces responsible for dendrite formation at their very origin, enabling smooth plating behavior during long-term cycling. The integration of hydrophobic units within the hydrogel framework establishes a nanoscale "hydrophobic confinement" or "H_2O-poor" microenvironment at the zinc-electrolyte interface [61; 89]. Such hydrophobic regions repel free water molecules, markedly increase the electrolyte's contact angle on the zinc surface, and form an effective water-repellent barrier. This structural feature significantly suppresses water-induced parasitic reactions, such as the hydrogen evolution reaction (HER) and zinc corrosion[46]. Concurrently, the hydrophobic confinement promotes Zn^{2+} desolvation by facilitating the removal of residual water molecules from the solvation sheath, thereby accelerating electrochemical reactions at the interface. In addition, bio-inspired designs, for instance the incorporation of dopamine or catechol groups, introduce strong adhesive properties to hydrogels. This adhesion ensures intimate and stable physical contact between the hydrogel electrolyte and the zinc surface, which is critical for preventing delamination,

localized current density spikes, and eventual failure during repeated cycling[91]. In summary, these cooperative mechanisms, including crystallographic orientation control, electric field and ion flux homogenization, and interfacial hydrophobization with strong adhesion, enable hydrophobic and amphiphilic hydrogels to fundamentally mitigate zinc dendrite growth and suppress parasitic side reactions. This comprehensive regulation strategy not only stabilizes the electrode-electrolyte interface but also provides a reliable pathway toward high-performance, long-life, and safe zinc-based batteries.

1.5.4 Hydrophobic association for high utilization of thick cathodes

The efficient utilization of thick cathodes is often limited by limited electrolyte penetration and poor ion accessibility in densely packed layers. Hydrophobic associations provide a coherent design approach that links molecular interactions, interfacial organization, and mesoscopic structure to overcome these limitations. In amphiphilic hydrogel electrolytes, hydrophobic side chains spontaneously aggregate into nanodomains that act as dynamic crosslinks in the hydrophilic network. These reversible associations support load sharing and local rearrangement while maintaining the continuity of ion channels in the water-rich phase, so that the polymer can deform with the electrode without interrupting transport[92; 93]. Chain length and grafting density regulate the extent of phase separation: longer alkyl groups favor the formation of more persistent polymer-rich domains that coexist with connected water channels, helping to reconcile mechanical integrity with ion conduction[93; 94].

At the electrode interface, nonpolar segments tend to orient toward hydrophobic surfaces. This self-directed hydrophobization expels interfacial water, promotes intimate contact with binder- or carbon-rich domains, and provides underwater adhesion that resists delamination during operation[95]. Once anchored, the hydrophobic moieties can “pull” the hydrophilic backbone into the porous interior, effectively threading electrolyte into tortuous pores and building continuous ion-access routes through previously under-wetted regions[93]. Electrostatic rearrangement between polar and nonpolar segments further stabilizes the interfacial layer, allowing adhesion and ion access to persist in aqueous and mixed environments without sacrificing the through-plane ion pathway[94]. Figure 9 shows that the hydrophobic chains connected to the hydrophilic part hydrophobically associate with the hydrophobic part in the positive electrode material, pulling and dragging the hydrophilic gel close to the internal cathode material, improving the electrode utilization.

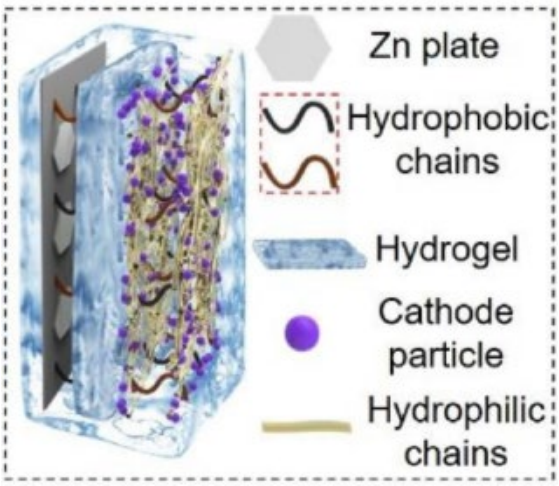

Figure 9. Schematic diagram of hydrophobic chains guiding the insertion of electrolyte into the cathode material[93]. Copyright 2023, Energy Storage Materials.

Mesoscale organization adds another layer of control. Surfactant micelles provide soft templates whose morphology changes with concentration and ionic milieu; simulations and experiments show transitions from spherical to rodlike, wormlike, and bilayer assemblies, which define progressively more confined and directional conduits for transport[96; 97]. Applying this principle to hydrogels, micelle-assisted polymerization or surfactant-templated association can position hydrophobic aggregates in locations that can direct permeation pathways and reduce diffusion distances through thick coatings, thereby increasing access to deeper redox sites without the need for rigid pores.

Surface-grafted polymer brush systems offer a complementary perspective on controlling accessibility through interfacial reorganization. Tethered block copolymer brushes can change their top-layer chemistry upon selective solvent exposure, forming stable nanodomains and altering the wettability of the outer few nanometers, an effect that improves wet contact while preventing water films that hinder ion transfer[98]. Mixed homopolymer brushes on nanoparticles reorganize in response to external cues such as solvent or pH. This reversible switching exposes hydrophobic or hydrophilic chains on the surface, thereby regulating adsorption, lubrication, and interfacial transport without changing the composition of the bulk polymer[99]. Thermo-responsive terpolymer brushes follow the same logic, where small changes in hydration cause the brushes to collapse or swell, thereby regulating the local chain density and the accessibility of charged or hydrophobic groups to molecules at the interface[100]. Although these brush systems are not battery electrodes, their potential for controlled surface presentation of groups, management of interfacial water, and formation of stable nanodomains can directly explain how amphiphilic hydrogels maintain close contact with thick composite

cathodes and regulate local ion/water distribution during operation.

1.5.5 Conversion cathode behaviour under hydrophilic-hydrophobic microenvironments

In aqueous zinc-ion battery systems, the dissolution of conversion-type cathodes is primarily controlled by reactions at the electrode-electrolyte interface. At the interface, local water activity and ion solvation determine three failure pathways for cathode materials: dissolution of the active phase, parasitic hydrogen/oxygen precipitation, and the persistence and outward diffusion of soluble intermediates such as polyiodides. Therefore, the key to stabilizing these cathodes lies in controlling interfacial water activity and solvation, rather than simply improving bulk ionic conductivity. In vanadium-oxide cathodes, water and protons at the interface attack the V-O bonds, bending and breaking the VOx polyhedral and the lattice loses its shape. This makes vanadium dissolve out of the solid, and the dissolved species then react with Zn^{2+}/OH^- to form basic zinc vanadates that are electrochemically inactive[101; 102]. A complementary failure route occurs in iodine cathodes. During conversion, highly soluble polyiodides (I_3^-, I_5^-) form, diffuse away from the cathode, and react at the zinc anode. This shuttle lowers Coulombic efficiency and causes self-discharge unless their formation and mobility are suppressed near the interface[103; 104]. At high areal loadings, the cathode becomes thicker and more porous, which increases the interfacial area and prolongs the residence time of interfacial water films. These factors amplify interfacial instabilities[105].

Hydrophilic-hydrophobic microenvironment engineering decouples bulk ion conduction from interfacial water chemistry. Amphiphilic gels and binders spontaneously enrich hydrophobic segments on the cathode surface (self-hydrophobization), displacing the thin interfacial water layer, reducing local water activity, and enhancing the boundaries for hydrolysis and oxygen evolution. At the same time, the hydrophilic segments maintain continuous Zn^{2+} channels within the porous matrix. The result resembles a local water-in-salt effect, where the interface has very little free water while the bulk still contains enough to support fast ion transport, and it avoids the high viscosity, reduced conductivity, and higher cost of making the entire electrolyte highly concentrated[102].

As mentioned in 1.5.4, the preferential insertion of long alkyl segments into hydrophobic composite regions pulls the hydrophilic backbone deep into the tortuous pores through hydrophobic association, thereby forming the same amphiphilic microenvironment where the

actual conversion reaction occurs.

In VOx cathodes, making the immediate interface drier cuts hydrolysis and reduces unwanted side reactions. Inside the crystal, methods such as guest pre-intercalation and surface anion exchange make the framework harder to dissolve and less stressed. Together these effects push the chemistry toward Zn^{2+}-driven pathways, limit H^+ involvement, and reduce the formation of basic zinc vanadates[101].

In iodine chemistry, hydrophilic-hydrophobic interactions restrict polyiodides and maintain the mobility of Zn^{2+}. Specifically, the soft microphase structure with a hydrophobic core and a hydrophilic shell can preferentially distribute polyiodides to hydrophobic regions or core-shell interfaces, while Zn^{2+} migrates along hydrated channels in the shell[103; 106]. The sticky and/or charged amphiphilic network further reduces the effective diffusion rate of polyiodides through steric and electrostatic interactions, thereby reducing the self-discharge rate and improving the Coulombic efficiency in practical Zn-I_2 batteries[103]. In the vanadium oxide and iodine titania system, the hydrophobic component acts as a selective barrier to water and soluble intermediates, while the hydrophilic component maintains a fast ion flux.

In MnO_2 cathodes, interfacial dehydration suppresses H^+-dominated routes that drive Mn-O hydrolysis, Mn^{3+} disproportionation to soluble Mn^{2+}, and oxygen evolution at high potentials. An amphiphilic interface simultaneously facilitates partial desolvation and guided insertion of Zn^{2+}, favoring Zn^{2+}-centric redox over proton pathways[107]. Preferential insertion of long alkyl segments into hydrophobic composite domains propagates these water-poor boundaries and hydrated Zn^{2+} channels onto internal pore walls, while strong wet adhesion maintains intimate contact during phase and volume changes, limiting fresh-surface exposure and further dissolution in thick electrodes[93; 105]. When employed, mesoscale soft-templating (micelles, core–shell microphases) and responsive brush skins provide confined, directional conduits through the thickness and programmable surface presentation in the top few nanometers, which shorten Zn^{2+} diffusion paths and smooth local fields without altering bulk composition[76]. Collectively, these effects reduce Mn dissolution and parasitic reactions and stabilize MnO_2 conversion under high areal loading and lean electrolyte conditions.

In aqueous Zn systems, conversion cathodes are stabilized when the interfacial region is rendered water-poor while the bulk remains highly conductive to Zn^{2+}. Lower interfacial water activity suppresses water-triggered side reactions and dissolution, while local confinement near the cathode limits the escape and reactivity of soluble intermediates without impeding cation

transport. Hydrophobic association enables deep penetration of the electrolyte into thick porous electrodes and preserves intimate, durable contact under mechanical strain, so continuous through-thickness ion pathways coexist with protected interfaces. Building on this foundation, micelle-derived architectures and responsive polymer-brush skins provide directional, confined conduits and tunable surface presentation, allowing interfacial protection and rapid transport to operate in the same structure. Together, these effects deliver chemical stability and high utilization at practical areal loadings and under lean-electrolyte conditions.

1.6 Multifunctional hydrophobic hydrogel electrolyte

Hydrophobic and amphiphilic hydrogels extend these principles through four coupled effects: reducing free-water activity to widen the electrochemical stability window, restructuring Zn^{2+} solvation to lower desolvation barriers and improve transference numbers, homogenizing local electric fields and ion flux to suppress dendrites, and forming nanoscale interphases that block parasitic reactions while preserving ion transport. To be effective in real devices, these molecular and interfacial functions must be embedded within hydrogel frameworks that tolerate strain, maintain intimate electrode contact, operate across wide temperature ranges, and resist uncontrolled swelling. For wearable and flexible applications, mechanical integrity is as essential as conductivity, since electrolytes must withstand repeated bending, stretching, and compression[108-110]. The central challenge lies in balancing robustness with dynamic features such as self-healing and resilience[111] , a trade-off that recent advances in network engineering are beginning to resolve.

1.6.1 Mechanical robustness and stretchability

Multifunctional hydrogel electrolytes need to possess both high stretchability and excellent toughness to ensure that the soft electrolyte does not break due to large deformation during battery cycling or repeated human movement. Traditional hydrogels often fail in this regard because their highly hydrated networks collapse upon expansion or mechanical stress. Introducing hydrophobic interactions into the hydrogel backbone has become a unifying strategy to resolve this contradiction, providing both energy dissipation and dimensional stability.

One representative approach is homogeneous hydrophobic crosslinking in high-saline environments, where divinylbenzene micelles serve as uniformly dispersed junctions. The high ionic strength compresses micelle size, producing defect-free networks that are exceptionally soft yet exhibit extreme extensibility (>10,000%) and high toughness (134 kJ m^{-2})[112]. As shown in Figure X, the PAMD-NaCl hydrogels sustain compressive stresses up to 52 MPa at 98% strain without fracture, maintain resilience under multiple compression cycles, and achieve a tensile stretch ratio as high as $\lambda = 102$, far exceeding the performance of salt-free controls. These results highlight the effectiveness of hydrophobic micelle crosslinking in simultaneously achieving softness, toughness, and extreme stretchability.

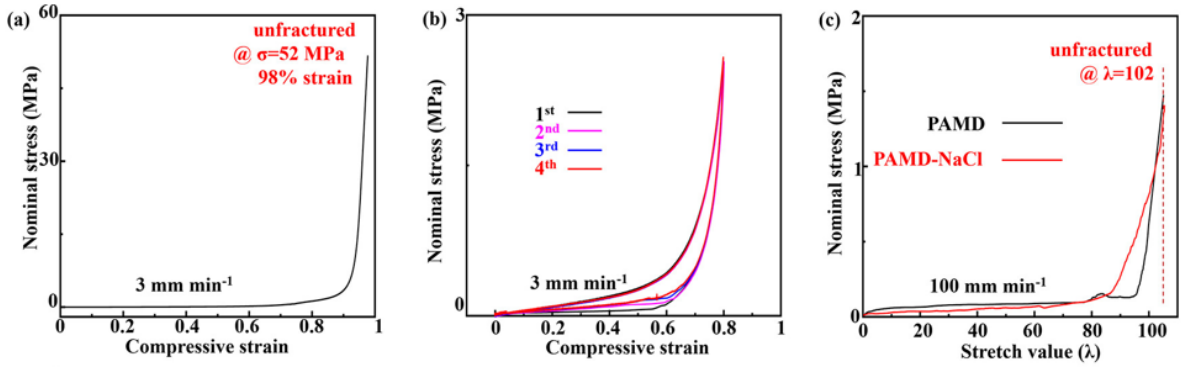

Figure 10. Mechanical properties of PAMD-NaCl hydrogels. (a) Stress–strain curve. (b) Cyclic compression tests at 80% strain over four successive loading–unloading cycles. (c) Tensile stress–strain comparison of PAMD and PAMD-NaCl hydrogels[112]. Copyright 2023, ACS Nano.

Similarly, the dual cross-linking design combining hydrophobic covalent bonds and dynamic electrostatic coordination also gives it extraordinary elasticity. In the PAAD-LM hydrogel, DVB provides permanent hydrophobic cross-linking, while Ga^{3+}/In^{3+} cations form reversible ionic bonds with carboxyl groups, resulting in an elongation of up to 5257% and an area strain tolerance of over 7000%[113].

Hierarchical architectures that integrate multiple noncovalent interactions can dissipate stress efficiently. For instance, the COMBIA hydrogel exploits bismuth coordination together with organic ligands, producing a cascade of bond strengths that distribute mechanical loads. This biomimetic strategy enables ultrahigh stretchability (5417%) and fracture toughness (12.14 MJ m^{-3}), while maintaining transparency, self-healing, and adhesion, making it highly suitable for skin-mimicking electronic platforms[111]. A similar principle applies to zwitterionic amphiphilic hydrogels, where hydrophobic alkyl side chains are interspersed with ionic motifs to create dynamic reversible junctions. Such systems allow controlled rehydration, preserving both

elasticity and conductivity through repeated dehydration–rehydration cycles, essential for sustainable wearable sensors[114].

Mechanically robust and highly stretchable hydrogel electrolytes prevent fracture or delamination during electrode breathing and external deformation, which avoids the formation of cracks that would interrupt ion pathways. As a result, ionic conduction remains continuous and stable, enabling reliable cycling performance in both high-loading and flexible device formats.

1.6.2 Self-healing and fatigue resistance

Self-healing and fatigue resistance are crucial for multifunctional hydrogel electrolytes, as microcracks or cuts can disrupt ionic conduction and mechanical integrity, while repeated deformation can gradually weaken the network without repair or energy dissipation mechanisms.

The COMBIA hydrogel demonstrates how a hierarchy of reversible noncovalent bonds enables spontaneous self-repair. After damage, its dynamic interactions re-form without external stimuli, restoring 91.45% of toughness and fully recovering ionic conductivity, ensuring uninterrupted electrochemical function[111]. A complementary example is the PAAD–LM hydrogel, where covalent hydrophobic crosslinks are coupled with dynamic electrostatic associations. Even when cut, this dual-crosslinked system reconnects and maintains stable operation[113]. In Figure X the schematic illustrates a self-healing process in which damage exposes hydrophobic moieties that tend to re-aggregate at the fractured surfaces. When the cut pieces are brought back into contact, these hydrophobic domains spontaneously reorganize to reduce interfacial free energy, re-establishing the network and restoring ion transport.

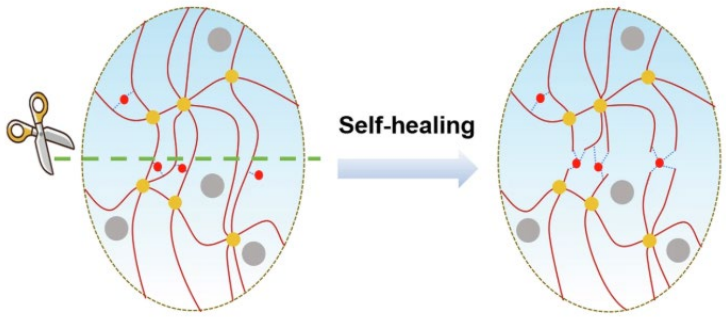

Figure 11. Self-healing schematic diagram[113].

In addition to bulk network engineering, surface and matrix-level strategies also contribute to fatigue resistance. A P(BA-co-HFBMA) elastomer shell serves as a protective skin, preserving both elasticity and conductivity under repeated drying–wetting cycles and thus mitigating cumulative environmental damage[115]. Constructing the entire framework from hydrophobic components yields ionogels with exceptional endurance: these systems sustain adhesion and ionic conductivity even after 5000 stretch–release cycles and over five months of continuous immersion in seawater[116].

In zinc-ion batteries, imparting self-healing and fatigue resistance to hydrogel electrolytes ensures that microdamage does not interrupt ion transport or electrode contact, thereby sustaining electrochemical stability over prolonged cycling and enabling safe operation even under frequent deformation in flexible device formats.

1.6.3 Adhesion and interfacial stability

The stability of soft electrochemical devices is fundamentally governed by the quality of the electrolyte–electrode interface. For zinc-ion batteries in particular, the interface must sustain intimate and uniform contact while accommodating repeated deformation, without generating resistive layers or losing ionic continuity. Hydrophobic design contributes to this goal on several levels. By lowering the activity of interfacial water and disrupting hydration shells, hydrophobic domains reduce the barrier between the gel and the electrode surface, which facilitates closer contact and enlarges the real bonding area. In parallel, dynamic and reversible interactions such as hydrogen bonding, coordination with metal ions, and hydrophobic associations provide effective pathways for stress dissipation. Instead of concentrating stress at sharp edges that can trigger debonding, the interface is able to reorganize under load and redistribute forces, thereby maintaining attachment through cycles of bending, stretching, or compression[109].

The practical outcome is that hydrogel electrolytes engineered with hydrophobic motifs display both strong and reversible adhesion to a wide range of substrates, including metals, oxides, polymers, and even biological tissue. This effect is particularly evident in systems where multiple bonding motifs coexist, enabling weaker bonds to open and release stress while stronger associations preserve overall contact. The result is an adhesive interface that remains intact in environments where conventional hydrophilic gels would delaminate, including underwater or saline conditions[111; 113]. In zinc-based cells, such adhesion translates directly

into stable electrode–electrolyte contact, minimized interfacial impedance, and reduced risk of delamination during long-term cycling. Another important function of hydrophobicity is the ability to modulate electrode–electrolyte interactions, where selective penetration into cathode or anode interfaces improves contact stability and contributes to more uniform electrochemical processes[93]. At the matrix level, fully hydrophobic ionogels exhibit robust adhesion both in air and under water, achieving peel strengths above 700 N m^{-2} on plastics and silicones and maintaining stable attachment over repeated cycles[116]. Surface-engineered strategies provide another route: in situ encapsulation with a P(BAcoHFBMA) elastomeric skin enhances bonding to diverse substrates including glass, metals, and polymers, while preserving compliance and conductivity in humid conditions[115]. these advances highlight that hydrophobic modification not only secures electrolyte–electrode interfaces mechanically but also extend adhesion performance into demanding environments such as aqueous and marine systems.

Reliable adhesion of the hydrogel electrolyte to electrodes is pivotal for minimizing interfacial resistance and preventing delamination during cycling, ensuring that intimate contact is preserved even under repeated deformation and thus supporting stable long-term operation in both rigid and flexible configurations.

1.6.4 Temperature adaptability

Extreme temperature poses distinct challenges for hydrogel electrolytes, as sub-zero conditions induce ice crystallization and sharp increases in viscosity that hinder ion mobility, while elevated temperatures accelerate water evaporation, soften networks, and destabilize electrode interfaces. Hydrophobic design has proven effective in moderating both regimes by lowering the activity of free water and by providing alternative ion-conduction pathways that remain functional when bulk water either freezes or escapes.

At low temperatures, hydrophobic crosslinking can suppress the formation of continuous water domains that would otherwise crystallize and fracture the network. PAMD–NaCl exemplifies this effect, where homogeneous hydrophobic junctions induced by saline conditions maintain elasticity and conduction at -20 °C, preventing catastrophic embrittlement during operation[112]. Cosolvent-based strategies further highlight the role of hydrophobic modification. In COMBIA, the incorporation of glycerol alongside coordinated bismuth ions interrupts ice percolation while stabilizing the polymer backbone, enabling the electrolyte to remain conductive down to

-32 °C[111]. Fully hydrophobic ionogels extend this principle by minimizing water uptake from the outset. Because ion transport occurs predominantly through ionic liquids and polar polymer segments, freezing of the external aqueous environment exerts little influence on conductivity or mechanics, and hydrophobic interfacial reorganization during soaking further suppresses molecular diffusion, yielding stable performance even after long-term immersion. Comparable approaches using zwitterionic amphiphiles or fluorinated comonomers also demonstrate enhanced low-temperature tolerance by confining water within restricted domains that resist crystallization[117; 118].

At elevated temperatures, the main priority shifts toward preventing water loss and maintaining interfacial integrity. Hydrophobic elastomer encapsulation slows evaporation while preserving the compliance of the underlying hydrogel, thereby avoiding interfacial shear and crack initiation under thermal cycling[115]. This protective skin also suppresses re-swelling when devices return to humid or aqueous conditions, reducing dimensional drift and interfacial impedance. Fully hydrophobic ionogels again offer robust performance under more aggressive environments, including hot saline media, where their negligible vapor pressure and water-repellent backbone allow both adhesion and conductivity to remain stable over extended operation[116]. Similar benefits have been reported in composite hydrogels incorporating hydrophobic nanodomains or supramolecular crosslinks, which resist thermally driven dehydration while maintaining ion conduction[114; 119].

For zinc-ion batteries, these advances in temperature adaptability are particularly significant. By preventing freezing-induced cracking at low temperatures and dehydration-induced delamination at elevated temperatures, hydrophobically engineered hydrogels enable cells to retain stable ionic conduction and intimate electrode contact across wide environmental ranges. This stability translates into prolonged cycle life, improved safety margins, and reliable function in both conventional and flexible configurations, extending the applicability of zinc-ion batteries to cold climates, wearable electronics, and marine or high-temperature settings.

1.6.5 Anti-swelling and dimensional stability

While the ability of hydrogels to absorb and retain large amounts of water is fundamental to their function as electrolytes, uncontrolled swelling can be detrimental in certain applications. Excessive swelling can compromise the mechanical integrity of the hydrogel, lead to delamination from electrodes, and cause dimensional instability, which is unacceptable for

devices requiring precise form factors, such as implantable electronics[110].

To address this challenge, extensive efforts have focused on incorporating hydrophobic components into hydrogel networks, thereby regulating water uptake and suppressing undesirable swelling. Hydrophobic domains can serve as physical barriers against excessive water penetration, while also providing secondary crosslinking points that stabilize the three-dimensional network. This strategy has been demonstrated across diverse material systems, ranging from supramolecular assemblies to zwitterionic copolymers and elastomer-encapsulated hydrogels.

One effective route involves the balance between hydrophilic and hydrophobic segments, as shown in chitosan-based double-network hydrogels. By integrating butyl acrylate (BA) and hydroxyethyl methacrylate (HEMA) into acrylic acid/chitosan matrices, a hydrophobic-hydrophilic equilibrium was achieved, leading to long-term volumetric stability and even negative swelling in water. These hydrogels retained both conductivity and toughness during long-term submersion, underscoring the role of hydrophobic modulation in underwater sensing applications[117]. Zwitterionic hydrogels incorporating hydrophobic alkyl side chains, such as octadecyl methacrylate (SMA), also demonstrated controlled swelling and rehydration. The hydrophobic microdomains limited water uptake, while the sulfobetaine methacrylate (SBMA) segments preserved strong hydrophilicity and reusability. This combined effect enabled stable anti-swelling behaviour through repeated dehydration-rehydration cycles and extended immersion, supporting the development of wearable strain sensors with high sensitivity and long-term durability[114].

Beyond covalent designs, supramolecular and amphiphilic interactions have been widely adopted. Hydrophobic association zones, often mediated by surfactants or host-guest chemistry like cyclodextrins, generate dynamic but stable crosslinking that resists volumetric expansion while maintaining ionic transport. For example, supramolecule-crosslinked hydrogels with embedded cyclodextrin cavities not only suppressed swelling but also homogenized ion flux in Zn anodes, thereby enhancing electrochemical stability[120]. Likewise, amphiphilic copolymers incorporating lauryl methacrylate or fluorinated chains provided water-resistant hydrogel matrices for underwater adhesion and strain sensing[118; 121; 122].

Hydrophobic encapsulation represents another powerful strategy. By coating hydrogel cores with hydrophobic elastomer shells such as silicone or fluoropolymer-based layers, interfacial water uptake can be minimized, dramatically reducing swelling and dehydration. Such

encapsulated systems achieve long-term dimensional stability and preserve mechanical compliance in aqueous or humid conditions[115; 119]. Combinations of hydrophobic engineering with other functionalities, such as antifreeze agents, zwitterions, or bioinspired catechol groups, further expand the design space. For instance, dual-functional anti-freezing/anti-swelling hydrogels exploit both hydrophobic modification and hydrogen-bond reinforcement, yielding sensors operable in cold and underwater environments[116; 122].

These studies underscore the central role of hydrophobic design in realizing swelling-resistant hydrogels. By precisely tuning the type, content, and distribution of hydrophobic moieties, researchers can achieve a delicate balance between water stability, ion conduction, and mechanical robustness, paving the way for hydrogel electrolytes and sensors with broad applicability in extreme environments.

Chapter 2: Design and Characterization of Electrolytes with Hydrophobic Spacers for Controlled Ion Transport

2.1 Introduction

Zinc metal anodes exhibit intrinsically low reactivity toward non-flammable aqueous electrolytes, compatibility with low-cost cathode materials, and a comparatively high resistance to persistent parasitic reactions[123]. Rechargeable aqueous zinc-ion batteries show considerable potential for large-scale energy-storage applications because of their low materials cost, inherent safety, established biocompatibility, and environmentally benign characteristics[124]. The overall performance of rechargeable aqueous zinc-ion batteries is largely dictated by interfacial phenomena at the electrode-electrolyte boundary, where zinc ions (Zn^{2+})migrate, undergo solvation and desolvation, and participate in reversible redox processes[125] [126]. Although the high ionic conductivity of water-based electrolytes supports operation at high current densities and enables rapid charge-discharge capability, it can also increase the likelihood of soft short circuits and other localized failure modes[127]. In addition, parasitic reactions such as hydrogen evolution and surface corrosion degrade the reversibility of the zinc anode, leading to unstable coulombic efficiency and limited areal capacity during extended cycling[128]. Because electrolytes governs ion transport, modulates the interfacial environment, and steers the operative reaction pathways, targeted electrolyte optimization is therefore critical for enhancing reversibility and stabilizing the electrode-electrolyte interface in rechargeable aqueous zinc-ion batteries.

Various electrolyte regulation strategies have been developed, including the deliberate incorporation of functional additives[129], systematic adjustment of the salt type [130] and concentration[131], and the use of structured hydrogel electrolytes. Hydrogel electrolytes, typically prepared from vinyl monomers such as acrylamide[132-134] or acrylic acid[135; 136], have been widely explored because they combine ionic transport with a mechanically compliant medium. Polyzwitterionic hydrogels have attracted growing attention owing to their dense population of oppositely charged groups along the polymer backbone, their strong capacity for electrostatic hydration, and their ability to modulate the transport behavior of zinc ions (Zn^{2+}) through tailored ion-polymer interactions. Hydrogels formed by physical or chemical cross-linking present a three-dimensional polymer network capable of absorbing and retaining substantial amounts of water while maintaining structural integrity[137], thereby offering a

tunable platform for electrolyte design. These materials have shown considerable promise in guiding zinc deposition morphology, suppressing the hydrogen evolution reaction (HER), and imparting flexibility and self-healing characteristics that are advantageous for mechanically robust devices[138; 139]. Relative to purely aqueous electrolytes, the reduced free-water content and constrained water activity within hydrogels help to mitigate dissolution of cathode materials and to stabilize electrode interfaces during cycling. As a representative example, poly(sulfobetaine methacrylate) provides abundant hydrophilic and charged moieties that engage in strong electrostatic hydration between the side-chain charges and surrounding water molecules[140] , enabling high water retention, spatially uniform zinc-ion distribution, and an elevated zinc-ion transference number. Nevertheless, excessive hydrophilicity can exacerbate parasitic side reactions by facilitating proton activity and gas evolution pathways[141] , highlighting the need for a balanced hydrophilic-hydrophobic design. Moreover, polyzwitterionic chains can undergo intra- and interchain self-association between oppositely charged groups[142] , which perturbs the network topology and, in turn, affects mechanical and transport performance. In electrolyte environments containing dissolved salts, ionic screening of interchain electrostatic attractions diminishes zwitterionic pairings and increases the osmotic driving force for water uptake, which collectively promote chain swelling and network expansion under saline conditions[[143].

To further regulate the state of water in hydrogels and suppress undesirable side reactions, the deliberate introduction of hydrophobic components into the polymer network has gained growing attention. The incorporation of hydrophobic segments establishes well-defined hydrophilic-hydrophobic microdomains, modulates water distribution and mobility, and enhances mechanical stability by strengthening secondary cross-linking and dissipating stress[144]. Such hydrophobization strategies have repeatedly been shown to suppress excessive swelling and limit volumetric drift under aqueous operation[59; 63]. In aqueous zinc systems, a judicious balance between hydrophilic and hydrophobic domains regulates interfacial water activity, facilitates zinc-ion (Zn^{2+}) desolvation, and guides uniform, dendrite-free zinc deposition by smoothing current distribution and reducing local supersaturation[79; 145]. Accordingly, achieving an appropriate hydrophilic-hydrophobic balance in polyzwitterionic hydrogels is essential for governing the water state while preserving network integrity and mechanical robustness.

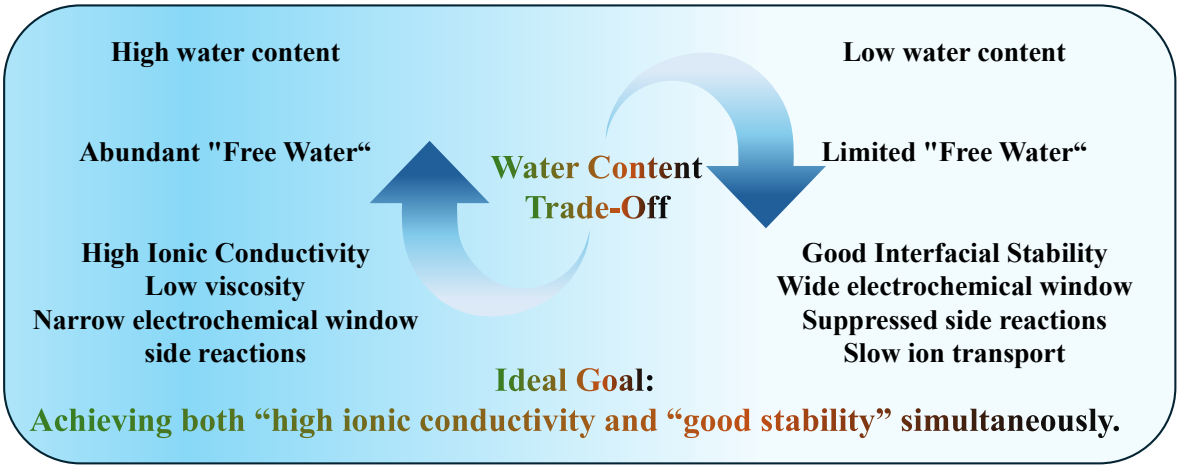

Figure 12. Managing free water for hydrogel electrolytes.

Herein, we propose a hydrophobic-spacer engineering strategy for zwitterionic hydrogel electrolytes that regulates water structure, optimizes Zn^{2+} solvation chemistry, and enhances ion transport in aqueous zinc-ion batteries. By incorporating rationally selected hydrophobic monomers into the zwitterionic polymer network, we induce controlled amphiphilicity that perturbs the water-water hydrogen-bond network, suppresses ion self-association and parasitic proton activity, and generates continuous, percolated ionic channels for Zn^{2+} migration. A coordinated suite of experimental characterizations together with fully atomistic molecular dynamics simulations confirms that the strategy restructures the Zn-centered solvation shell, accelerates Zn^{2+} diffusion, and stabilizes the electrode-electrolyte interface during cycling. As a result, the optimized zwitterionic hydrogel electrolyte based on the fluorinated methacrylate comonomer (denoted ZWHE-F) delivers markedly improved interfacial stability, effective dendrite suppression, and long-term cycling durability in Zn||Zn symmetric cells as well as zinc||sodium vanadium oxide (Zn||NaVO) full cells. Furthermore, the approach is generalizable, as demonstrated by its effectiveness when employing additional hydrophobic monomers with distinct chemical structures and steric profiles. Collectively, this hydrophobic-spacer design provides a versatile framework for next-generation hydrogel electrolytes featuring tailored water confinement, elevated Zn^{2+} mobility, mitigated side reactions, and durable electrochemical stability.

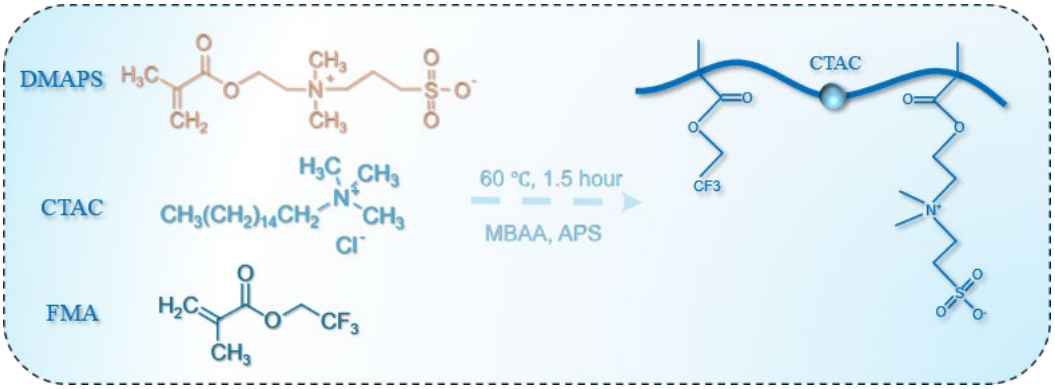

Figure 13. CTAC mediated construction of an amphiphilic copolymer chain

2.2 Experimental Methodology

2.2.1 Chemicals and materials

[2-(Methacryloyloxy)ethyl]N, Nethyl-(3-sulfopropyl)ammonium hydroxide (DMAPS, 279.35 g/mol, CAS: 3637-26-1), 2,2,2-Trifluoroethyl methacrylate (FMA ,184.11 g/mol, CAS: 352-87-4), CTAC (25 wt% aqueous solution), zinc sulfate heptahydrate ($ZnSO_4 \cdot 7H_2O$), crosslinker N,N′-methylenebisacrylamide (MBAA), initiator ammonium persulfate (APS), vanadium pentoxide (V_2O_5, 98%), and deionized (DI) water were used. All reagents purchased from Sigma-Aldrich and used without further purification.

2.2.2 Hydrogel electrolytes synthesis

A. Preparation of DMAPS-FMA Hydrogel

A CTAC/ Zn^{2+} micellar solution was first prepared by dissolving CTAC (1.28 g of a 25 wt% aqueous stock, 0.32 g CTAC, 1.0 mmol) and $ZnSO_4 \cdot 7H_2O$ (1.4378 g, 5.00 mmol) in deionized water and adjusting the total volume to 5.0 mL. The mixture stirred at room temperature until homogeneous. DMAPS (2.2348 g, 8.00 mmol, 1.60 M in the final prepolymer mixture) then added and stirred until fully dissolved. FMA (0.3362 g, 2.00 mmol, 0.40 M) introduced and the solution stirred for 10 min to promote solubilization within the CTAC micellar cores. MBAA (5 mg, 0.032 mmol, 6.5 mM) added and mixed thoroughly, followed by APS (15 mg, 0.0657 mmol, 13.1 mM) with vigorous stirring for 30 s. The precursor cast into a sealed mold and thermally polymerized at 65 °C for 2 h. The as-prepared hydrogel removed and equilibrated in

2 M $ZnSO_4$ prior to electrochemical testing.

B. Variant Hydrogels

DMAPS-isobornyl acrylate (DMAPS-IBA) and DMAPS-ethylene glycol phenyl ether acrylate (DMAPS-EGPEA) hydrogels were prepared identically by replacing FMA with IBA or EGPEA at the same molar amount (2.00 mmol in 5 mL). A DMAPS-only hydrogel obtained by omitting the hydrophobic comonomer. FMA-only and IBA-only hydrogels were prepared by substituting DMAPS with the corresponding hydrophobic monomer under otherwise identical conditions.

2.2.3 Preparation of electrodes

A. Synthesis of NaVO powders

Sodium vanadate (NaVO) powders are synthesized via a solution route. Commercial V_2O_5 powder (3.0 g) dispersed in 100 mL of 2 M NaCl aqueous solution and magnetically stirred at 400 rpm for 72 h at room temperature. The resulting orange colour precipitates collected by centrifugation, washed sequentially with deionized water and ethanol five times, and dried at 80 °C for 10 h to obtain NaVO powders.

B. Fabrication of NaVO cathodes

Cathode slurries were prepared by thoroughly blending NaVO powder, Super P carbon (conductive additive), and poly (vinylidene fluoride) (PVDF) in a mass ratio of 8:1:1, followed by grinding. N-methyl-2-pyrrolidone (NMP) then added to form a homogeneous slurry under stirring. The slurry blade-coated onto carbon cloth (CC) and titanium (Ti) foil substrates and dried in a vacuum oven at 70 °C for 10 h to yield the NaVO electrodes.

C. Fabrication of activated carbon (AC) electrodes

Activated carbon electrodes were prepared following the same procedure as the NaVO cathodes, except that NaVO powder replaced with activated carbon. Specifically, activated carbon (AC), Super P carbon, and poly (vinylidene fluoride) (PVDF) were mixed in a mass ratio of 8:1:1, thoroughly blended and ground, and then dispersed with N-methyl-2-pyrrolidone (NMP) to form homogeneous slurry under stirring. The slurry blade-coated onto carbon cloth (CC) and titanium (Ti) foil substrates and dried in a vacuum oven at 60 °C for 10 h to obtain the AC electrodes.

2.2.4 Hydrogel electrolytes Characterization

Fourier-transform infrared spectroscopy (FTIR) in attenuated total reflectance mode (Nicolet 6700 ATR-FTIR) used to analyze characteristic functional groups in the hydrogel electrolytes. Thermogravimetric analysis (TGA, TA Instruments Q5000) was employed to evaluate thermal properties and water content, while decomposition products formed on the zinc surface identified by X-ray diffraction (XRD, Rigaku SmartLab SE). Differential scanning calorimetry (DSC, TA Instruments Discovery SDT 650) conducted to determine phase-transition behaviors. NMR spectra were recorded at 303 K on a Bruker AVIII 500 MHz NMR spectrometer. For ^7Li DOSY measurements, a 16-step linearly incremented gradient array was used. The observation interval between gradient pulses was 2 s, the gradient pulse length was 0.8 ms, and the acquisition time was 3 s. The gradient pulse duration was set to δ = 400 μs.

X-ray diffraction (XRD) patterns of zinc indexed to the (002), (100), and (101) reflections, in agreement with the JCPDS reference card No. 87-0713. Preferred orientation quantified by the relative texture coefficient (RTC), defined for a reflection (hkl) as:

$$RTC_{(hkl)} = \frac{I_{(hkl)}/I_{0(hkl)}}{\sum\left(I_{(hkl)}/I_{0(hkl)}\right)} \times 100\% \quad (1)$$

where $I_{(hkl)}$ is the background-corrected integrated intensity of the sample, and $I_{0(hkl)}$ is the corresponding intensity from the JCPDS card. By definition, $RTC_{(hkl)} = 100\%$, values exceeding 33.3% indicate preferred orientation along the plane[146; 147].

2.2.5 MD calculation details

The molecular simulations were done in Gromacs 2023[148] using the OPLS-AA/L force field[149]. A cubic simulation box containing an aqueous 2.0 M $ZnSO_4$ solution and 25 polymer chains constructed to model the hydrogel system. After energy minimization, the system was equilibrated in the NPT ensemble at 298 K and 1 atm for 5 ns using the V-rescale thermostat[150] (temperature-coupling constant τ_t = 2.0 ps) and the Parrinello-Rahman barostat[151] (pressure-coupling constant τ_p = 5.0 ps). Long-range electrostatics were treated with the Particle-Mesh Ewald method[152] real-space cut-offs for both electrostatic and van der Waals interactions were 1.0 nm.

Subsequently, 15 ns production runs conducted in the NVT ensemble at 298 K with the V-

rescale thermostat (τ_t = 2.0 ps). Trajectories saved every 0.2 ps and used to compute the mean-squared displacement (MSD), radial distribution functions (RDFs), and coordination numbers (CNs).

Initial polymer-chain structures were pre-optimized with xtb 6.7.0[153] using the **GFN2** method[154]. RESP charges were obtained from single-point quantum-chemical calculations with ORCA 6.0.1[155] and subsequent fitting in Multiwfn 3.8[156; 157]. Electrostatic potentials were evaluated at the RIJCOSX[158]/B3LYP[159]/def2-SVP[160] level of theory.

2.2.6 Electrochemical measurement

A. Ionic conductivity

The ionic conductivity, σ (reported in mS cm^{-1}), measured by electrochemical impedance spectroscopy (EIS) over 0.1 Hz-10 kHz. A hydrogel electrolyte specimen sandwiched between two stainless-steel (SS) blocking electrodes. The bulk resistance R_b obtained from the high-frequency intercept of the Nyquist plot, and σ calculated as:

$$\sigma = \frac{L}{R_b \times A} \times 10^3 \tag{2}$$

where L (cm) is the electrolyte thickness, A (cm^2) is the electrode-electrolyte contact area, and $R_b(\Omega)$ is the bulk resistance. The factor 10^3 converts S cm^{-1} to mS cm^{-1}.

B. Zinc-ion transference number

The Zn^{2+} transference number was determined by the Evans method using symmetric Zn||hydrogel||Zn cells under a small DC polarization ΔV. The value of t_+ obtained from:

$$t_{Zn^{2+}} = \frac{I_s(\Delta V - I_0 R_0)}{I_0(\Delta V - I_s R_s)} \tag{3}$$

Where I_0 and I_s are the initial and steady-state currents, respectively, and R_0 and R_s are the interfacial resistances extracted from EIS before and after polarization. ΔV (20 mV) is the constant polarization potential.

C. Other electrochemical measurements

Electrochemical impedance spectroscopy (EIS), linear sweep voltammetry (LSV), cyclic voltammetry (CV), and galvanostatic charge-discharge (GCD) tests performed on an

electrochemical workstation. For LSV, titanium (Ti) foil served as the working electrode, while a zinc (Zn) plate functions as both the counter and quasi-reference electrode. GCD measurements conducted using a LAND battery testing system. Symmetric Zn||Zn cells assembled to evaluate the electrochemical stability of the hydrogel electrolytes, in which two identical bare Zn disks (10 mm in diameter) used as the positive and negative electrodes. All measurements conducted under ambient conditions unless otherwise specified.

2.3 Water-state in hydrogel electrolytes

To analyze the water state in the hydrogel electrolytes, the ZWHEF and ZWHE hydrogel electrolytes were characterized by Raman spectroscopy, Fourier-transform infrared (FTIR) spectroscopy, low-field nuclear magnetic resonance (LFNMR), differential scanning calorimetry (DSC), and thermogravimetric analysis (TGA).

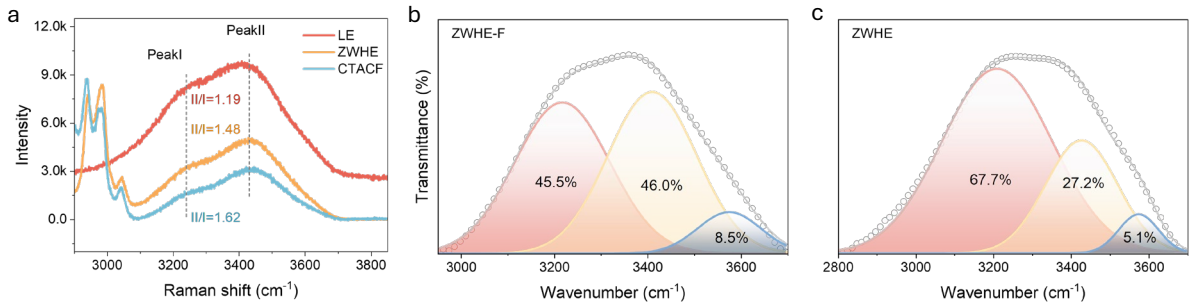

Figure 14. Water-state modulation in zwitterionic hydrogel electrolytes: **(a)** Raman O-H stretching and FTIR deconvolution **(b)** ZWHE-F and **(c)** ZWHE.

The hydration structure first examined by Raman spectroscopy in the O-H stretching region (3000-3800 cm^{-1}) (Fig. 14a). The band centered at ~3225 cm^{-1} is assigned to the symmetric O-H stretching of strongly hydrogen-bonded water in tetrahedral coordination (double donor-double acceptor, DDAA-OH), whereas the band at ~3420 cm^{-1}corresponds to the asymmetric O-H stretching of weakly hydrogen-bonded water in an incomplete tetrahedral environment (single donor-single acceptor, DA-OH)[161]. Quantification employed the intensity ratio III/II (weak/strong H-bond), obtained by integrating the ~3420 cm^{-1}band and dividing by the integrated intensity of the ~3225 cm^{-1}band. The resulting values, 1.19, 1.48, and 1.62 for LE, ZWHE, and ZWHEF, respectively indicate progressive disruption of the bulk water-water hydrogen-bond network and its reorganization into water-ion and water-polymer interactions,

consistent with a larger fraction of confined or coordinated water molecules that display reduced chemical activity and a diminished propensity for side reactions. Relative to ZWHE, hydrogels incorporating hydrophobic FMA comonomers exhibited more pronounced water-polymer interactions, in line with the larger weak/strong H-bond ratio observed for ZWHEF.

To further resolve hydrogen-bond states, FTIR spectra in the O-H stretching region were deconvoluted into strongly and weakly hydrogen-bonded components after baseline correction using a multi-peak Gaussian fitting protocol (Fig. 14b,c)[162]. For ZWHE (Fig. 14b), the area fractions corresponding to strongly hydrogen-bonded ("ice-like"), intermediate/partially hydrogen-bonded, and weakly hydrogen-bonded or "free" water are 45.5%, 46.0%, and 8.5%, respectively. For ZWHEF (Fig. 14c), the corresponding fractions are 67.7%, 27.2%, and 5.1%. The introduction of hydrophobic segments redistributes water within the polymer network and disrupts portions of the extended tetrahedral hydrogen-bonding framework. The weakly bonded water thereby coordinates more dynamically with ions and polar groups, suppressing ice-like ordering, decreasing effective water activity, and imparting enhanced electrochemical stability together with improved antifreeze behavior in the hydrogel electrolyte. Compared with ZWHE, ZWHEF displays an increased proportion of strong hydrogen-bonded water and a reduced proportion of weakly bonded/free water, evidencing stronger water confinement and more pronounced water-polymer/ion coordination.

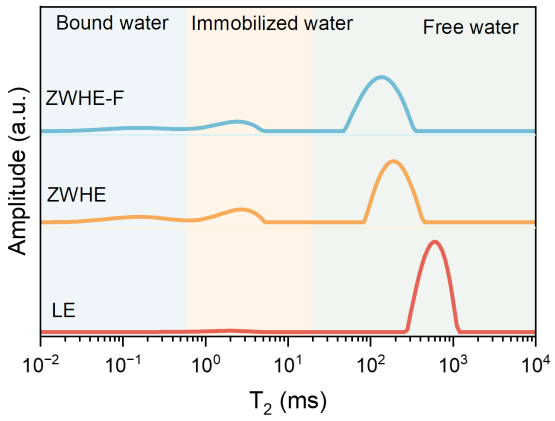

Figure 15. LF-NMR T_2 relaxation distributions reveal water-state partitioning (bound/immobilized/free) in LE, ZWHE, and ZWHE-F hydrogel electrolytes.

Low-field nuclear magnetic resonance (LF-NMR) analysis (Fig. 15) provides complementary, dynamics-sensitive evidence. Transverse relaxation (T_2) distributions obtained from inverse-Laplace transformation of Carr-Purcell-Meiboom-Gill decays resolve two well-separated components: a short-T_2 population (<10 ms) attributed to bound/confined water experiencing

restricted rotational and translational motion, and a long-T_2 population (>50 ms) assigned to bulk-like, mobile water in relatively open environments[163]. The short-T_2 peak reflects water molecules subject to strong spatial confinement within polymer/ionic microdomains and frequent dipolar interactions with nearby nuclei, whereas the long-T_2 peak arises from water with weaker motional constraints and longer rotational correlation times characteristic of free or loosely associated water. In the ZWHE-F electrolyte, the short-T_2 component shifts to lower relaxation times and its relative integral (area fraction) increases markedly, accompanied by a pronounced diminution of the long-T_2 contribution. This spectral evolution signifies that a larger fraction of water resides in confined environments and participates in localized interactions with polymer functional groups and coordinated ions. Concomitantly, the pool of bulk-like mobile water reduced. The further decrease of T_2 for the bound-water peak indicates slower molecular reorientation and enhanced confinement within the polymer/ionic microenvironment, behavior consistent with water engaged in weaker, more localized hydrogen bonds compared with the extended, cooperative tetrahedral water-water network[164]. Collectively, the T_2 profiles corroborate that hydrophobic-spacer engineering promotes water sequestration into constrained domains while suppressing the bulk-like water reservoir.

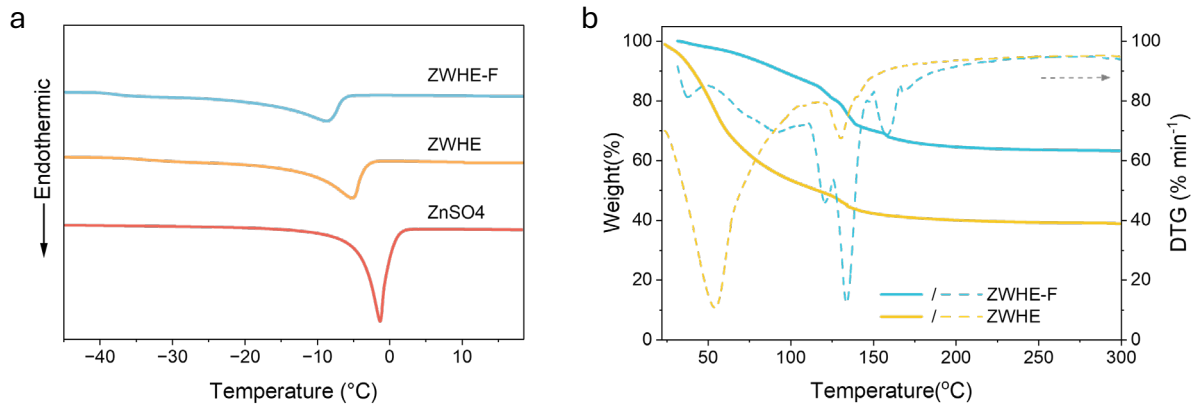

Figure 16. (a) DSC and **(b)** TGA evidence for a significant reduction of free/freezable water in ZWHE-F relative to ZWHE hydrogel electrolytes.

Differential scanning calorimetry (DSC) and thermogravimetric analysis (TGA) provide complementary confirmation of the hydrophobic-spacer-induced modulation of water states. In the DSC heating/cooling traces (Fig. 16a), the endothermic absorption associated with ice melting and the corresponding crystallization exotherm shifted to lower temperatures for ZWHE-F relative to both the aqueous liquid electrolyte and the zwitterionic hydrogel without the fluorinated comonomer. These downward shifts are most consistently interpreted as colligative/confinement effects that reduce the fraction of free/freezable water and weaken

cooperative water-water interactions within the gel matrix, rather than as a direct kinetic suppression of ice nucleation or growth. Concomitantly, the integrated melting enthalpy (ΔH) decreases, indicating a smaller inventory of freezable water and, by implication, an increased proportion of bound or immobilized water confined by polymer and ionic microdomains. TGA profiles (Fig. 16b) further corroborate this picture: the initial mass-loss stage around 150 °C, commonly attributed to the evaporation of free and loosely bound water, diminished in ZWHE-F compared with ZWHE, evidencing a lower reservoir of labile water. At higher temperatures, the comparatively attenuated mass-loss rate prior to the onset of polymer degradation is consistent with stronger water-polymer/ion associations and a reduced volatility of confined water, in agreement with the DSC-inferred decrease in free/freezable water content.

Incorporation of hydrophobic segments into the zwitterionic network perturbs the extended tetrahedral water-water hydrogen-bond framework, converting a significant portion of strongly bonded, cooperative water into a weaker hydrogen-bonded population confined within polar microdomains. The concomitant reduction in freezable/loosely bound water that evidenced by depressed freezing/melting transitions and lower initial TGA mass loss, correlates with decreased effective water activity and underpins the enhanced electrochemical stability and low-temperature tolerance of the hydrophobic-modified hydrogel electrolyte.

2.4 Molecular dynamics and spectroscopic insights into Zn^{2+} solvation and transport

To gain molecular-level insight into the structural origins of the spectroscopic and thermal trends above, we conducted molecular dynamics (MD) simulations together with complementary spectroscopy (Figs. 17-23).

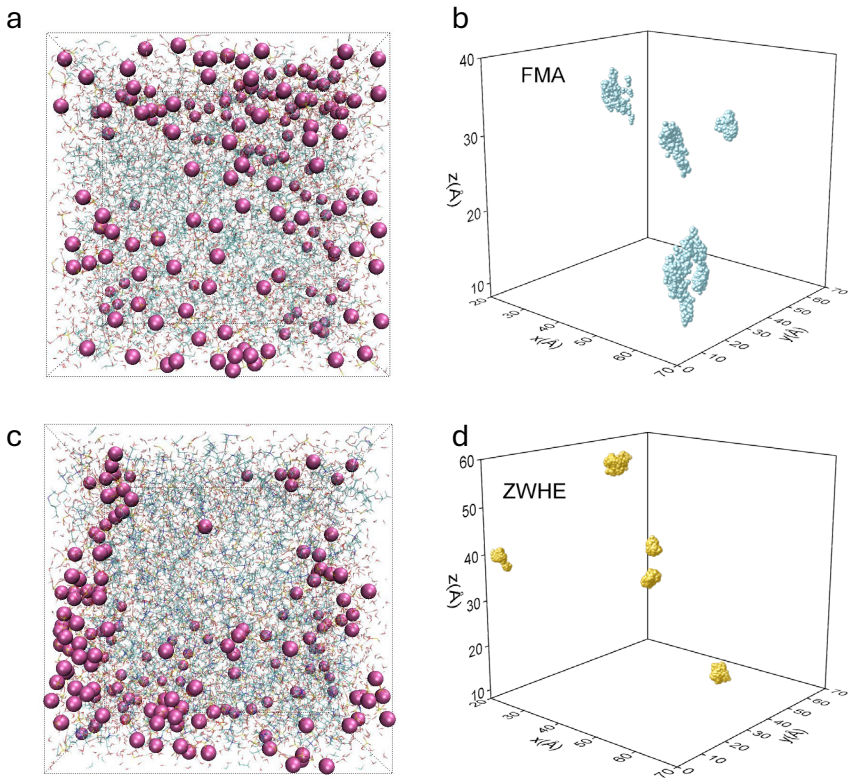

Figure 17. Molecular-dynamics snapshots and Zn^{2+} cluster-size distributions in **(a, b)** ZWHE-F vs **(c, d)** ZWHE

In the equilibrated MD snapshots (Fig. 17a, c), Zn^{2+} ions (red spheres) in the ZWHE-F matrix more uniformly dispersed throughout the zwitterionic network and display greater spatial freedom, whereas in ZWHE they preferentially localize within denser ionic regions and form mesoscale aggregates. Cluster analysis of Zn^{2+} coordinates (Fig. 17b, d) quantitatively corroborates these observations: the introduction of hydrophobic segments weakens strong zwitterion-zwitterion correlations and promotes a percolated amphiphilic morphology that offers continuous migration pathways, thereby inhibiting Zn^{2+} aggregation within the polymeric network[61; 165].

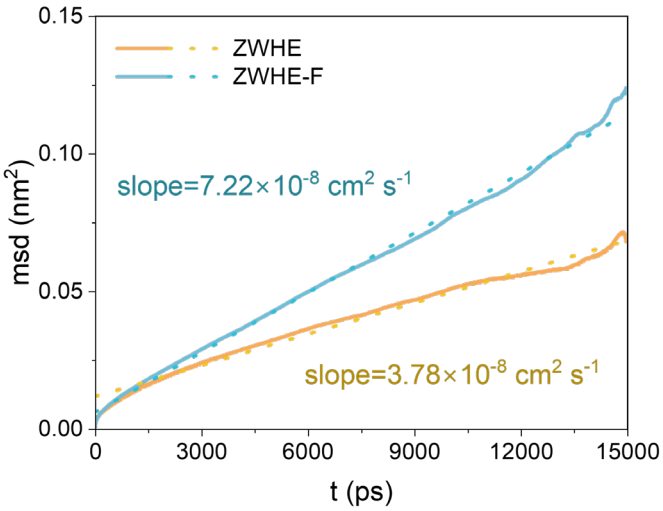

Figure 18. Mean-square displacement of Zn^{2+} in ZWHE and ZWHE-F

The dynamical consequence of this morphological change was captured by the mean-squared displacement (MSD) of Zn^{2+} (Fig. 18). In the diffusive regime, the MSD increases linearly with time and the slope is appreciably steeper for ZWHE-F than for ZWHE, evidencing faster Zn^{2+} motion in the hydrophobically modified network. This enhanced mobility is consistent with reduced trapping within ion-rich clusters and with the formation of more continuous ionic channels.

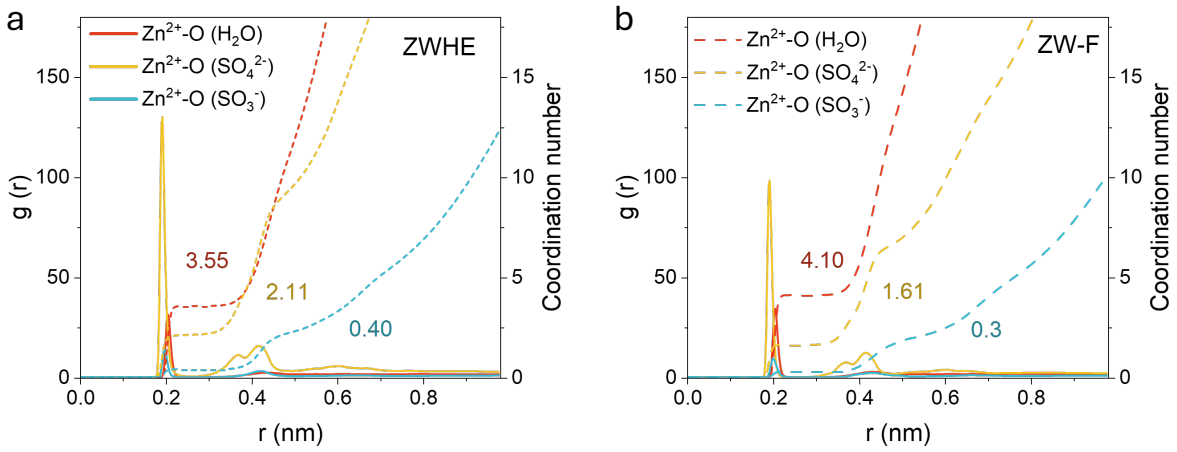

Figure 19. Radial distribution functions and first-shell coordination numbers for Zn-O (H_2O), Zn-O(SO_4^{2-}), and Zn-O (SO_3^-/polymer) in **(a)** ZWHE and **(b)** ZWHE-F.

Consistently, radial distribution functions g(r) and the corresponding coordination numbers around Zn^{2+} (Fig. 19) reveal a reconfigured first-shell solvation. Integration of the primary peaks to the first minima shows a decrease in Zn-O (H_2O) coordination together with an increase in Zn-O (SO_4^{2-}) and Zn-O (SO_3^-/polymer) contacts for ZWHE-F relative to ZWHE, indicating partial replacement of bulk-like hydration by anion-/polymer-coordinated species

within the gel microenvironment. This shift in local coordination is consistent with the spectroscopic signatures of strengthened water-ion/polymer interactions and diminished "free" water.

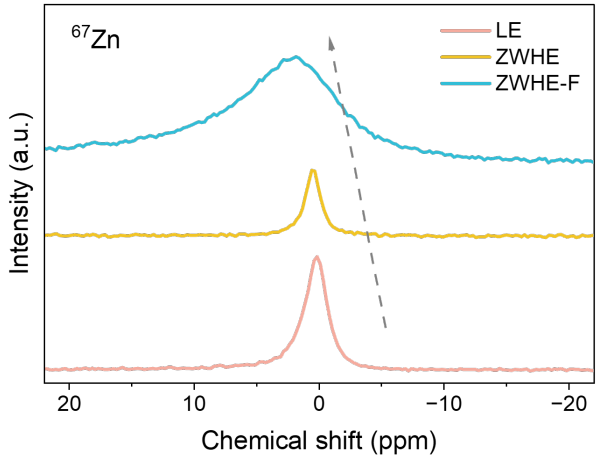

Figure 20. ^{67}Zn NMR spectra of ZWHE and ZWHE-F hydrogel electrolytes.

Direct experimental evidence for this solvation restructuring provided by ^{67}Zn NMR spectroscopy (Fig. 20). Relative to ZWHE, ZWHE-F exhibits a downfield (positive) chemical-shift displacement accompanied by line broadening, features consistent with reduced electronic shielding at the zinc center and a broader distribution of coordination environments caused by partial substitution of water ligands with anion and polymer donors. The broadened profile further suggests slower exchange and a wider spread of Zn^{2+} microstates within the amphiphilic network.

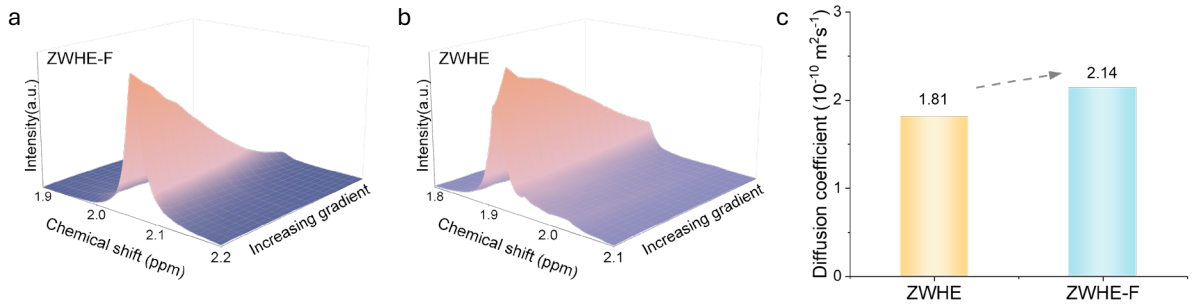

Figure 21. DOSY NMR of Zn-containing species: **(a)** ZWHE-F, **(b)** ZWHE, **(c)** comparison of the apparent diffusion coefficients D extracted from the DOSY fits.

Diffusion-ordered NMR spectroscopy (DOSY) then used to quantify the apparent diffusion coefficient of Zn-containing species (Fig. 21). The gradient-dependent signal attenuation surfaces yield larger extracted diffusion coefficients for ZWHE-F than for ZWHE, in

agreement with the MD-derived MSD trends and supporting the conclusion that hydrophobic-spacer engineering enhances the mobility of Zn-bearing species in the gel phase.

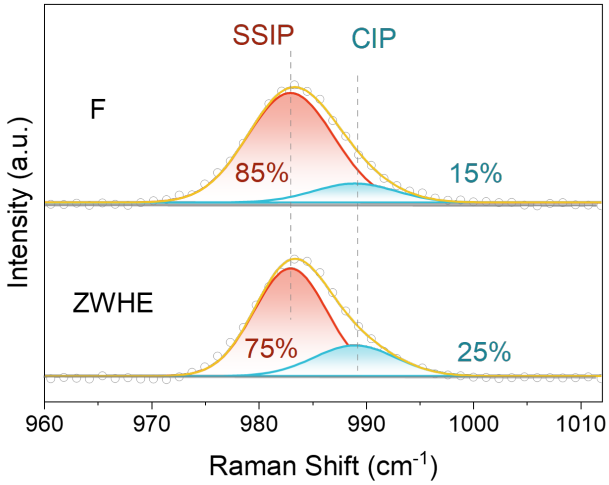

Figure 22. Raman ν(S-O) spectra with deconvolution into ion-pair species (SSIP, CIP) for ZWHE and ZWHE-F.

Raman spectroscopy of the ν(S-O) region (Fig. 22) was deconvoluted to resolve ion-pair speciation. ZWHE-F displays an increased fraction of solvent-separated ion pairs (SSIP) and a decreased fraction of contact ion pairs (CIP) relative to ZWHE, indicating that the amphiphilic microenvironment favors partially dissociated states with intervening solvent/polymer mediation rather than direct anion-cation contact. This speciation shift is consistent with the observed enhancement in Zn^{2+} mobility and with the reduced propensity for ion-cluster formation.

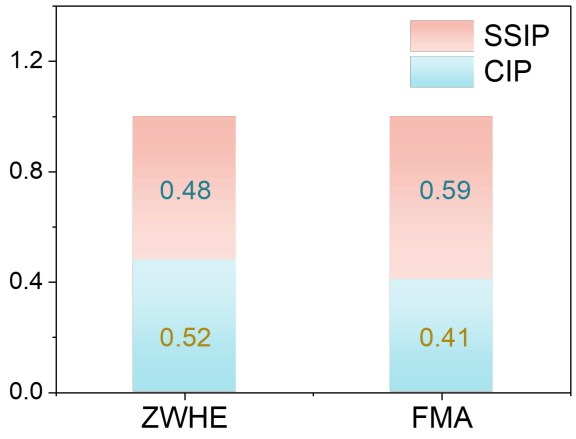

Figure 23. Molecular-dynamics ion-pair statistics in ZWHE and ZWHE-F.

Finally, MD-based ion-pair population statistics (Fig. 23) corroborate the spectroscopic analysis: hydrophobic-induced microphase separation spatially separates cationic and anionic sites, elevates the SSIP population, and suppresses CIP formation.

Hydrophobic-spacer engineering induces amphiphilic microphase separation that weakens zwitterion self-association and creates continuous ionic pathways, shifting Zn^{2+} solvation from water-dominated to polymer/anion-assisted, suppressing ion clustering, and thereby increasing effective Zn^{2+} mobility and stabilizing interfaces in ZWHE-F. By disrupting zwitterionic self-association and establishing continuous ionic channels, the hydrophobic segments keep Zn^{2+} more uniformly dispersed and mobile, thereby laying the molecular-level foundation for the improved transport characteristics observed for ZWHE-F.

2.5 Basic properties of the electrolyte

To evaluate the influence of hydrophobic segments on electrochemical transport, linear sweep voltammetry (LSV, 2 mV s^{-1}) was employed.

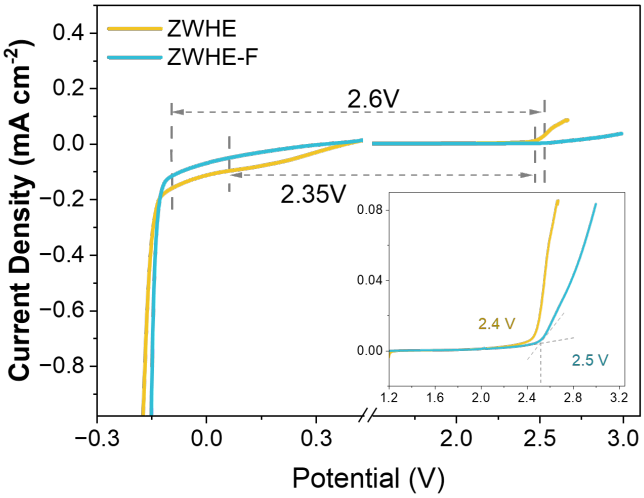

Figure 24. Linear sweep voltammetry (LSV, 2 mV s^{-1}) for ZWHE-F and ZWHE.

Figure 24 displays the LSV curves of ZWHE-F and ZWHE recorded under identical conditions. The onset potentials at the cathodic and anodic ends define the practical electrochemical stability window, which is ≈ 2.6 V for ZWHE-F and ≈ 2.35 V for ZWHE. The wider window for ZWHE-F is consistent with fewer parasitic currents near both limits. The traces also highlight the low-current baseline region used to identify the potential thresholds.

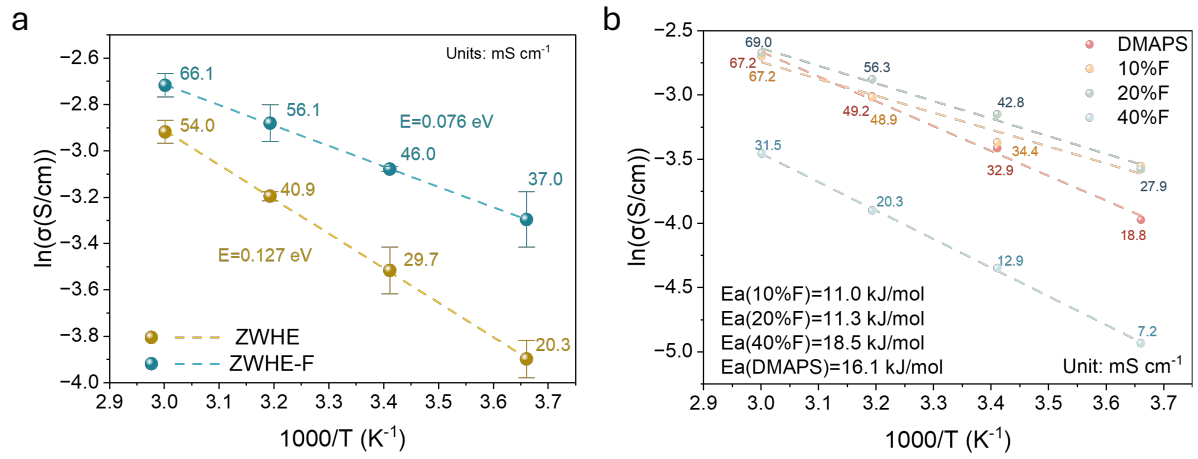

Figure 25. Temperature-dependent ionic conductivity and Arrhenius analysis. **(a)** ZWHE-F and ZWHE: σ vs temperature with activation energies from linear fits. **(b)** Formulation screening: Arrhenius plots for a series of ZWHE-F different ratios used to identify the optimal composition.

Temperature-dependent ionic conductivity measurements further compare bulk transport. In Figure 25a, σ(T) for ZWHE-F (the optimized hydrophobic formulation) and ZWHE (control) plotted over the same temperature range. ZWHE-F exhibits higher conductivity at all temperatures and a weaker temperature dependence. Linear fits of ln σ versus 1/T (Arrhenius analysis) yield a lower activation energy for ZWHE-F, indicating a reduced migration barrier and suggesting more continuous conduction pathways. Figure 25b documents the ratio-selection process for the hydrophobic comonomer: conductivity (and corresponding Arrhenius fits) shown for a series of ZWHE-F formulations with different monomer ratios, from which the optimal composition used in panel (a) selected.

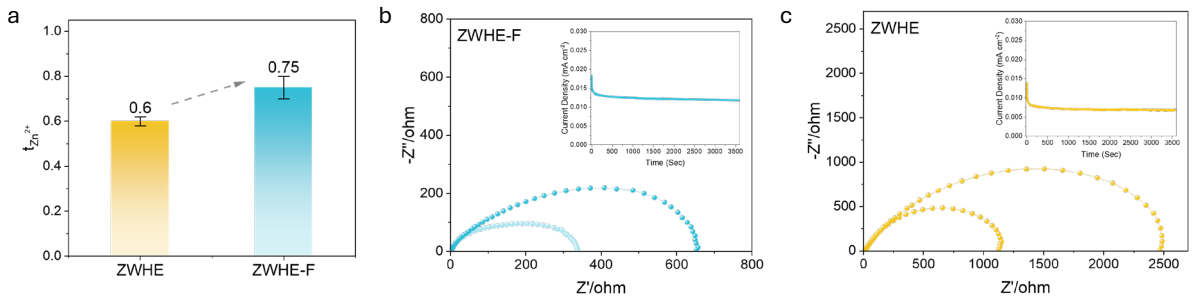

Figure 26. Determination of Zn^{2+} transference number: **(a)** t_{Zn}^{2+} for ZWHE and ZWHE-F measured in symmetric Zn||hydrogel||Zn cells under a 20-mV polarization, **(b)** EIS of the cell before polarization ($R0$), **(c)** EIS of the same cell after reaching steady state (Rs).

The zinc-ion transference number was quantified using the Evans method in symmetric Zn||hydrogel||Zn cells under a small DC polarization (ΔV = 20 mV), with the initial/steady-

state currents taken from the polarization trace and the interfacial resistances obtained from EIS immediately before and after polarization. Figure 26a compiles the resulting t_{Zn}^{2+} values as a bar chart showing an increase from 0.60 for ZWHE to 0.75 for ZWHE-F at the test temperature. A higher t_{Zn}^{2+} indicates that a larger fraction of the total ionic current carried by Zn^{2+} rather than anions, which alleviates concentration polarization during galvanostatic operation, mitigates anion accumulation/depletion near electrodes, and facilitates more uniform interfacial transport. The enhancement in t_{Zn}^{2+} for ZWHE-F is consistent with strengthened anion/polymer interactions and the formation of continuous cation-conduction pathways inferred from MD, RDF/CN analysis, and spectroscopic speciation.

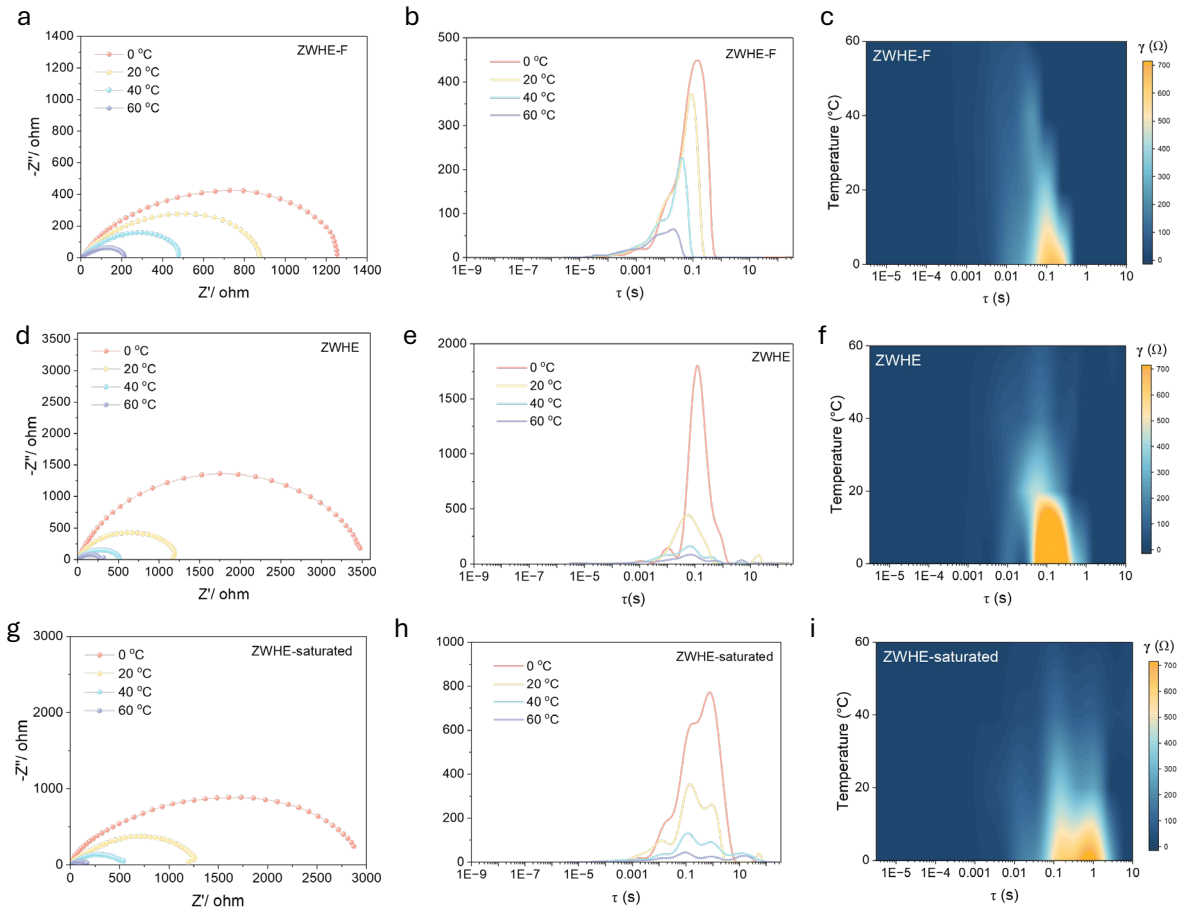

Figure 27. Temperature-dependent interfacial spectroscopy: Nyquist plots, 1D DRT spectra, and 2D DRT intensity maps vs temperature for ZWHE-F, ZWHE, and ZWHE-saturated measured in identical symmetric cells.

To probe interfacial behavior over temperature, Figure 27 compiles temperature-dependent EIS with distribution of relaxation times (DRT) analysis for ZWHE-F, ZWHE, and a ZWHE-saturated condition, all in identical symmetric configurations. For ZWHE-F, the Nyquist plots show a single, compact depressed semicircle whose diameter changes modestly with

temperature. The corresponding 1D-DRT spectra displays a narrow, well-defined peak that shifts regularly to higher frequency on heating, and the 2D-DRT map remains sharply localized across the temperature range. By contrast, ZWHE develops a broadened interfacial response: the semicircle enlarges and becomes more depressed, a second low-frequency feature emerges (visible as a shoulder/tail in Nyquist and as a broad, low-frequency peak in the DRT), and the 2D-DRT intensity spreads toward lower frequencies with increasing temperature. The ZWHE-saturated case accentuates this behavior, exhibiting the widest relaxation distribution and the most pronounced low-frequency contribution. These differences are consistent with passivation-related processes and parasitic reactions such as interphase growth and slow diffusion/charge-transfer through a non-conductive surface layer in ZWHE and particularly in ZWHE-saturated, whereas ZWHE-F—containing hydrophobic segments—retains a more stable, conductive interface with a single dominant kinetic process.

Mechanistically, the clearer, temperature-regular DRT signature of ZWHE-F aligns with its lower free-water content, reconfigured Zn^{2+} solvation, and wider electrochemical window reported elsewhere: reduced interfacial water activity and polymer/anion-assisted solvation lower desolvation/charge-transfer barriers and curb side-reaction pathways. In ZWHE, higher water activity facilitates film formation and gas/parasite channels that manifest as additional, temperature-amplified low-frequency relaxations. ZWHE-saturated amplifies these trends due to excess free water.

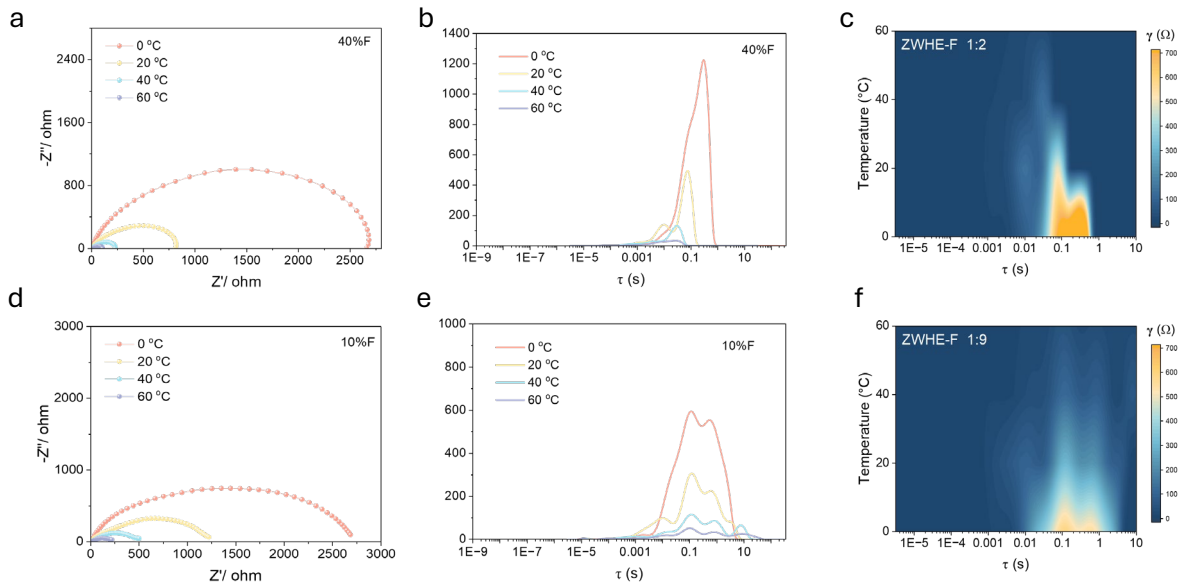

Figure 28. Formulation dependence of interfacial response: temperature-dependent Nyquist plots, 1D DRT spectra, and 2D DRT maps for ZWHE-F at ratios **(a, b, c)** 1:2 and **(d, e, f)** 1:9.

Relative to the zwitterionic baseline (ZWHE) in Fig. 27, the low-hydrophobic formulation in Fig. 28 shows Nyquist and DRT signatures that closely resemble ZWHE: a larger, more depressed semicircle with a developing low-frequency shoulder and a broadened DRT that spreads toward lower frequencies at elevated temperature features consistent with passivation-related processes and diffusion-coupled polarization. By contrast, the higher-hydrophobic formulation (ZWHE-F 1:2) exhibits a single, compact semicircle with minimal low-frequency tailing and a narrow, temperature-regular DRT peak, indicating one prevailing interfacial kinetic process and a cleaner interface with fewer side reactions. These interfacial trends align with the σ(T) results in Fig. 25b: enrichment in hydrophobic comonomer raises ionic conductivity and lowers the apparent activation energy (more continuous ion-conduction pathways), whereas at low hydrophobic content the conductivity and temperature dependence approach the ZWHE baseline. Mechanistically, increasing the hydrophobic fraction reduces interfacial water activity and zwitterion self-association, promotes polymer/anion-assisted Zn^{2+} transfer, and attenuates slow parasitic processes that manifest as broad, low-frequency relaxations.

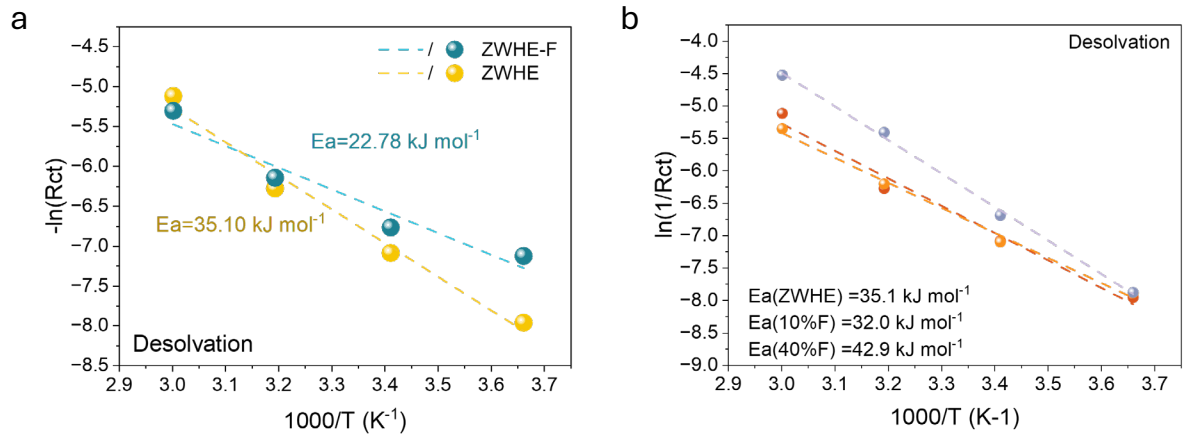

Figure 29. Arrhenius analysis of charge-transfer resistance Rct: **(a)** ZWHE vs ZWHE-F (1:4), **(b)** ZWHE-F formulations 1:2, 1:4, and 1:9. Dashed lines are linear fits, activation energies are extracted from the slopes.

Temperature-dependent EIS with DRT analysis (Fig. 29) reveals distinct interfacial behaviors for the two electrolytes: ZWHE develops a broadened response with an emergent low-frequency contribution at elevated temperatures, characteristic of passivation-related processes, whereas ZWHE-F retains a single, sharply defined relaxation whose positions shift regularly with temperature, indicative of a more stable and conductive interface. Quantifying the temperature dependence of the interfacial process, Arrhenius fits of $\ln R_{ct}$ versus 1/T (Fig. 29) yield a lower apparent desolvation/charge-transfer activation energy for ZWHE-F (22.78 kJ

mol⁻¹) than for ZWHE (35.10 kJ mol⁻¹), consistent with easier ligand exchange at the zinc/electrolyte boundary. Compositionally, the formulation study (Figs. 25b, 28, 29b) shows that increasing the hydrophobic fraction narrows the DRT feature and reduces both R_{ct} and its activation barrier while simultaneously raising ionic conductivity and weakening its temperature dependence. The 1:4 ZWHE-F formulation combines the highest conductivity with the lowest interfacial barrier, reflecting a hydrophobic-spacer-induced reconfiguration of the Zn^{2+} solvation shell and reduced interfacial water activity. These macroscopic transport characteristics accord with the molecular-level picture established earlier, in which controlled amphiphilicity weakens zwitterion self-association, maintains continuous cation-conduction pathways, and suppresses side-reaction channels.

2.6 Zn Plating/Stripping Performance Evaluation

The electrochemical performance of Zn||Zn symmetric cells with ZWHE-F and ZWHE electrolytes systematically evaluated to clarify the effect of hydrophobic segment incorporation on Zn interfacial stability.

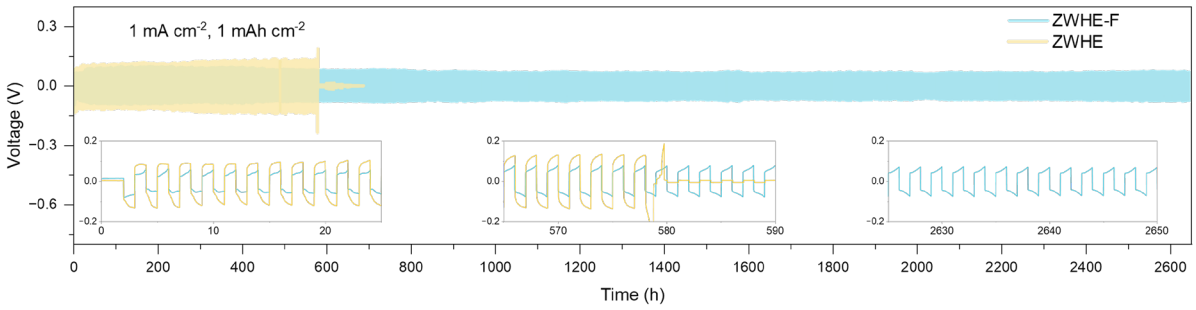

Figure 30. Long-term galvanostatic cycling curves of Zn||Zn symmetric cells at 1 mA cm^{-2} and 1 mAh cm^{-2}.

Under long-term galvanostatic cycling at 1 mA cm^{-2} and 1 mAh cm^{-2} (Fig. 30), the voltage-time curves clearly demonstrate the superior durability of ZWHE-F. The blue profile corresponding to ZWHE-F maintains a flat and stable hysteresis for more than 2500 h, reflecting highly reversible Zn plating and stripping. In contrast, the yellow curve for ZWHE undergoes rapid voltage fluctuations and short-circuits after 800 h, which is attributed to the growth and penetration of Zn dendrites. The insects further magnify specific cycling segments, showing that ZWHE-F preserves a consistent oscillation amplitude whereas ZWHE exhibits significant drift, confirming that hydrophobic modification effectively suppresses interfacial instability.

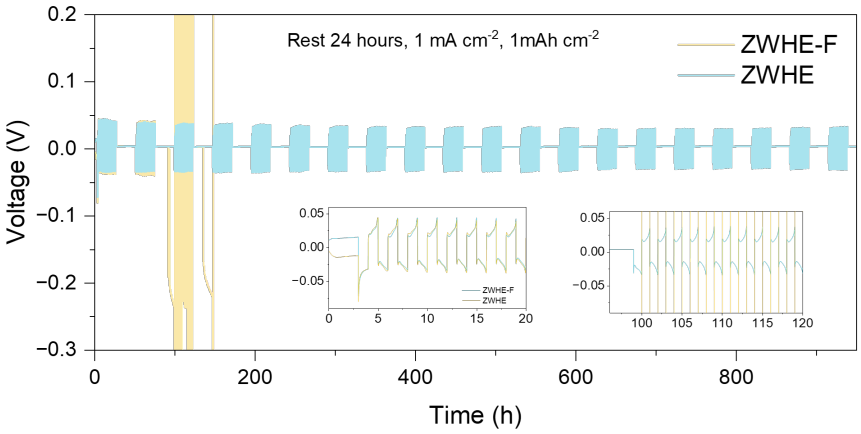

Figure 31. Rest-enabled cycling curves of Zn||Zn symmetric cells.

When rest-enabled cycling applied (Fig. 31), the distinction between the two electrolytes became even more pronounced. The ZWHE curve displays severe voltage overshoot upon restarting after the rest period, indicating uncontrolled dendrite regrowth during the idle time. Conversely, ZWHE-F resumes cycling with unchanged hysteresis, highlighting its ability to stabilize the Zn surface even in dynamic resting-cycling conditions.

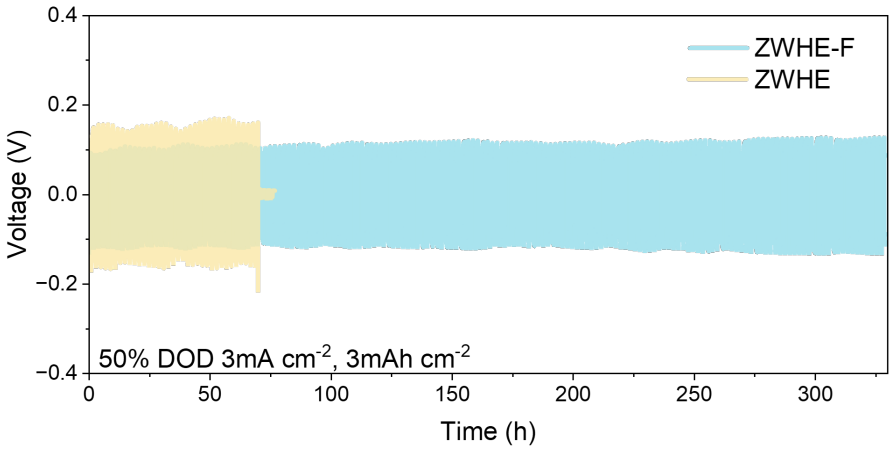

Figure 32. Galvanostatic cycling curves of Zn||Zn symmetric cells at an areal capacity of 3 mAh cm^{-2}.

At higher areal capacity of 3 mAh cm^{-2} (Fig. 32), ZWHE shows voltage polarization and irregular profiles, whereas ZWHE-F continues to deliver steady plating/stripping without obvious degradation, thereby confirming its robustness under demanding capacity conditions.

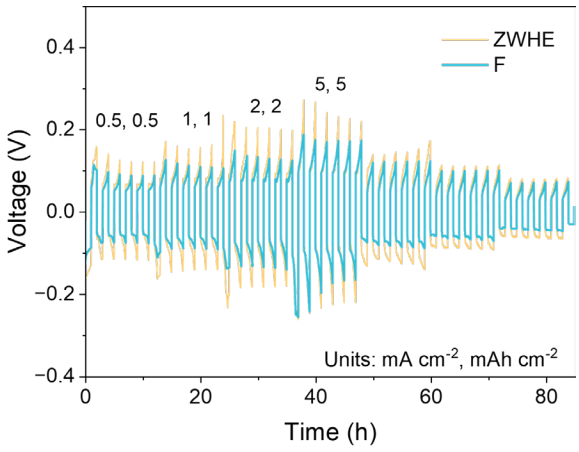

Figure 33. Rate-capability tests of Zn||Zn symmetric cells at various current densities.

Rate-capability tests (Fig. 33) provide additional insights into the kinetics of Zn deposition. As the current density increased stepwise up to 5 mA cm^{-2}, the voltage profiles of ZWHE gradually diverge and exhibit large overpotentials, suggesting sluggish kinetics and aggravated polarization at high rates. In sharp contrast, ZWHE-F maintains narrow voltage gaps across all current densities, indicating facilitated ion transport and uniform Zn nucleation even at accelerated cycling conditions.

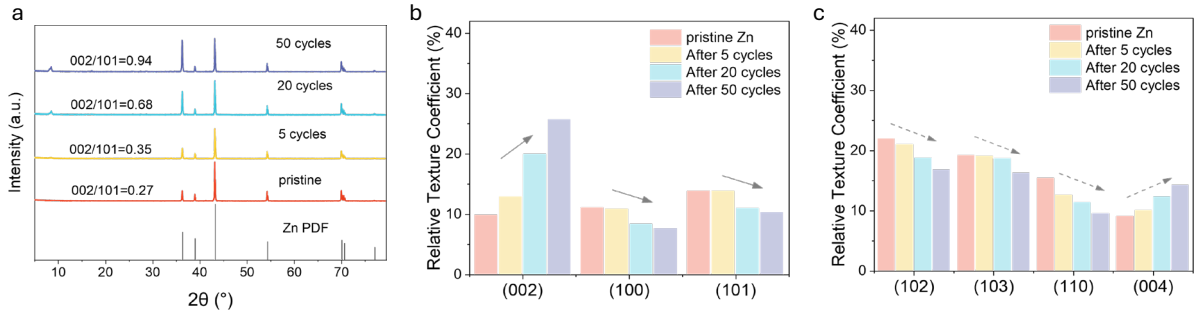

Figure 34. (a) XRD patterns of Zn deposits obtained in different electrolytes after cycling. Relative Texture coefficient (RTC) values of the **(b)** (002), (100), and (101) and (c) (102), (103), (110) and (004) planes for Zn deposits.

XRD-based texture coefficient analysis (Fig. 34) further supports these electrochemical observations. The diffraction patterns reveal that in ZWHE-F, the (002) plane retains a strong preferred orientation during cycling, favoring lateral Zn growth with densely packed basal planes. This orientation is well known to inhibit vertical dendritic protrusions. On the other hand, ZWHE loses (002) dominance and shows broader peaks with increased contributions from high-index planes, a signature of disordered nucleation and uneven vertical deposition.

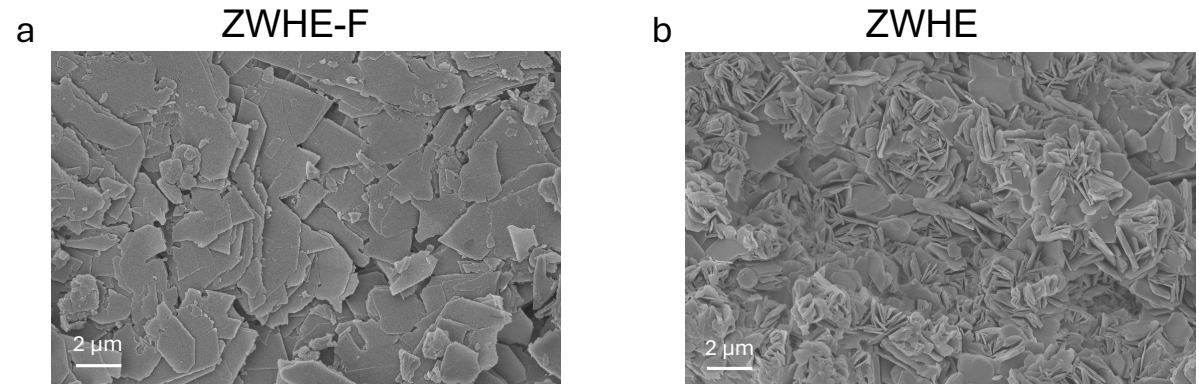

Figure 35. SEM images of Zn anode surfaces after cycling in **(a)** ZWHE-F hydrogel electrolyte and **(b)** ZWHE hydrogel electrolyte.

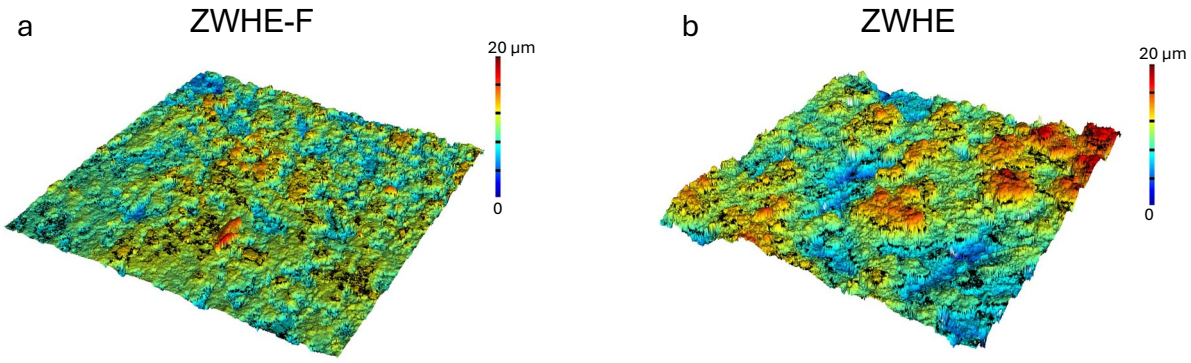

Figure 36. 3D surface profilometry of Zn anode surfaces after cycling obtained by confocal microscopy of **(a)** ZWHE-F and **(b)** ZWHE hydrogel electrolytes.

Post-cycling morphological analysis by SEM (Fig. 35) provides direct visual evidence. The ZWHE-F cycled anode surface appears smooth, compact, and layered, consistent with homogeneous lateral growth. In comparison, the ZWHE cycled surface exhibits rough, porous, and needle-like structures, confirming uncontrolled dendritic growth. Three-dimensional surface profilometry (Fig. 36) further highlights the disparity in roughness: ZWHE-F maintains a flat topology with small height variations, while ZWHE exhibits pronounced protrusions and a rugged surface morphology, in agreement with dendritic formation.

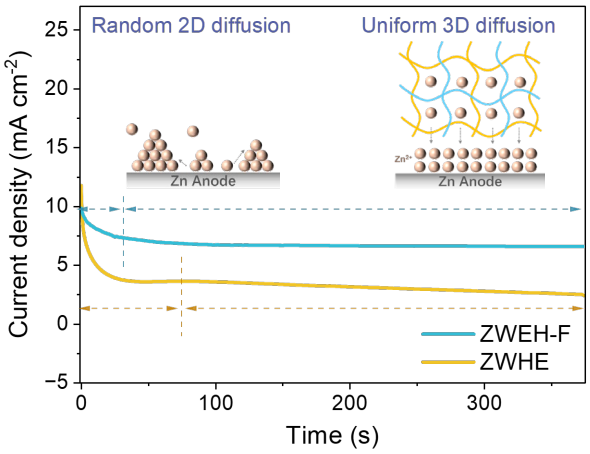

Figure 37. Chronoamperometry curves and schematic illustration of Zn deposition mechanisms in different hydrogel electrolytes.

To probe the deposition mechanism in real time, chronoamperometry (CA) performed (Fig. 37). In ZWHE, the current density first drops steeply but then undergoes a prolonged increase in absolute magnitude, indicative of an extended two-dimensional surface diffusion process, where nuclei spread across the electrode surface and promote random vertical growth. By contrast, ZWHE-F quickly reaches a steady plateau after a short transient, which corresponds to a diffusion-limited three-dimensional process. This suggests that Zn nuclei evolve into compact and laterally oriented layers rather than forming high-aspect-ratio dendrites. The schematic illustration further contrasts random 2D diffusion in ZWHE with uniform 3D diffusion in ZWHE-F, linking the hydrophobic modification to controlled nucleation pathways.

These electrochemical and structural characterizations consistently demonstrate that the incorporation of hydrophobic segments in ZWHE-F suppresses dendrite formation and stabilizes the Zn/electrolyte interface. The macroscopic enhancements in interfacial stability and cycling life originate from the tailored solvation structure and optimized ion-transport pathways introduced by hydrophobic-spacer engineering, which ensure uniform Zn^{2+} flux, regulated nucleation, and long-term dendrite-free cycling.

2.7 Electrochemical Performances

The markedly improved Zn plating/stripping reversibility, dendrite suppression, and interfacial stability achieved with ZWHE-F anticipated to translate into superior full-cell performance. To validate this, Zn||NaVO full cells assembled and systematically investigated.

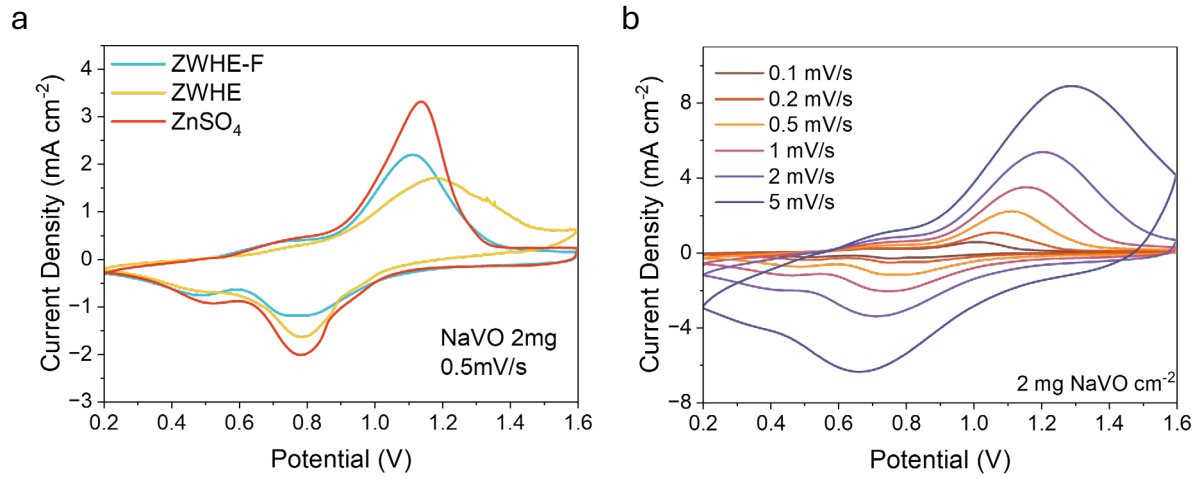

Figure 38. Electrochemical characterization of the prepared materials. **(a)** Cyclic voltammetry (CV) curves Zn||NaVO cell in ZWHE-F, ZWHE and $ZnSO_4$ electrolytes at a scan rate of 0.5mV/s. **(b)** CV curves of Zn||NaVO cell in ZWHE-F electrolyte at various scan rates.

The electrochemical redox behavior first examined by cyclic voltammetry (Fig. 38). In comparison between different electrolytes, the ZWHE-F cell exhibits clearer and more symmetric anodic and cathodic peaks, while the corresponding current response is consistently higher. When the scan rate was varied from 0.1 to 1.0 mV s^{-1}, both systems showed diffusion-controlled features, yet the peak separation remained smaller and the current growth more pronounced with ZWHE-F, evidencing faster charge-transfer kinetics.

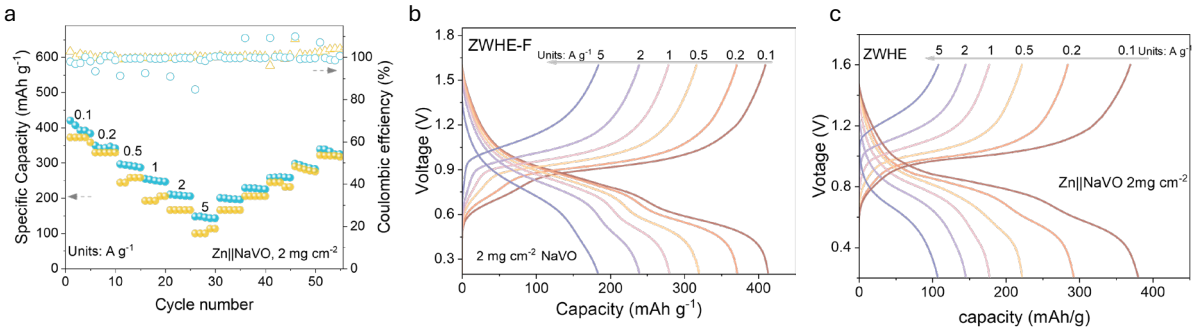

Figure 39. (a) Rate capability and corresponding Coulombic efficiency of ZWHE-F and ZWHE electrolytes at different current densities. Galvanostatic charge-discharge (GCD) profiles of **(b)** ZWHE-F and (c) ZWHE electrolytes.

The rate capability of the full cells then evaluated (Fig. 39). As the current density increased from 0.1 to 5.0 A g^{-1}, ZWHE-F maintained higher reversible capacities compared with ZWHE. The corresponding galvanostatic charge-discharge profiles reveal that in ZWHE-F distinct voltage plateaus persist even at high rates, accompanied by low polarization. In contrast, cells with ZWHE display sloping and distorted plateaus, which reflects increased internal resistance

and sluggish ion transport.

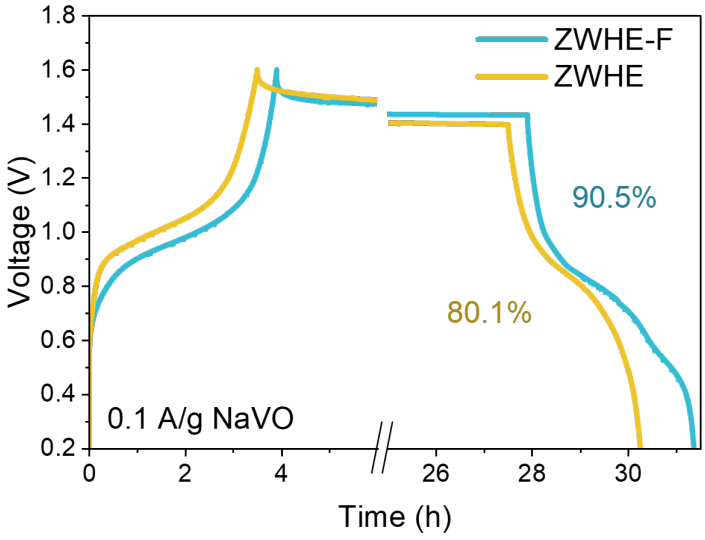

Figure 40. Comparison of self-discharge behavior between ZWHE and ZWHE-F after a 24-hour idle period at 0.1 A g^{-1}.

Self-discharge performance further assessed by introducing 24 h rest intervals at 0.1 A g^{-1} (Fig. 40). The voltage-capacity curves clearly indicate that ZWHE-F retains about 90.5% of its capacity after the rest period, whereas ZWHE falls to about 80.1%. This comparison highlights parasitic side reactions effectively suppressed in the hydrophobically modified system, enabling improved capacity retention during idle storage.

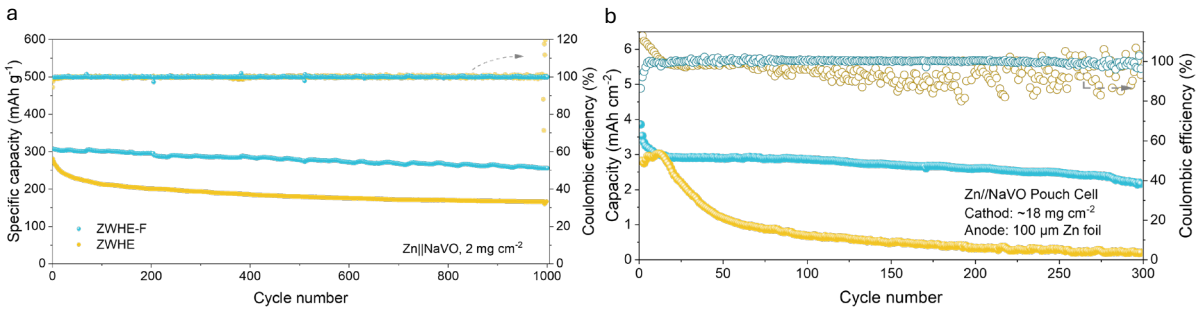

Figure 41. Comparison of the long-term cycling stability for ZWHE and ZWHE-F electrolytes in **(a)** coin cells and **(b)** pouch cells.

In the coin-cell configuration (Fig. 41a), Zn||NaVO full cells with ZWHE-F maintained highly stable discharge capacity for over 300 cycles, accompanied by Coulombic efficiencies consistently above 98%. By contrast, cells assembled with the unmodified ZWHE electrolyte exhibited progressive capacity fading, reflecting increased side reactions and interfacial instability. These results highlight the critical role of the fluorinated amphiphilic design in

stabilizing Zn deposition and ensuring efficient Zn^{2+} transport at the electrode-electrolyte interface.

To further challenge the electrolyte under more practical and demanding conditions, pouch-cell tests were performed (Fig. 41b). Despite the higher areal capacity, enlarged electrode area, and more severe dendrite-driving factors in the soft-pack configuration, ZWHE-F still sustained long-term cycling with excellent capacity retention and minimal fluctuation in Coulombic efficiency. In contrast, the ZWHE-based pouch cell underwent rapid degradation, underscoring the importance of suppressing water activity and regulating ion solvation in large-format cells.

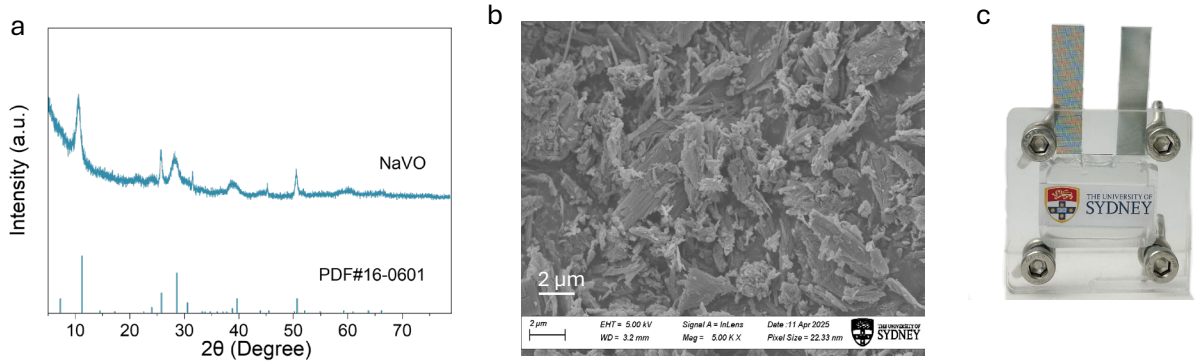

Figure 42. (a) X-ray diffraction (XRD) pattern of the as-synthesized NaVO powder compared with the standard reference pattern. **(b)** Scanning electron microscopy (SEM) image of NaVO. **(c)** A digital photograph of the pouch cell used for electrochemical measurements.

The structural properties of the NaVO cathode confirmed by XRD analysis (Fig. 42a). The diffraction peaks are sharp and well defined, matching well with the standard reference pattern, which indicates high crystallinity and phase purity of the material. SEM observations further reveal a layered and sheet-like microstructure (Fig. 42b), where the loosely stacked nanosheets create an open framework that is favorable for electrolyte infiltration and ion diffusion. Such morphology provides abundant electrochemically active sites and is expected to enhance the reaction kinetics during cycling. To validate the feasibility of practical device integration, a Zn||NaVO pouch cell assembled using the hydrogel electrolyte (Fig. 42c). The soft-pack configuration not only demonstrates scalability beyond coin-cell tests but also highlights the mechanical flexibility and compatibility of the electrolyte with realistic battery architectures.

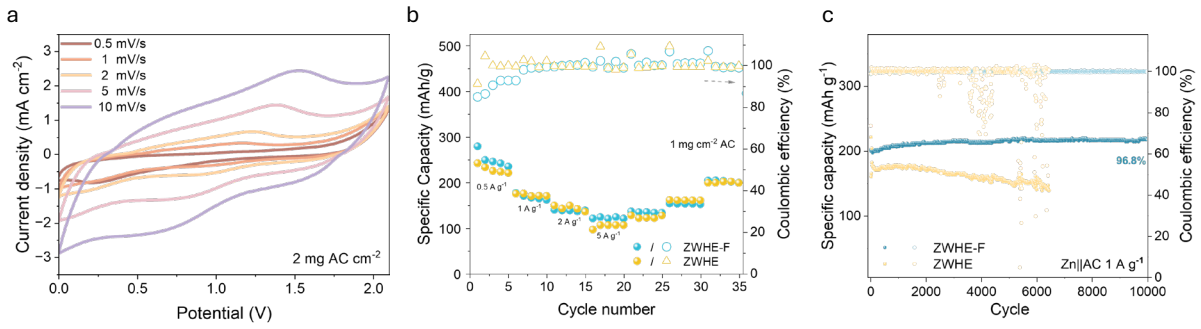

Figure 43. (a) CV curves for the AC||ZWHE-F||Zn cell at different scan rates. **(b)** Rate capability of ZWHE-F and ZWHE electrolytes at different current densities. **(c)** long-term cycling stability and coulombic efficiency of ZWHE-F and ZWHE.

Beyond Zn||NaVO batteries, the versatility of ZWHE-F tested in Zn||activated carbon (AC) hybrid capacitors (Fig. 43). The cyclic voltammetry (CV) profiles of Zn||AC cells with ZWHE-F maintain ideal rectangular shapes even at high scan rates, demonstrating fast charge-discharge kinetics and capacitive-dominated storage behavior. In comparison, the ZWHE electrolyte shows more pronounced distortion, suggesting slower ion transport and increased polarization. Figure 44b reveals that ZWHE-F-based devices achieve markedly higher energy retention over a broad power density range, thereby overcoming the typical trade-off between energy and power in aqueous hybrid systems. Long-term cycling measurements further confirm that the ZWHE-F hybrid capacitors deliver superior capacity retention and nearly 100% coulombic efficiency over extended operation, whereas ZWHE counterparts suffer from significant fading. These results highlight that the hydrophobic-modified hydrogel design enhances battery-type Zn||NaVO cells and proves effective in capacitor-type Zn||AC systems, underscoring its universality for diverse aqueous Zn-based energy storage technologies.

Collectively, the results from Figures 39-44 demonstrate that hydrophobic-spacer engineering in ZWHE-F enables a unified improvement across diverse device configurations. From symmetric Zn cells to Zn||NaVO full batteries and Zn||AC hybrid capacitors, the fluorinated amphiphilic electrolyte consistently delivers fast charge-transfer kinetics, suppressed parasitic reactions, and prolonged cycling stability. Such versatility underscores its potential as a generalizable strategy to advance aqueous Zn-based energy storage from laboratory prototypes toward practical, high-performance devices.

2.8 Mechanical and Adhesion Properties

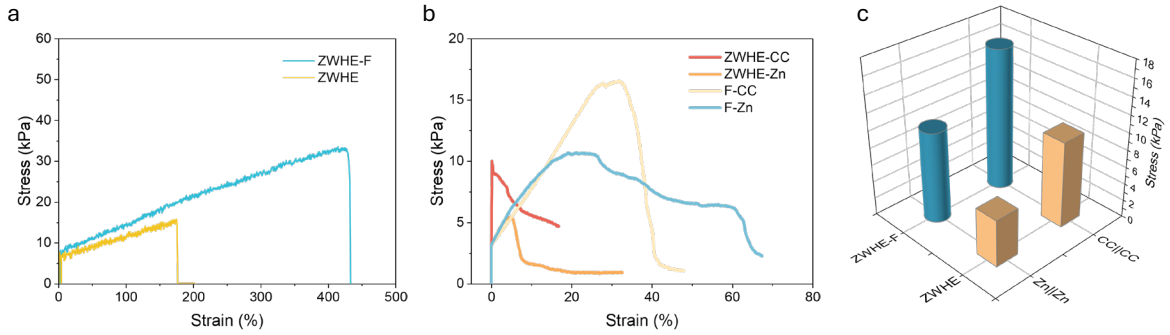

Figure 44. Mechanical and adhesion properties of hydrogel electrolytes. **(a)** Tensile stress-strain curves of different electrolytes. **(b)** Adhesion tests on carbon cloth and Zinc foil of different electrolytes. **(c)** Quantitative comparison of adhesion strength.

The mechanical and interfacial properties of the hydrogel electrolytes systematically evaluated. The tensile stress-strain curves (Fig. 44a) show that ZWHE-F possesses substantially higher tensile strength and elongation at break compared with ZWHE, indicating that hydrophobic modification reinforces the polymer network and enhances toughness. In addition to intrinsic mechanical robustness, interfacial adhesion is critical for maintaining intimate contact between the electrolyte and electrodes during long-term operation. As shown in Fig. 44b, ZWHE-F exhibits markedly stronger adhesion to both carbon cloth and Zn foil, ensuring reliable electrode-electrolyte interfaces even under external deformation or prolonged cycling. The corresponding quantitative comparison (Fig. 44c) further confirms that the adhesion strength of ZWHE-F nearly doubled relative to ZWHE. These enhancements arise from the amphiphilic design, where hydrophobic domains provide reversible physical anchoring while the hydrophilic matrix ensures conformal contact. Such a synergy not only prevents delamination but also improves ion transport at the interface, thereby coupling mechanical integrity with electrochemical stability in practical device configurations.

2.9 Exploring the generality of hydrophobic monomer engineering in tailoring ZWHE electrolyte performance.

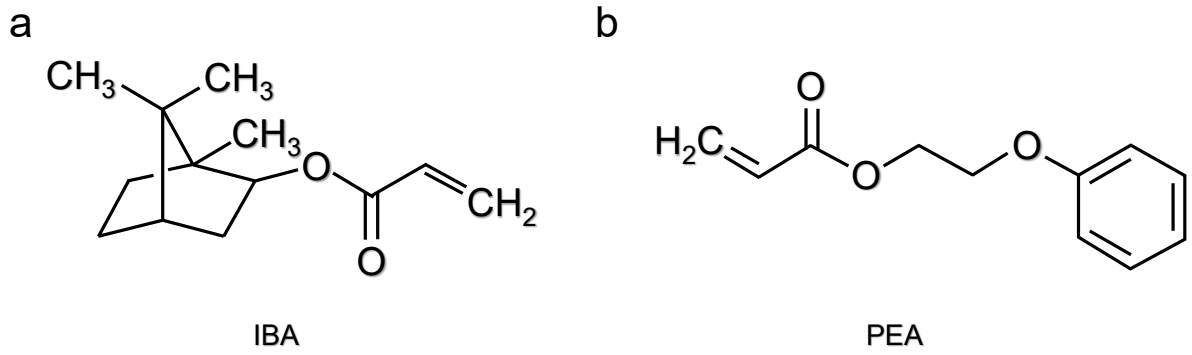

Figure 45. The molecular structures of **(a)** Isobornyl Acrylate (IBA) and **(b)** ethylene glycol phenyl ether acrylate (PEA).

To further validate the generality of the hydrophobic-spacer concept established with ZWHE-F, two additional zwitterionic hydrogel electrolytes were synthesized: ZWHE-IBA, incorporating a bulky bicyclic isobornyl acrylate (IBA) unit to impose pronounced steric hindrance, and ZWHE-PEA, containing an ethylene glycol phenyl ether acrylate (PEA) moiety with high intrinsic hydrophobicity (Fig. 45). These two structural motifs represent complementary design routes—one dominated by steric effects and the other by hydrophobicity—that enable systematic evaluation of spacer functionality in zwitterionic hydrogel electrolytes.

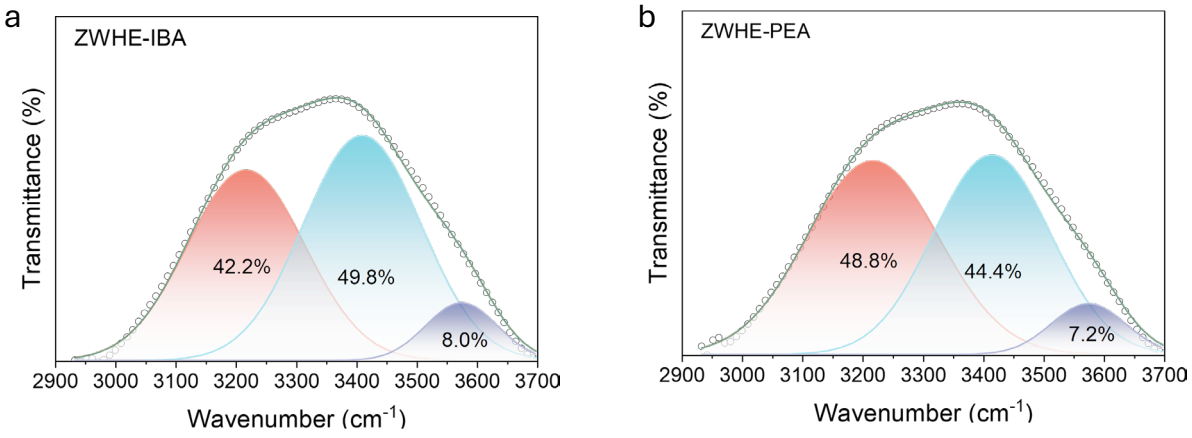

Figure 46. Water-state modulation in zwitterionic hydrogel electrolytes: FTIR deconvolution **(a)** IBA and **(b)** PEA.

Spectroscopic and thermal analyses first confirmed the impact of these spacers on the water environment. FTIR OH-stretch deconvolution revealed a redistribution of hydrogen-bonding

states, with both ZWHE-IBA and ZWHE-PEA showing increased fractions of weakly hydrogen-bonded water and reduced strongly bonded populations relative to ZWHE (Fig. 46).

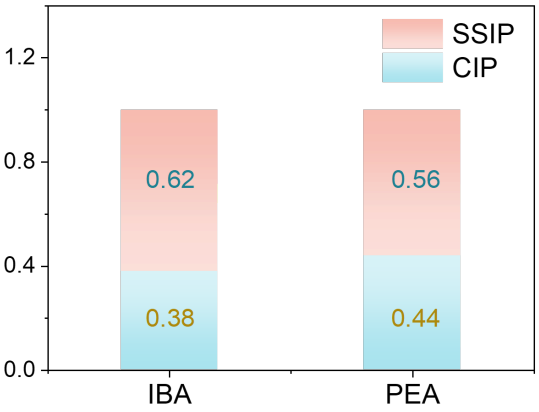

Figure 47. Molecular-dynamics ion-pair statistics in ZWHE-IBA and ZWHE-PEA.

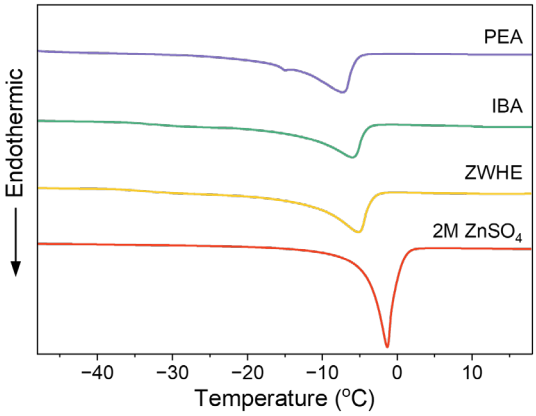

Figure 48. DSC test in ZWHE-IBA and ZWHE-PEA.

Quantitative analysis of water environments further corroborated this trend, indicating a shift toward less structured water (Fig. 47). DSC thermograms exhibited markedly suppressed freezing transitions in spacer-containing systems compared with pristine ZWHE, consistent with lower free-water activity and enhanced confinement (Fig. 48). Together, these results demonstrate that hydrophobic domains disrupt bulk-like hydrogen-bond networks and confine water into ionic/polar domains.

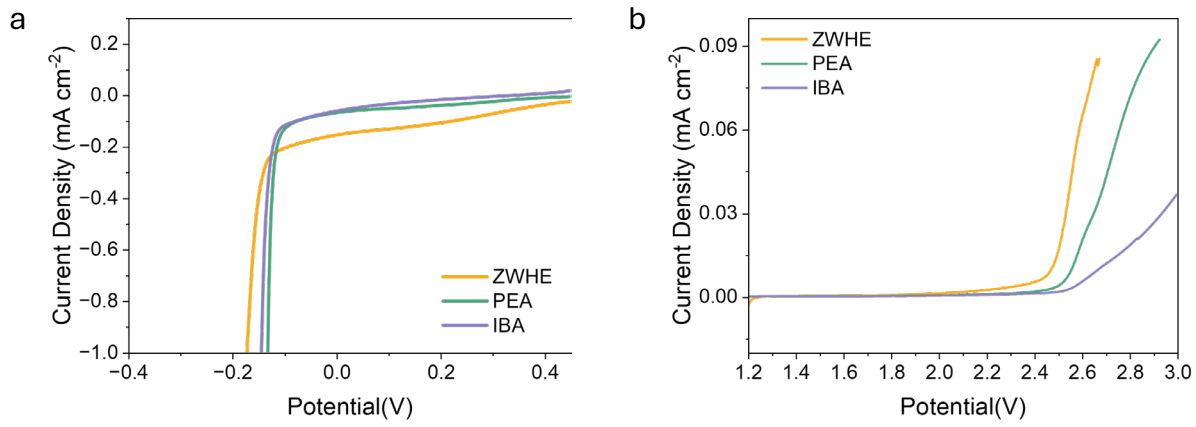

Figure 49. Linear sweep voltammetry (LSV, 2 mV s^{-1}) in different electrolytes.

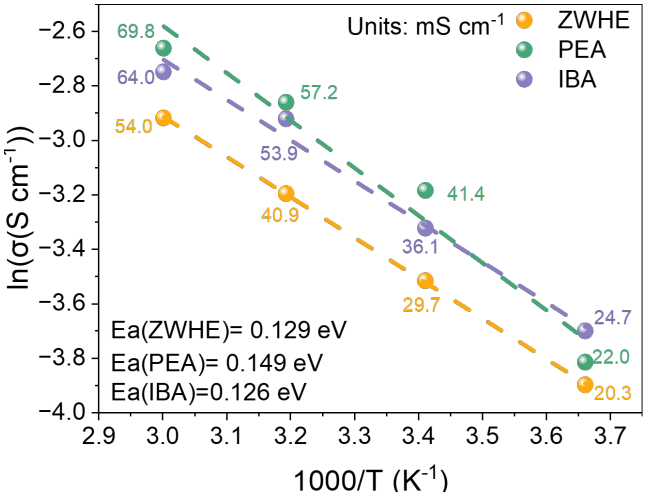

Figure 50. Ionic conductivity of ZWHE-IBA and ZWHE-PEA.

Electrochemical stability was also substantially improved. Linear sweep voltammetry showed that ZWHE-IBA and ZWHE-PEA extended the electrochemical stability window, suppressing hydrogen evolution at the cathodic side and delaying oxygen-related side reactions anodically (Fig. 49). Correspondingly, temperature-dependent conductivity analysis revealed reduced activation energies for ion conduction in the spacer-containing hydrogels (Fig. 50), evidencing facilitated Zn^{2+} migration.

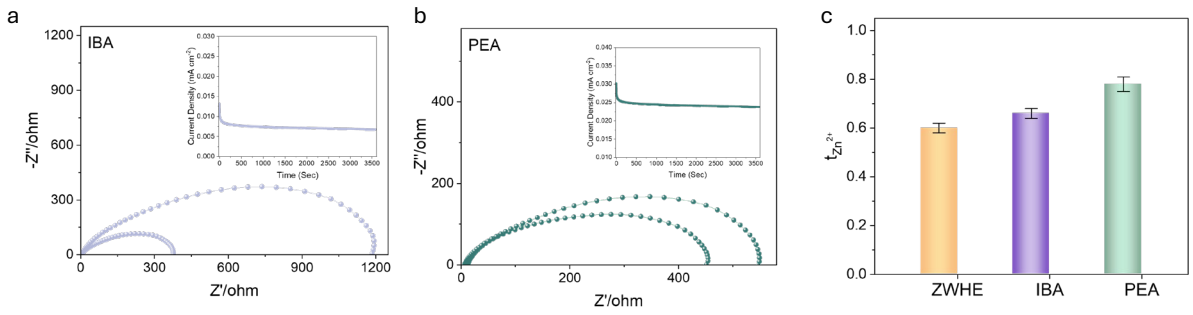

Figure 51. Zn^{2+} transference number of ZWHE-IBA and ZWHE-PEA.

The zinc-ion transference numbers of the spacer-modified hydrogels were determined using symmetric Zn||Zn cells (Figure 51). Both IBA and PEA containing electrolytes exhibit enhanced cation selectivity, with transference numbers of 0.66 and 0.78, respectively, compared with 0.60 for the pristine ZWHE. These results indicate that the incorporation of hydrophobic spacers strengthens anion–polymer interactions and promotes preferential Zn^{2+} transport, thereby mitigating concentration polarization and enabling more uniform interfacial ion flux.

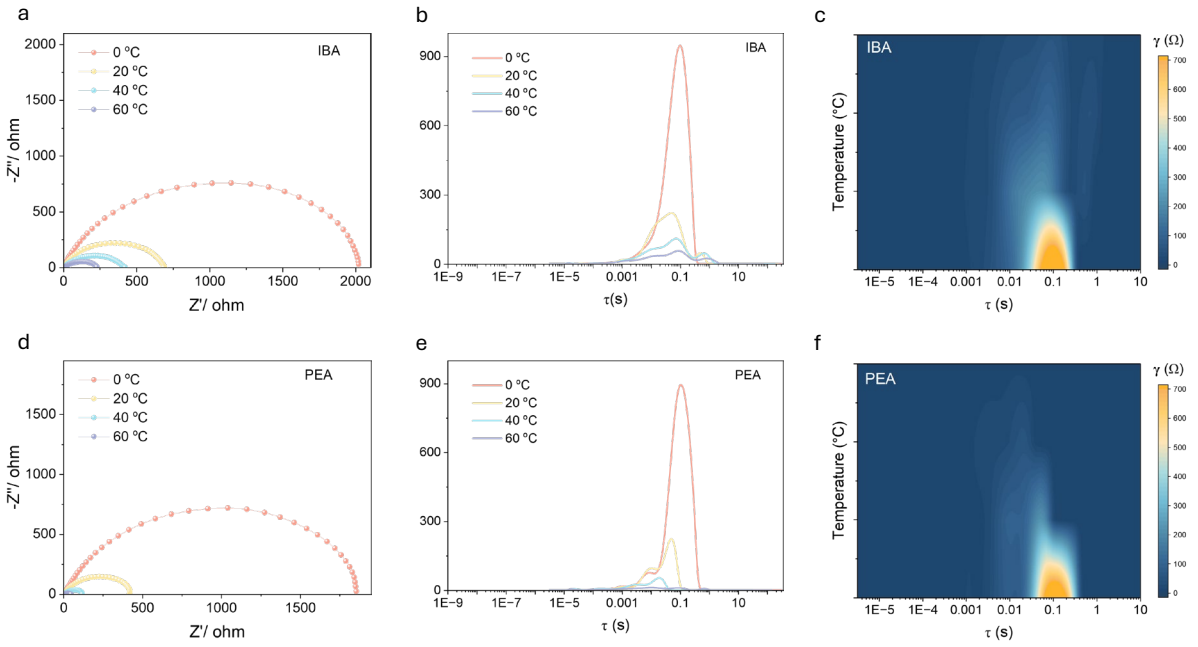

Figure 52. Temperature-dependent interfacial spectroscopy: Nyquist plots, 1D DRT spectra, and 2D DRT intensity maps vs temperature for ZWHE-IBA and ZWHE-PEA measured in identical symmetric cells.

Electrochemical impedance spectroscopy (EIS) combined with distribution of relaxation times (DRT) analysis was further employed to probe the interfacial behavior of spacer-modified hydrogels under different temperatures. As shown by the IBA- and PEA-containing systems, the Nyquist plots retain compact semicircles with minimal distortion upon heating, and the

corresponding 1D DRT spectra exhibit single, narrow peaks that shift regularly toward higher frequency. Two-dimensional DRT intensity maps further confirm that the relaxation processes remain highly localized, with negligible low-frequency contributions. This sharply contrasts with the broadened, multi-component relaxations observed in pristine zwitterionic hydrogels, indicating that hydrophobic spacers effectively suppress side-reaction pathways and stabilize the interfacial kinetics of Zn^{2+} deposition and stripping.

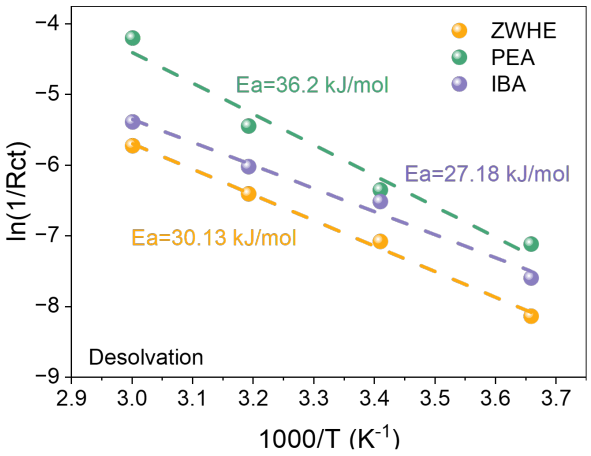

Figure 53. Arrhenius analysis of charge-transfer resistance Rct: of ZWHE-IBA and ZWHE-PEA.

The impact of these molecular modifications on interfacial energetics was quantitatively assessed through Arrhenius analysis of the charge-transfer resistance (Rct). The apparent activation energies extracted for ZWHE, ZWHE-IBA, and ZWHE-PEA were 30.1, 27.2 and 36.2 kJ mol^{-1}, respectively. While both spacer-containing systems exhibit improved interfacial stability compared with pristine ZWHE, the PEA-based electrolyte shows a relatively higher activation energy. This result suggests that the strong hydrophobicity of PEA may impose additional interfacial reorganization barriers, even though it still contributes to suppressing parasitic reactions and maintaining a clean interfacial process. Together, the impedance and activation-energy results corroborate the spectroscopic and molecular dynamics analyses, establishing that spacer engineering regulates Zn^{2+} solvation, reduces free-water activity, and tailors interfacial transport pathways.

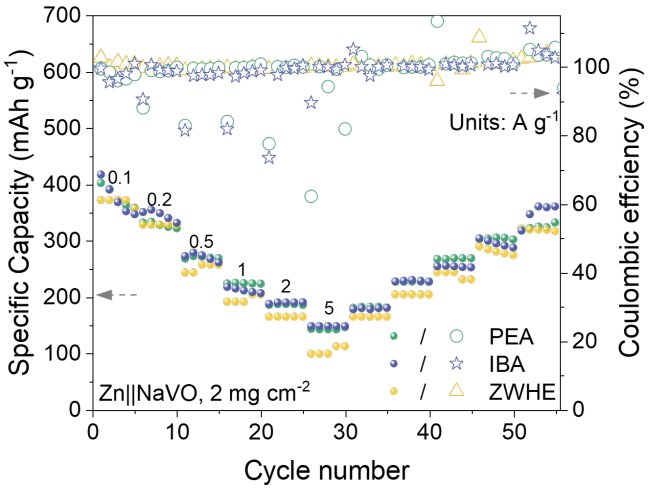

Figure 54. Rate capability and corresponding Coulombic efficiency of ZWHE-IBA and ZWHE-PEA electrolytes at different current densities.

To further evaluate the general applicability of the hydrophobic-spacer strategy, we tested the rate performance of Zn||NaVO full cells under varying current densities (Figure 54). The results clearly demonstrate that spacer-modified hydrogels enable markedly improved capacity retention compared with the pristine system. At low current densities, all electrolytes deliver comparable discharge capacities, indicating sufficient ionic conduction. However, as the current density increases, the capacity of the control cell drops sharply due to sluggish Zn^{2+} transport and aggravated polarization, while cells with IBA and PEA containing hydrogels maintain stable and reversible capacities. Notably, the PEA-modified system achieves the highest capacity retention across the full range of rates, underscoring the critical role of strong hydrophobic interactions in stabilizing ion transport pathways. These findings confirm that hydrophobic-spacer engineering not only improves symmetric-cell cycling stability but also translates into superior high-rate capability in practical full-cell configurations.

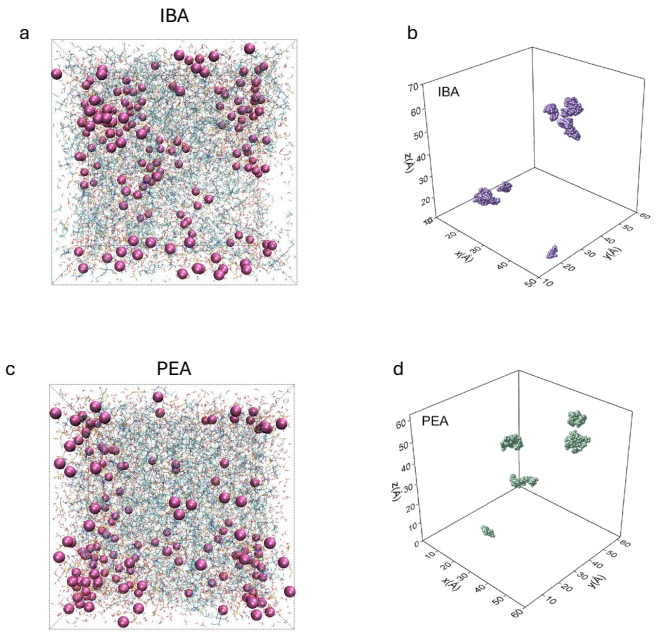

Figure 55. MD snapshots and ion trajectories maps of IBA and PEA.

Molecular dynamics (MD) simulations provided mechanistic insight at the atomistic scale. Ion-pair statistics indicated higher fractions of solvent-separated ion pairs (SSIP) and fewer contact ion pairs (CIP) for both ZWHE-IBA and ZWHE-PEA compared with ZWHE (Fig. 47), suggesting weakened Zn^{2+} anion association. Radial distribution functions (RDFs) and coordination numbers further confirmed a reorganized Zn^{2+} solvation shell, with reduced Zn-O(H_2O) coordination and increased Zn-O(sulfate/polymer) contacts (Fig. 57). This reconfiguration highlights a transition from bulk-like hydration toward a more polymer-involved solvation environment.

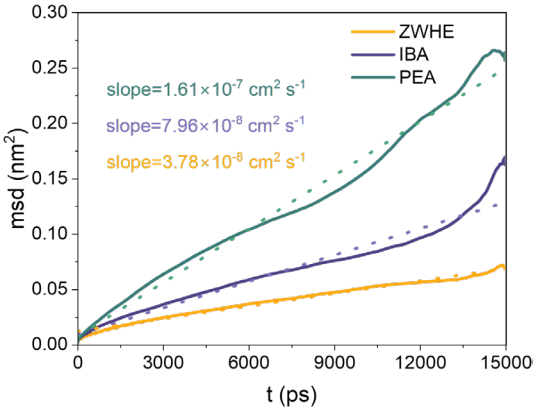

Figure 56. Mean-squared displacement of Zn^{2+} in ZWHE-IBA and ZWHE-PEA.

Dynamic transport properties were likewise improved. Arrhenius analysis of ionic conductivity

yielded lower activation energies for ZWHE-IBA and ZWHE-PEA (Fig. 50), while MD-derived mean-square displacement curves revealed significantly higher Zn^{2+} diffusivities, following the order PEA > IBA > ZWHE (Fig. 56).

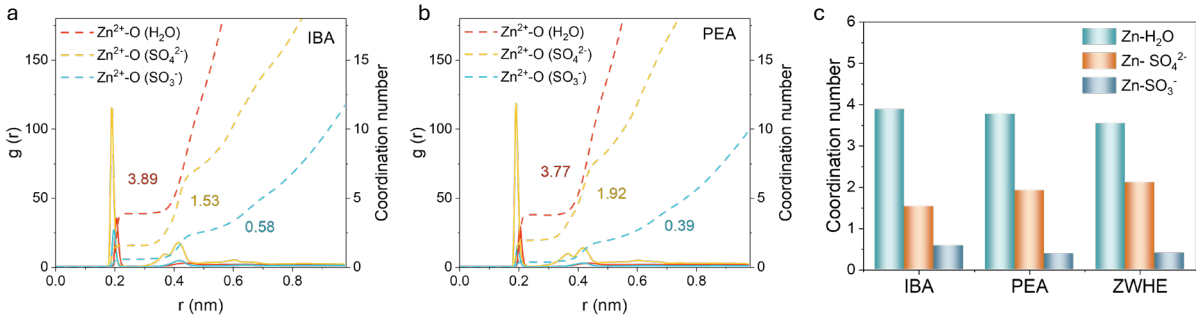

Figure 57. Radial distribution functions and first-shell coordination numbers for Zn-O(H_2O), Zn-O(SO_4^{2-}), and Zn-O(SO_3^-/polymer) in **(a)** ZWHE-IBA and **(b)** ZWHE-PEA.

At the mesoscale, Zn^{2+} density maps and clustering analyses from MD simulations demonstrated that ZWHE-IBA and ZWHE-PEA suppress local ion aggregation and promote a more uniform spatial distribution of Zn^{2+} compared with spacer-free ZWHE. These findings align with the improved electrochemical performance observed experimentally.

Taken together, the evidence from Figures 46-58 establishes that both steric-hindrance-dominated (IBA) and high-hydrophobicity-dominated (PEA) spacers exert convergent effects: they weaken ion pairing, restructure Zn^{2+} solvation, confine free water, and accelerate Zn^{2+} transport. The combination of experimental and computational results demonstrates that hydrophobic-spacer engineering in zwitterionic hydrogels provides a unified strategy to balance water stability with electrochemical kinetics, thereby enabling dendrite-free Zn cycling, fast charge transfer, and long-term cycling stability. This work highlights hydrophobic monomer incorporation as a general and versatile design principle for advancing aqueous Zn-ion batteries toward practical implementation.

Chapter 3: Conclusion and outlook

3.1 Conclusion: A Paradigm Shift from Physical Management to Interfacial Chemical Engineering

Aqueous zinc-ion batteries (AZIBs) have emerged as a highly compelling next-generation energy storage technology, predicated on the intrinsic merits of zinc metal—high theoretical capacity, natural abundance, and low cost—and the unparalleled safety of aqueous electrolytes. However, the very component that ensures safety, water, is also the root cause of technology's most persistent challenges. The thermodynamic instability of the zinc anode in aqueous environments leads to a cascade of debilitating issues, including uncontrollable dendritic growth, parasitic hydrogen evolution reactions (HER), and pervasive corrosion, which collectively undermine the battery's Coulombic efficiency, cycle life, and overall viability.

In response, traditional hydrophilic hydrogel electrolytes were introduced as an initial, logical step forward. By immobilizing a large volume of water within a three-dimensional polymer network such as polyvinyl alcohol or polyacrylamide, these quasi-solid-state systems offered immediate advantages. They provided a physical barrier with sufficient mechanical strength to mechanically suppress the growth of nascent dendrites and, by reducing the content of "free" water, could partially mitigate parasitic reactions and prevent electrolyte leakage. However, this approach represented only a partial solution. At the critical electrode-electrolyte interface, a water-rich environment persisted, meaning the fundamental thermodynamic driving forces for HER and corrosion remained largely unaddressed.

The core thesis of recent advanced research, and the focus of this report, represents a fundamental paradigm shift in electrolyte design: the strategic incorporation of hydrophobic or amphiphilic components into the hydrogel matrix. This evolution in strategy moves beyond the passive, physical management of water to an active, sophisticated approach of interfacial chemical engineering. This design philosophy provides a multi-pronged, synergistic platform that systematically addresses the core challenges of AZIBs through several interconnected mechanisms.

The primary function of introducing hydrophobic moieties is to fundamentally re-engineer the microenvironment at the zinc anode surface. Hydrophobic domains—whether from polymer backbones, additives, or self-assembled monolayers—create a "hydrophobic shield" that physically repels water molecules from the electrode surface. This selective exclusion of water

serves as the first line of defence, kinetically inhibiting the water-induced parasitic reactions of HER and corrosion at their source. By preventing the formation of insulating, the anode surface remains electrochemically clean and active, which is a prerequisite for achieving uniform, dendrite-free zinc deposition. This principle has been demonstrated effectively through various means, from incorporating additives like Tween-85 that form a hydrophobic interface to engineering in-situ grafted layers of poly(dimethylsiloxane) (PDMS) and dynamic monolayers of hydrophobic carbon dots.

A narrow electrochemical stability window (ESW), limited by water's decomposition, has historically constrained the energy density of aqueous batteries. Amphiphilic hydrogels overcome this limitation through a powerful dual-mechanism approach. On a thermodynamic level, the introduction of trace hydrophobic moieties can paradoxically enhance the hydrogen bonding between the hydrophilic groups of the polymer and the surrounding water molecules. This, along with the addition of strong hydrogen-bond acceptors like dimethyl sulfoxide (DMSO), reconstructs the native hydrogen-bond network of water. The formation of stronger polymer-water or additive-water bonds raises the energetic barrier for water decomposition, thereby thermodynamically suppressing both HER and the oxygen evolution reaction. Complementing this, the hydrophobic shield at the interface acts as a kinetic barrier, physically preventing water molecules from reaching the electrode surfaces where decomposition occurs. This synergistic combination has enabled the development of amphiphilic hydrogels with an impressively wide ESW of up to ~3.0 V, even at a remarkably high water-content of ~76 wt%, paving the way for high-voltage AZIBs.

Beyond the interface, amphiphilic hydrogels fundamentally alter the behavior of ions within the electrolyte bulk. In standard aqueous electrolytes, Zn^{2+} ions are tightly coordinated by six water molecules, forming a stable $[Zn\ (H_2O)_6]^{2+}$ solvation sheath, which presents a high energetic penalty for desolvation and delivers reactive water directly to the anode surface. Functional groups within the hydrogel network, such as either bonds or the carbonyl groups in tetramethyl urea (TMU), act as competitive ligands. They partially or fully displace water molecules from the primary solvation shell, reconfiguring the sheath to significantly lower the desolvation energy barrier, facilitate faster interfacial kinetics, and improve rate performance. Simultaneously, these hydrogels are engineered for highly efficient ion transport. The interconnected hydrophilic domains ensure high ionic conductivity, often comparable to liquid electrolytes, while the incorporation of fixed anionic groups or cationic polymer chains achieves exceptionally high Zn^{2+} transference numbers often exceeding 0.8. A high t_{zn}^{2+} is

critical as it minimizes concentration polarization at the anode, ensuring a uniform ion flux that is fundamental to suppressing dendrite formation.

To be commercially viable, batteries must deliver high energy density on an areal basis, which necessitates the use of thick, high-mass-loading electrodes. However, thick electrodes, often fabricated with conventional hydrophobic binders like PVDF, suffer from poor wettability by aqueous electrolytes and highly tortuous ion transport pathways, leading to severe underutilization of the active material. Amphiphilic hydrogels uniquely solve this challenge. The hydrophobic chains within the hydrogel can engage in "hydrophobic association" with the cathode material, effectively anchoring the electrolyte directly onto the surface of the active particles. This targeted adhesion dramatically improves the wetting of the entire thick electrode structure and establishes a continuous, efficient ion-conductive network throughout the cathode. This transforms the electrolyte from a separate component into an integrated, functional part of the electrode architecture, enabling high utilization of active materials and achieving the high areal capacities essential for practical applications.

3.2 Outlook: Challenges and Future Research Directions

Despite the profound progress enabled by functionalized hydrogel electrolytes, the path toward widespread commercialization requires addressing several remaining challenges and exploring next-generation design concepts.

A critical area for investigation is the long-term chemical and mechanical stability of these complex polymer networks under realistic, dynamic operating conditions. While many hydrogels demonstrate excellent performance in laboratory-scale cell cycling, they must ultimately withstand thousands of cycles in a highly oxidative and reductive electrochemical environment, often coupled with mechanical stresses from flexible applications and wide temperature fluctuations. Understanding and preventing material fatigue and chemical degradation over extended periods is paramount for ensuring the reliability required for grid-scale storage or consumer electronics. Furthermore, the scalability and cost-effectiveness of these advanced materials must be addressed. The synthesis of novel functional monomers or the implementation of complex, multi-step polymerization processes can be costly and difficult to adapt for industrial production. For hydrogel electrolytes to be commercially viable, the development of simpler, more economical, and environmentally benign synthesis routes using

abundant raw materials is essential. Finally, a deeper, dynamic understanding of the electrode-hydrogel interface is needed. The evolution of this interface, including potential degradation, stress accumulation, and changes in adhesion, particularly within thick electrodes over thousands of cycles, requires sophisticated in situ and operando characterization techniques to fully elucidate and control.

Looking forward, several exciting research avenues promise to overcome these challenges and unlock new levels of performance. To accelerate the discovery of new materials and move beyond empirical approaches, advanced computational methods are indispensable. Molecular dynamics (MD) simulations and density functional theory (DFT) can be employed to predict ion solvation structures, transport properties, and interfacial interactions, providing a powerful tool for the rational, bottom-up design of next-generation amphiphilic polymer architectures with targeted properties.

The next frontier in hydrogel design lies in creating more sophisticated, hierarchical structures. Inspired by natural materials like wood, anisotropic hydrogels with vertically aligned channels can be fabricated. Such structures offer the dual benefit of enhanced mechanical modulus specifically in the direction of dendrite growth while simultaneously providing low-tortuosity pathways for rapid ion transport. Another transformative approach is in situ polymerization, where the hydrogel is formed directly within the assembled battery cell. This technique creates a perfectly conformal, seamless, and strongly adhered electrode-electrolyte interface, eliminating voids and contact issues inherent to ex-situ fabrication. Pushing the mechanical properties to their limits is also a key strategy. By tuning hydrophobic and crystalline domains, hydrogels with ultra-high moduli (approaching 200 MPa) have been developed, which can physically overcome the growth stress of zinc dendrites while maintaining high water content and ionic conductivity.

Future hydrogels can also be designed as intelligent, responsive platforms. Integrating self-healing capabilities can enable the electrolyte to autonomously repair mechanical damage, drastically extending the lifespan of flexible and wearable batteries. Furthermore, incorporating stimuli-responsive moieties that react to changes in temperature or local pH could allow for active, on-demand regulation of battery performance and safety. Pushing the boundaries of water control, novel concepts like the "Möbius Solvation Structure"—surfactant-free "water-in-oil" microemulsion electrolytes—are emerging, offering an ultimate level of water activity suppression and potentially unlocking unprecedented interfacial stability. Finally, to fully

realize the "green" potential of AZIBs, future research should increasingly focus on sustainability. This includes exploring the use of abundant, renewable, and biodegradable biopolymers such as cellulose, alginates, and gelatin as the foundation for high-performance amphiphilic hydrogel networks, thereby creating a truly environmentally benign energy storage lifecycle.

By systematically addressing these challenges and vigorously pursuing these innovative research avenues, the scientific community can propel functionalized hydrogel electrolytes from the laboratory to widespread practical application, solidifying the role of aqueous zinc-ion batteries as a safe, reliable, and sustainable pillar of our future energy landscape.

References list:

1. Chao, D., Zhou, W., Xie, F., Ye, C., Li, H., Jaroniec, M., & Qiao, S.-Z. (2020). Roadmap for advanced aqueous batteries: From design of materials to applications. *Science advances*, *6*(21), eaba4098.
2. Sui, Y., & Ji, X. (2024). Electrolyte interphases in aqueous batteries. *Angewandte Chemie International Edition*, *63*(2), e202312585.
3. Bi, S., Zhang, Y., Deng, S., Tie, Z., & Niu, Z. (2022). Proton-assisted aqueous manganese-ion battery chemistry. *Angewandte Chemie*, *134*(17), e202200809.
4. Pasta, M., Wessells, C. D., Huggins, R. A., & Cui, Y. (2012). A high-rate and long cycle life aqueous electrolyte battery for grid-scale energy storage. *Nature communications*, *3*(1), 1149.
5. Ju, Z., Zhao, Q., Chao, D., Hou, Y., Pan, H., Sun, W., Yuan, Z., Li, H., Ma, T., & Su, D. (2022). Energetic aqueous batteries. *Advanced Energy Materials*, *12*(27), 2201074.
6. Geng, X., Hou, X., He, X., & Fan, H. J. (2024). Challenges and strategies on interphasial regulation for aqueous rechargeable batteries. *Advanced Energy Materials*, *14*(12), 2304094.
7. Li, X., Wang, X., Ma, L., & Huang, W. (2022). Solvation structures in aqueous metal-ion batteries. *Advanced Energy Materials*, *12*(37), 2202068.
8. Liu, Y., Lu, X., Lai, F., Liu, T., Shearing, P. R., Parkin, I. P., He, G., & Brett, D. J. (2021). Rechargeable aqueous Zn-based energy storage devices. *Joule*, *5*(11), 2845-2903.
9. Cui, Y., Li, D., Shao, Z., Zhao, Y., Geng, K., Huang, J., Zhang, Y., & Hou, H. (2024). Construction of hydration layer for proton transport by implanting the hydrophilic center Ag0 in nickel metal-organic frameworks. *Small*, *20*(15), 2307964.
10. Mallick, S., & Raj, C. R. (2021). Aqueous Rechargeable Zn-ion Batteries: Strategies for Improving the Energy Storage Performance. *ChemSusChem*, *14*(9), 1987-2022.
11. Meng, Y. S., Srinivasan, V., & Xu, K. (2022). Designing better electrolytes. *Science*, *378*(6624), eabq3750.
12. Cao, X., Jia, H., Xu, W., & Zhang, J.-G. (2021). Localized high-concentration electrolytes for lithium batteries. *Journal of The Electrochemical Society*, *168*(1), 010522.
13. Karuppasamy, K., Theerthagiri, J., Vikraman, D., Yim, C.-J., Hussain, S., Sharma, R., Maiyalagan, T., Qin, J., & Kim, H.-S. (2020). Ionic liquid-based electrolytes for energy storage devices: A brief review on their limits and applications. *Polymers*, *12*(4), 918.
14. Xu, J., Zhang, J., Pollard, T. P., Li, Q., Tan, S., Hou, S., Wan, H., Chen, F., He, H., & Hu, E. (2023). Electrolyte design for Li-ion batteries under extreme operating conditions. *Nature*, *614*(7949), 694-700.
15. Zhang, X., Xue, D., Jiang, S., Xia, H., Yang, Y., Yan, W., Hu, J., & Zhang, J. (2022). Rational confinement engineering of MOF-derived carbon-based electrocatalysts toward CO2 reduction and O2 reduction reactions. *InfoMat*, *4*(3), e12257.
16. Li, M., Wang, C., Chen, Z., Xu, K., & Lu, J. (2020). New Concepts in Electrolytes. *Chemical reviews*, *120*(14), 6783-6819.
17. Tiago, G. A. O., Matias, I. A. S., Ribeiro, A. P. C., & Martins, L. M. D. R. S. (2020). Application of Ionic Liquids in Electrochemistry—Recent Advances. *Molecules*, *25*(24), 5812.
18. Yan, J., Ang, E. H., Yang, Y., Zhang, Y., Ye, M., Du, W., & Li, C. C. (2021). High-Voltage Zinc-Ion Batteries: Design Strategies and Challenges. *Advanced Functional Materials*,

31(22), 2010213. https://doi.org/10.1002/adfm.202010213
19. Tan, Y., Liao, R., Mu, Y., Dong, L., Chen, X., Xue, Y., Zheng, Z., Wang, F., Ni, Z., & Guo, J. (2024). Hierarchically-Structured and Mechanically-Robust Hydrogel Electrolytes for Flexible Zinc-Iodine Batteries. *Advanced Functional Materials*, *34*(45), 2407050.
20. Li, C., Yang, S., Guo, Y., Lv, H., Li, P., Bai, X., Li, X., Zhi, C., & Li, H. (2023). Hydrogel Electrolyte with High Tolerance to a Wide Spectrum of pHs and Compressive Energy Storage Devices Based on It. *Small Methods*, *7*(3), 2201448.
21. Hao, Y., Feng, D., Hou, L., Li, T., Jiao, Y., & Wu, P. (2022). Gel Electrolyte Constructing Zn (002) Deposition Crystal Plane Toward Highly Stable Zn Anode. *Advanced Science*, *9*(7), 2104832. https://doi.org/10.1002/advs.202104832
22. Zhang, W., Guo, F., Mi, H., Wu, Z.-S., Ji, C., Yang, C., & Qiu, J. (2022). Kinetics-Boosted Effect Enabled by Zwitterionic Hydrogel Electrolyte for Highly Reversible Zinc Anode in Zinc-Ion Hybrid Micro-Supercapacitors. *Advanced Energy Materials*, *12*(40), 2202219.
23. Chen, Z. J., Shen, T. Y., Xiao, X., He, X. C., Luo, Y. L., Jin, Z., & Li, C. H. (2024). An Ultrahigh-Modulus Hydrogel Electrolyte for Dendrite-Free Zinc Ion Batteries. *Advanced Materials*, *36*(52), 2413268.
24. Peng, H., Wang, D., Zhang, F., Yang, L., Jiang, X., Zhang, K., Qian, Z., & Yang, J. (2024). Improvements and challenges of hydrogel polymer electrolytes for advanced zinc anodes in aqueous zinc-ion batteries. *ACS Nano*, *18*(33), 21779-21803.
25. Zhang, B., Qin, L., Fang, Y., Chai, Y., Xie, X., Lu, B., Liang, S., & Zhou, J. (2022). Tuning Zn^{2+} coordination tunnel by hierarchical gel electrolyte for dendrite-free zinc anode. *Science Bulletin*, *67*(9), 955-962.
26. Fu, Q., Hao, S., Meng, L., Xu, F., & Yang, J. (2021). Engineering self-adhesive polyzwitterionic hydrogel electrolytes for flexible zinc-ion hybrid capacitors with superior low-temperature adaptability. *ACS Nano*, *15*(11), 18469-18482.
27. Dong, H., Li, J., Guo, J., Lai, F., Zhao, F., Jiao, Y., Brett, D. J., Liu, T., He, G., & Parkin, I. P. (2021). Insights on flexible zinc-ion batteries from lab research to commercialization. *Advanced Materials*, *33*(20), 2007548.
28. Xu, L., Meng, T., Zheng, X., Li, T., Brozena, A. H., Mao, Y., Zhang, Q., Clifford, B. C., Rao, J., & Hu, L. (2023). Nanocellulose-carboxymethylcellulose electrolyte for stable, high-rate zinc-ion batteries. *Advanced Functional Materials*, *33*(27), 2302098.
29. Ji, G., Sun, M., Li, M., & Zheng, J. (2025). Sulfonate-Modified Covalent Organic Framework Integrated Hydrogel Electrolyte: Enhancing AZIBs Performances by Tailoring Microstructures and Functional Groups. *Advanced Functional Materials*, 2500110.
30. Huang, S., Hou, L., Li, T., Jiao, Y., & Wu, P. (2022). Antifreezing hydrogel electrolyte with ternary hydrogen bonding for high-performance zinc-ion batteries. *Advanced Materials*, *34*(14), 2110140.
31. Meng, Y., Zhang, L., Peng, M., Shen, D., Zhu, C., Qian, S., Liu, J., Cao, Y., Yan, C., & Zhou, J. (2022). Developing Thermoregulatory Hydrogel Electrolyte to Overcome Thermal Runaway in Zinc-Ion Batteries. *Advanced Functional Materials*, *32*(46), 2206653.
32. Li, C., Zhu, X., Wang, D., Yang, S., Zhang, R., Li, P., Fan, J., Li, H., & Zhi, C. (2024). Fine Tuning Water States in Hydrogels for High Voltage Aqueous Batteries. *ACS Nano*, *18*(4), 3101-3114.
33. Zhu, X., Ji, C., Meng, Q., Mi, H., Yang, Q., Li, Z., Yang, N., & Qiu, J. (2022). Freeze-Tolerant Hydrogel Electrolyte with High Strength for Stable Operation of Flexible Zinc-Ion Hybrid Supercapacitors. *Small*, *18*(16), 2200055.

34. Yang, F., Yuwono, J. A., Hao, J., Long, J., Yuan, L., Wang, Y., Liu, S., Fan, Y., Zhao, S., & Davey, K. (2022). Understanding H2 evolution electrochemistry to minimize solvated water impact on Zinc-anode performance. *Advanced Materials*, *34*(45), 2206754.
35. Wan, J., Wang, R., Liu, Z., Zhang, S., Hao, J., Mao, J., Li, H., Chao, D., Zhang, L., & Zhang, C. (2024). Hydrated Eutectic Electrolyte Induced Bilayer Interphase for High-Performance Aqueous Zn-Ion Batteries with 100° C Wide-Temperature Range. *Advanced Materials*, *36*(11), 2310623.
36. Li, G., Zhao, Z., Zhang, S., Sun, L., Li, M., Yuwono, J. A., Mao, J., Hao, J., Vongsvivut, J., & Xing, L. (2023). A biocompatible electrolyte enables highly reversible Zn anode for zinc ion battery. *Nature communications*, *14*(1), 6526.
37. Zhao, S., Zuo, Y., Liu, T., Zhai, S., Dai, Y., Guo, Z., Wang, Y., He, Q., Xia, L., & Zhi, C. (2021). Multi-functional hydrogels for flexible zinc-based batteries working under extreme conditions. *Advanced Energy Materials*, *11*(34), 2101749.
38. Yan, Y., Duan, S., Liu, B., Wu, S., Alsaid, Y., Yao, B., Nandi, S., Du, Y., Wang, T. W., & Li, Y. (2023). Tough hydrogel electrolytes for anti-freezing zinc-ion batteries. *Advanced Materials*, *35*(18), 2211673.
39. Wang, X., Wang, B., & Cheng, J. (2023). Multi-healable, mechanically durable double cross-linked polyacrylamide electrolyte incorporating hydrophobic interactions for dendrite-free flexible zinc-ion batteries. *Advanced Functional Materials*, *33*(43), 2304470.
40. Cho, J., Turney, D. E., Yadav, G. G., Nyce, M., Wygant, B. R., Lambert, T. N., & Banerjee, S. (2024). Use of hydrogel electrolyte in Zn-MnO2 rechargeable batteries: Characterization of safety, performance, and Cu2+ ion diffusion. *Polymers*, *16*(5), 658.
41. Chen, M., Chen, J., Zhou, W., Han, X., Yao, Y., & Wong, C. P. (2021). Realizing an all-round hydrogel electrolyte toward environmentally adaptive dendrite-free aqueous Zn–MnO2 batteries. *Advanced Materials*, *33*(9), 2007559.
42. Shin, K. H., Ji, D., Park, J. M., Joe, Y. S., Park, H. S., & Kim, J. (2024). Structural composite hydrogel electrolytes for flexible and durable Zn metal batteries. *Advanced Functional Materials*, *34*(3), 2309048.
43. Wang, Y., Wang, Z., Yang, F., Liu, S., Zhang, S., Mao, J., & Guo, Z. (2022). Electrolyte engineering enables high performance zinc-ion batteries. *Small*, *18*(43), 2107033.
44. Sun, M., Ji, G., & Zheng, J. (2023). A hydrogel electrolyte with ultrahigh ionic conductivity and transference number benefit from Zn^{2+} “highways” for dendrite-free Zn-MnO2 battery. *Chemical Engineering Journal*, *463*, 142535.
45. Shi, Y., Wang, R., Bi, S., Yang, M., Liu, L., & Niu, Z. (2023). An Anti-Freezing Hydrogel Electrolyte for Flexible Zinc-Ion Batteries Operating at −70 °C. *Advanced Functional Materials*, *33*(24), 2214546.
46. Wang, Y., Li, Q., Hong, H., Yang, S., Zhang, R., Wang, X., Jin, X., Xiong, B., Bai, S., & Zhi, C. (2023). Lean-water hydrogel electrolyte for zinc ion batteries. *Nature communications*, *14*(1), 3890.
47. Yang, J.-L., Yu, Z., Wu, J., Li, J., Chen, L., Xiao, T., Xiao, T., Cai, D.-Q., Liu, K., Yang, P., & Fan, H. J. (2023). Hetero-Polyionic Hydrogels Enable Dendrites-Free Aqueous Zn-I2 Batteries with Fast Kinetics. *Advanced Materials*, *35*(44), 2306531.
48. Yang, J.-L., Xiao, T., Xiao, T., Li, J., Yu, Z., Liu, K., Yang, P., & Fan, H. J. (2024). Cation-Conduction Dominated Hydrogels for Durable Zinc–Iodine Batteries. *Advanced Materials*, *36*(21), 2313610.
49. Chen, Z.-J., Shen, T.-Y., Zhang, M.-H., Xiao, X., Wang, H.-Q., Lu, Q.-R., Luo, Y.-L., Jin, Z.,

& Li, C.-H. (2024). Tough, Anti-Fatigue, Self-Adhesive, and Anti-Freezing Hydrogel Electrolytes for Dendrite-Free Flexible Zinc Ion Batteries and Strain Sensors. *Advanced Functional Materials*, *34*(26), 2314864.

50. Lu, H., Hu, J., Wei, X., Zhang, K., Xiao, X., Zhao, J., Hu, Q., Yu, J., Zhou, G., & Xu, B. (2023). A recyclable biomass electrolyte towards green zinc-ion batteries. *Nature communications*, *14*(1), 4435.
51. Hou, X., Huang, B., Zhou, L., Liu, S., Kong, J., & He, C. (2023). An amphiphilic entangled network design toward ultratough hydrogels. *Advanced Materials*, *35*(28), 2301532.
52. Shen, Z., Zhang, C., Wang, T., & Xu, J. (2023). Advances in functional hydrogel wound dressings: a review. *Polymers*, *15*(9), 2000.
53. Tuncaboylu, D. C., Sari, M., Oppermann, W., & Okay, O. (2011). Tough and self-healing hydrogels formed via hydrophobic interactions. *Macromolecules*, *44*(12), 4997-5005.
54. Nian, G., Kim, J., Bao, X., & Suo, Z. (2022). Making highly elastic and tough hydrogels from doughs. *Advanced Materials*, *34*(50), 2206577.
55. Jiang, H., Duan, L., Ren, X., & Gao, G. (2019). Hydrophobic association hydrogels with excellent mechanical and self-healing properties. *European Polymer Journal*, *112*, 660-669.
56. Mredha, M. T. I., Le, H. H., Cui, J., & Jeon, I. (2020). Double-Hydrophobic-Coating through Quenching for Hydrogels with Strong Resistance to Both Drying and Swelling. *Advanced Science*, *7*(6), 1903145.
57. Du, P., Wang, J., Hsu, Y.-I., & Uyama, H. (2024). Hydrophobic association hydrogel enabled by multiple noncovalent interactions for wearable bioelectronics in amphibious environments. *Chemistry of Materials*, *36*(3), 1318-1332.
58. Liang, M., Ge, X., Dai, J., Ren, P., Wei, D., Xu, L., Zhang, Q., He, C., Lu, Z., & Zhang, T. (2021). High-strength hydrogel adhesive formed via multiple interactions for persistent adhesion under saline. *ACS applied bio materials*, *4*(6), 5016-5025.
59. Han, L., Wang, M., Prieto-López, L. O., Deng, X., & Cui, J. (2020). Self-hydrophobization in a dynamic hydrogel for creating nonspecific repeatable underwater adhesion. *Advanced Functional Materials*, *30*(7), 1907064.
60. Zheng, D.-f., Hu, L., & Qiu, X.-q. (2021). Recent Advances in Lignin-Based Hydrogels and Its Synthesis and Applications. *Lignin Utilization Strategies: From Processing to Applications*, 207-229.
61. Wang, X., Wang, B., Lei, P., Wang, X., Zhou, L., Zhang, J., Zhang, J., & Cheng, J. (2024). Polycation-regulated hydrogel electrolytes with nanoscale hydrophobic confinement inducing Zn (002) deposition for highly reversible zinc anodes. *Energy & Environmental Science*, *17*(18), 6640-6655.
62. Yang, H., Lu, H., Miao, Y., Cong, Y., Ke, Y., Wang, J., Yang, H., & Fu, J. (2022). Non-swelling, super-tough, self-healing, and multi-responsive hydrogels based on micellar crosslinking for smart switch and shape memory. *Chemical Engineering Journal*, *450*, 138346.
63. Gosecka, M., Gosecki, M., & Jaworska-Krych, D. (2023). Hydrophobized hydrogels: construction strategies, properties, and biomedical applications. *Advanced Functional Materials*, *33*(25), 2212302.
64. Xu, C., Li, M., Wang, Y., Jiang, Y., Yin, J., Ma, W., Hu, X., Zeng, W., Ma, Y., & Wu, S. (2025). Bioinspired Tough and Antiswelling Hydrogel via in Situ Self-Assembly of Amphiphilic Copolymers within a Hydrophilic Network. *ACS Macro Letters*, *14*(6), 709-715.
65. Nichifor, M. (2023). Role of hydrophobic associations in self-healing hydrogels based on

amphiphilic polysaccharides. *Polymers*, *15*(5), 1065.
66. Abdurrahmanoglu, S., Can, V., & Okay, O. (2009). Design of high-toughness polyacrylamide hydrogels by hydrophobic modification. *Polymer*, *50*(23), 5449-5455.
67. Hao, J., & Weiss, R. (2016). Tuning the viscoelastic behavior of hybrid hydrogels composed of a physical and a chemical network by the addition of an organic solvent. *Macromolecules*, *49*(17), 6687-6693.
68. Liu, X., Zhang, Q., Duan, L., & Gao, G. (2019). Bioinspired nucleobase-driven nonswellable adhesive and tough gel with excellent underwater adhesion. *ACS applied materials & interfaces*, *11*(6), 6644-6651.
69. Huang, G., Tang, Z., Peng, S., Zhang, P., Sun, T., Wei, W., Zeng, L., Guo, H., Guo, H., & Meng, G. (2021). Modification of hydrophobic hydrogels into a strongly adhesive and tough hydrogel by electrostatic interaction. *Macromolecules*, *55*(1), 156-165.
70. Qin, Y., He, G., Li, Y., Liu, Y., Liu, W., Dong, L., Yu, L., & Wang, L. (2023). Preparation and properties of composite amphiphilic hydrogel anti-fouling materials. *Progress in Organic Coatings*, *179*, 107527.
71. Yang, M., Liu, C., Li, Z., Gao, G., & Liu, F. (2010). Temperature-responsive properties of poly (acrylic acid-co-acrylamide) hydrophobic association hydrogels with high mechanical strength. *Macromolecules*, *43*(24), 10645-10651.
72. Zhu, K., Niu, X., Xie, W., Yang, H., Jiang, W., Ma, M., & Yang, W. (2024). An integrated Janus hydrogel with different hydrophilicities and gradient pore structures for high-performance zinc-ion batteries. *Energy & Environmental Science*, *17*(12), 4126-4136.
73. Chen, H., Meng, C., Jiao, Z., Yuan, A., & Zhou, H. (2025). Amphiphilic Dodecanoic Monolayer Protects Zinc Anode from Water-Involved Side Reactions. *Energy & Fuels*, *39*(8), 4069-4078.
74. Wang, Y., Mo, L. e., Zhang, X., Ren, Y., Wei, T., He, Y., Huang, Y., Zhang, H., Tan, P., & Li, Z. (2024). Regulating water activity for all-climate aqueous zinc-ion batteries. *Advanced Energy Materials*, *14*(33), 2402041.
75. Zhai, C., Zhao, D., He, Y., Huang, H., Chen, B., Wang, X., & Guo, Z. (2022). Electrolyte additive strategies for suppression of zinc dendrites in aqueous zinc-ion batteries. *Batteries*, *8*(10), 153.
76. Yu, J., Li, M., Kong, X., Wang, T., Zhang, H., Zhu, X., Zhao, J., Ma, Z., & Yang, H. (2025). Polyanion hydrogel electrolyte with a high Zn 2+ transference number for dendrite-free aqueous zinc-ion batteries. *Journal of Materials Chemistry A*, *13*(21), 16182-16192.
77. Sun, M., Ji, G., Li, M., & Zheng, J. (2025). Molecularly Engineered Hydrogel Electrolyte Embedded with Multifunctional Oxygen-Rich Macrocyclic Units for Uniform Zinc Deposition. *Advanced Science*, e07377.
78. Eom, T. P., Lee, G., Cho, Y. H., Lim, Y., & Yoo, S. J. (2025). Hydrophobic Deep Eutectic Solvent (DES) Design Enables Optimally Hydrated DES-in-Water Electrolytes for High-Performance Bromine Redox-Enhanced Energy Storage Systems. *Advanced Functional Materials*, *35*(32), 2424243.
79. Li, C., Wang, T., Lai, H. C. J., Park, S. W., Chan, W. Y. K., Li, Q., Zhao, Y., Fan, J., Pei, Z., & Zhi, C. (2025). Hydrophobic-unit-regulated hydrogel electrolytes with high water content and low salt concentration for high-voltage aqueous batteries. *Joule*, *9*(4).
80. Chen, Z., Lin, Y., Shi, D., Song, K., Luo, J., Qiu, Y., Liu, Z., Yu, Y., & Yang, C. (2025). Rational hierarchical micellar gel electrolytes with synergistic hydrophobic–hydrophilic integration for dendrite-free zinc-ion batteries [10.1039/D4TA08537J]. *Journal of Materials*

Chemistry A, *13*(9), 6709-6718.
81. Li, H., Chen, Z., Zheng, L., Wang, J., Adenusi, H., Passerini, S., & Zhang, H. (2024). Electrolyte Strategies Facilitating Anion-Derived Solid-Electrolyte Interphases for Aqueous Zinc–Metal Batteries. *Small Methods*, *8*(6), 2300554.
82. Yin, W., Hu, K., Wan, F., Liu, R., & Chen, W. (2025). Gel Electrolyte with Excellent Zinc-Ion Conductivity for Achieving Highly Reversible Zinc Anodes. *ACS Sustainable Chemistry & Engineering*.
83. Cao, L., Li, D., Hu, E., Xu, J., Deng, T., Ma, L., Wang, Y., Yang, X.-Q., & Wang, C. (2020). Solvation Structure Design for Aqueous Zn Metal Batteries. *Journal of the American Chemical Society*, *142*(51), 21404-21409.
84. Lin, P., Cong, J., Li, J., Zhang, M., Lai, P., Zeng, J., Yang, Y., & Zhao, J. (2022). Achieving ultra-long lifespan Zn metal anodes by manipulating desolvation effect and Zn deposition orientation in a multiple cross-linked hydrogel electrolyte. *Energy Storage Materials*, *49*, 172-180.
85. Wang, K., Qiu, T., Lin, L., Zhan, H., Liu, X.-X., & Sun, X. (2024). Solvation Sheath Regulation to Induce Sulfide Solid–Electrolyte Interphase on Zn Metal Anode. *ACS Energy Letters*, *9*(3), 1000-1007.
86. Fu, C., Wang, Y., Lu, C., Zhou, S., He, Q., Hu, Y., Feng, M., Wan, Y., Lin, J., & Zhang, Y. (2022). Modulation of hydrogel electrolyte enabling stable zinc metal anode. *Energy Storage Materials*, *51*, 588-598.
87. Cheng, X., Zuo, Y., Zhang, Y., Zhao, X., Jia, L., Zhang, J., Li, X., Wu, Z., Wang, J., & Lin, H. (2024). Superfast Zincophilic Ion Conductor Enables Rapid Interfacial Desolvation Kinetics for Low-Temperature Zinc Metal Batteries. *Advanced Science*, *11*(28), 2401629.
88. Liu, L., Hu, Z., Wang, X., Wang, X., Zheng, Q., Han, C., Xu, X., Liu, H., Dou, S. X., & Li, W. (2024). Electrolyte Regulation Methods for Improving the Cycle-Life of Zinc Metal Anodes. *Journal of Materials Chemistry A*.
89. Yan, X., Tong, Y., Liu, Y., Li, X., Qin, Z.-b., Wu, Z., & Hu, W. (2023). Highly Reversible Zn Anodes through a Hydrophobic Interface Formed by Electrolyte Additive. *Nanomaterials*, *13*.
90. Li, C., Liang, B., Chen, Z., Zhang, R., Cui, H., Wang, Y., Li, Q., Peng, C., Fan, J., & Pei, Z. (2025). Scalable high-voltage Zn|| MnO2 batteries achieved by mild amphiphilic hydrogel electrolytes. *Proceedings of the National Academy of Sciences*, *122*(33), e2501935122.
91. Gu, Y., Zheng, X., Zhou, Z., Chen, G., Chen, S., & Li, Q. (2024). Amphiphilic ionic liquid hydrogel electrolytes with high ionic conductivity towards dendrite-free ultra-stable aqueous zinc ion batteries. *Journal of Energy Storage*, *89*, 111892.
92. Jiang, G., Liu, C., Liu, X., Chen, Q., Zhang, G., Yang, M., & Liu, F. (2010). Network structure and compositional effects on tensile mechanical properties of hydrophobic association hydrogels with high mechanical strength. *Polymer*, *51*(6), 1507-1515.
93. Li, C., Zhu, J., Zhang, R., Wu, Z., Cui, H., Chen, Z., Zhang, S., Zhang, W., Huang, Z., & Pei, Z. (2023). Hydrogels with amphiphilic chains and targeted adhesion for high-areal-capacity zinc batteries. *Energy Storage Materials*, *60*, 102858.
94. Fu, C., Shen, L., Liu, L., Tao, P., Zhu, L., Zeng, Z., Ren, T., & Wang, G. (2023). Hydrogel with Robust Adhesion in Various Liquid Environments by Electrostatic-Induced Hydrophilic and Hydrophobic Polymer Chains Migration and Rearrangement. *Advanced Materials*, *35*(15), 2211237.
95. Han, L., Wang, M., Prieto-López, L. O., Deng, X., & Cui, J. (2020). Self-Hydrophobization

in a Dynamic Hydrogel for Creating Nonspecific Repeatable Underwater Adhesion. *Advanced Functional Materials*, *30*(7), 1907064.

96. Gao, J., Ge, W., & Li, J. (2005). Effect of concentration on surfactant micelle shapes —A molecular dynamics study. *Science in China Series B: Chemistry*, *48*(5), 470-475.
97. Su, C., & Wang, H. (2012). Capsule-like α-Fe2O3 nanoparticles: Synthesis, characterization, and growth mechanism. *Crystal Research and Technology*, *47*(8), 896-902.
98. Zhao, B., Brittain, W. J., Zhou, W., & Cheng, S. Z. (2000). Nanopattern formation from tethered PS-b-PMMA brushes upon treatment with selective solvents. *Journal of the American Chemical Society*, *122*(10), 2407-2408.
99. Li, D., Sheng, X., & Zhao, B. (2005). Environmentally responsive "hairy" nanoparticles: Mixed homopolymer brushes on silica nanoparticles synthesized by living radical polymerization techniques. *Journal of the American Chemical Society*, *127*(17), 6248-6256.
100. Nagase, K., Yuk, S. F., Kobayashi, J., Kikuchi, A., Akiyama, Y., Kanazawa, H., & Okano, T. (2011). Thermo-responsive protein adsorbing materials for purifying pharmaceutical protein on exposed charging surface. *Journal of Materials Chemistry*, *21*(8), 2590-2593.
101. Chen, Z., Liu, H., Fan, S., Zhang, Q., Yuan, C., Peng, W., Li, Y., & Fan, X. (2024). Inhibition of vanadium cathode dissolution in zinc-ion batteries on thermodynamics and kinetics by guest pre-intercalation. *Advanced Energy Materials*, *14*(25), 2400977.
102. Zhu, S., Zhang, W., Liao, X., Zhang, L., An, Q., & Wang, X. (2024). "Water-in-Salt" Electrolyte Suppressed MnVOPO4· 2H2O Cathode Dissolution for Stable High-Voltage Platform and Cycling Performance for Aqueous Zinc Metal Battery. *Materials*, *17*(18), 4456.
103. Li, M., Wu, J., Li, H., & Wang, Y. (2024). Suppressing the shuttle effect of aqueous zinc–iodine batteries: Progress and prospects. *Materials*, *17*(7), 1646.
104. Bai, Z., Wang, G., Liu, H., Lou, Y., Wang, N., Liu, H., & Dou, S. (2024). Advancements in aqueous zinc–iodine batteries: a review. *Chemical Science*, *15*(9), 3071-3092.
105. Choi, S., Seo, J. K., Park, H., Park, J. H., Kim, S. W., Shin, S. W., Bang, J. A., Jung, K. N., & Kim, B. G. (2025). A Multifunctional Crosslinked F-Free Binder for MnO2 Microparticle Thick Cathode in Aqueous Zinc-Ion Batteries. *Advanced Functional Materials*, *35*(11), 2417179.
106. Zhang, X., Li, J., Xie, F., Xu, X., Sun, X., Su, L., Lu, F., Zheng, L., & Gao, X. (2025). Polyzwitterionic Gel Electrolyte: Dual Optimization of Polyiodide Shuttle Suppression and Anode Stabilization in Aqueous Zn-I2 Batteries. *Advanced Functional Materials*, 2505132.
107. Vandeginste, V., & Wang, J. (2024). A Review of the Synthesis of Biopolymer Hydrogel Electrolytes for Improved Electrode–Electrolyte Interfaces in Zinc-Ion Batteries. *Energies*, *17*(2), 310.
108. Kang, G., Lu, N., Li, L., Wang, S., Liu, S., Yang, Y., Luan, J., Zhang, S., & Wang, G. (2025). Stretchable/Compressible Supercapacitors Based on High-Elasticity and Fatigue-Resistant Hydrogel Electrolyte Cross-Linked by Hydrophobic Nanospheres. *Nano Letters*, *25*(10), 3858-3866.
109. Ma, R., Xu, Z., & Wang, X. (2023). Polymer hydrogel electrolytes for flexible and multifunctional zinc-ion batteries and capacitors. *Energy & Environmental Materials*, *6*(5), e12464.
110. Liang, X., Zhong, H.-J., Ding, H., Yu, B., Ma, X., Liu, X., Chong, C.-M., & He, J. (2024). Polyvinyl alcohol (PVA)-based hydrogels: Recent progress in fabrication, properties, and

multifunctional applications. *Polymers*, *16*(19), 2755.
111. Guo, X., Zhang, S., Patel, S., Sun, X., Zhu, Y.-L., Wei, Z., Wang, R., He, X., Wang, Z., & Yu, C. (2025). A skin-mimicking multifunctional hydrogel via hierarchical, reversible noncovalent interactions. *Science advances*, *11*(20), eadv8523.
112. Wang, C., Yang, B., Xiang, R., Ji, J., Wu, Y., & Tan, S. (2023). High-saline-enabled hydrophobic homogeneous cross-linking for extremely soft, tough, and stretchable conductive hydrogels as high-sensitive strain sensors. *ACS Nano*, *17*(22), 23194-23206.
113. Li, Y., Jiang, F., Li, X., Wu, Y., Wang, Y., Peng, H., Peng, J., Li, J., & Zhai, M. (2025). An ultrastretchable and multifunctional hydrophobic/electrostatic dual-crosslinked hydrogel for self-healing flexible touch panel and sensor. *npj Flexible Electronics*, *9*(1), 45.
114. Xu, T., Zhang, L., Song, B., Bai, X., Huang, Z., Bu, X., Chen, T., Fu, H., & Guo, P. (2022). High-strain sensitive zwitterionic hydrogels with swelling-resistant and controllable rehydration for sustainable wearable sensor. *Journal of Colloid and Interface Science*, *620*, 14-23.
115. Yuan, H., Zhu, T., Huang, Y., Wang, Z., Han, P., Tan, L., Wu, J., Chen, X., Yao, P., & Zhu, C. (2024). Hydrophobic and adhesive elastomer encapsulation for anti-drying, non-swelling, and adhesive hydrogels. *Advanced Functional Materials*, *34*(51), 2409703.
116. Wei, J., Zheng, Y., & Chen, T. (2021). A fully hydrophobic ionogel enables highly efficient wearable underwater sensors and communicators. *Materials Horizons*, *8*(10), 2761-2770.
117. Bi, M., Guan, X., Sun, S., Jin, Z., Gao, H., Sun, J., & Gao, Z. (2024). An anti-swelling chitosan-based hydrogel driven by balance of hydrophilic segment and hydrophobic segment strategy for underwater detection of human motion. *European Polymer Journal*, *205*, 112715.
118. Wang, S., Liu, J., Wang, L., Cai, H., Wang, Q., Wang, W., Shao, J., & Dong, X. (2023). Underwater adhesion and anti-swelling hydrogels. *Advanced Materials Technologies*, *8*(6), 2201477.
119. Luo, C., Guo, A., Zhao, Y., Sun, J., & Li, Z. (2021). Facile fabrication of nonswellable and biocompatible hydrogels with cartilage-comparable performances. *Materials Today Communications*, *27*, 102375.
120. Luo, X., Nian, Q., Dong, Q., Ruan, D., Cui, Z., Wang, Z., Xiong, B. Q., & Ren, X. (2025). Anti-Swelling Supramolecule-Crosslinked Hydrogel Interphase for Stable Zn Metal Anodes. *Advanced Energy Materials*, *15*(6), 2403187.
121. Qi, C., Dong, Z., Huang, Y., Xu, J., & Lei, C. (2022). Tough, anti-swelling supramolecular hydrogels mediated by surfactant–polymer interactions for underwater sensors. *ACS applied materials & interfaces*, *14*(26), 30385-30397.
122. Wang, Y., Gao, X., Wu, J., Jiang, M., Zhang, H., & Yan, C. (2024). Antifreezing/antiswelling hydrogels: synthesis strategies and applications as flexible motion sensors. *ACS applied materials & interfaces*, *16*(43), 58100-58120.
123. Zheng, J., Zhao, Q., Tang, T., Yin, J., Quilty, C. D., Renderos, G. D., Liu, X., Deng, Y., Wang, L., & Bock, D. C. (2019). Reversible epitaxial electrodeposition of metals in battery anodes. *Science*, *366*(6465), 645-648.
124. Han, D., Cui, C., Zhang, K., Wang, Z., Gao, J., Guo, Y., Zhang, Z., Wu, S., Yin, L., & Weng, Z. (2022). A non-flammable hydrous organic electrolyte for sustainable zinc batteries. *Nature Sustainability*, *5*(3), 205-213.
125. Zou, Y., Yang, X., Shen, L., Su, Y., Chen, Z., Gao, X., Zhou, J., & Sun, J. (2022). Emerging strategies for steering orientational deposition toward high-performance Zn metal

anodes. *Energy & Environmental Science*, *15*(12), 5017-5038.
126. Jiang, L., Li, D., Xie, X., Ji, D., Li, L., Li, L., He, Z., Lu, B., Liang, S., & Zhou, J. (2023). Electric double layer design for Zn-based batteries. *Energy Storage Materials*, *62*, 102932.
127. Li, Q., Chen, A., Wang, D., Pei, Z., & Zhi, C. (2022). "Soft shorts" hidden in zinc metal anode research. *Joule*, *6*(2), 273-279.
128. Wu, Z., Wang, Y., & Zhi, C. (2024). Zinc-anode reversibility and capacity inflection as an evaluation criterion. *Joule*, *8*(9), 2442-2448.
129. Long, T., Zhao, Q. Y., Yin, G. Y., Xie, P. X., Liu, S., Ma, X., Wu, Q., Lu, B. Y., Dai, Z., & Zeng, X. X. (2024). Regulating interfacial ion adsorption for smooth and durable zinc cycling at high area capacity. *Advanced Functional Materials*, *34*(24), 2315539.
130. Qiu, M., Sun, P., Han, K., Pang, Z., Du, J., Li, J., Chen, J., Wang, Z. L., & Mai, W. (2023). Tailoring water structure with high-tetrahedral-entropy for antifreezing electrolytes and energy storage at− 80° C. *Nature Communications*, *14*(1), 601.
131. Suo, L., Borodin, O., Gao, T., Olguin, M., Ho, J., Fan, X., Luo, C., Wang, C., & Xu, K. (2015). "Water-in-salt" electrolyte enables high-voltage aqueous lithium-ion chemistries. *Science*, *350*(6263), 938-943.
132. Jiang, Y., Luo, D., Peng, C., Niu, B., Gan, P., & He, X. (2025). "Cyano group bridge"-based enabling high zinc-ion transference number and cycling stability of aqueous zinc-ion batteries. *Journal of Materials Chemistry A*, *13*(22), 16816-16824.
133. Nageshwar, P., Wajge, S. W., Dhakar, G. L., Thakre, A. A., Tripathi, S., Singh, S., Maji, P. K., & Das, C. (2025). Fabrication of Zinc (II) Mediated Poly (Acrylamide Co Acrylic Acid) Hydrogel with Thixotropic and Tribological Properties. *Macromolecular Rapid Communications*, *46*(2), 2400670.
134. Wang, L., Wang, H., Cao, J., Yan, J., Dai, C., Sun, W., Du, Q., Huang, Z., Liu, D., & Li, C. (2025). Restructuring Hydrogen Bond Networks in Polyacrylamide Hydrogels via Trehalose Additives for Wide-Temperature-Range Zn-Ion Batteries. *ACS Nano*.
135. Wang, X., Wang, F., Wang, L., Li, M., Wang, Y., Chen, B., Zhu, Y., Fu, L., Zha, L., & Zhang, L. (2016). An aqueous rechargeable Zn//Co3O4 battery with high energy density and good cycling behavior. *Advanced Materials*, *28*(24), 4904-4911.
136. Paswan, A. M., Thakur, V. S., Banerjee, S., & Raj, C. R. (2025). Electrochemical engineering of anode with zincophilic polymer interface for reversible zinc battery. *Advanced Functional Materials*, *35*(2), 2412370.
137. Guo, Y., Fang, Z., & Yu, G. (2021). Multifunctional hydrogels for sustainable energy and environment. *Polymer International*, *70*(10), 1425-1432.
138. Guo, Y., Bae, J., Fang, Z., Li, P., Zhao, F., & Yu, G. (2020). Hydrogels and hydrogel-derived materials for energy and water sustainability. *Chemical reviews*, *120*(15), 7642-7707.
139. Duan, J., Xie, W., Yang, P., Li, J., Xue, G., Chen, Q., Yu, B., Liu, R., & Zhou, J. (2018). Tough hydrogel diodes with tunable interfacial adhesion for safe and durable wearable batteries. *Nano Energy*, *48*, 569-574.
140. Leng, K., Li, G., Guo, J., Zhang, X., Wang, A., Liu, X., & Luo, J. (2020). A safe polyzwitterionic hydrogel electrolyte for long-life quasi-solid state zinc metal batteries. *Advanced Functional Materials*, *30*(23), 2001317.
141. Lalani, R., & Liu, L. (2012). Electrospun zwitterionic poly (sulfobetaine methacrylate) for nonadherent, superabsorbent, and antimicrobial wound dressing applications. *Biomacromolecules*, *13*(6), 1853-1863.
142. Shao, Q., & Jiang, S. (2014). Influence of charged groups on the properties of zwitterionic

moieties: a molecular simulation study. *The Journal of Physical Chemistry B*, *118*(27), 7630-7637.
143. Kumar, R., & Fredrickson, G. H. (2009). Theory of polyzwitterion conformations. *The Journal of Chemical Physics*, *131*(10).
144. Su, X., Hao, D., Xu, X., Guo, X., Li, Z., & Jiang, L. (2020). Hydrophilic/hydrophobic heterogeneity anti-biofouling hydrogels with well-regulated rehydration. *ACS applied materials & interfaces*, *12*(22), 25316-25323.
145. Yao, L., Wang, G., Zhang, F., Chi, X., & Liu, Y. (2023). Highly-reversible and recyclable zinc metal batteries achieved by inorganic/organic hybrid separators with finely tunable hydrophilic–hydrophobic balance. *Energy & Environmental Science*, *16*(10), 4432-4441.
146. Zhang, H., Zhong, Y., Li, J., Liao, Y., Zeng, J., Shen, Y., Yuan, L., Li, Z., & Huang, Y. (2023). Inducing the preferential growth of Zn (002) plane for long cycle aqueous Zn-Ion batteries. *Advanced Energy Materials*, *13*(1), 2203254.
147. Song, G., Li, S., Liu, G., Fu, Q., & Pan, C. (2018). Influence of graphene oxide content on the Zn-Gr composite layer prepared by pulse reverse electro-plating. *Journal of The Electrochemical Society*, *165*(11), D501.
148. Abraham, M. J., Murtola, T., Schulz, R., Páll, S., Smith, J. C., Hess, B., & Lindahl, E. (2015). GROMACS: High performance molecular simulations through multi-level parallelism from laptops to supercomputers. *SoftwareX*, *1*, 19-25.
149. Kaminski, G. A., Friesner, R. A., Tirado-Rives, J., & Jorgensen, W. L. (2001). Evaluation and reparametrization of the OPLS-AA force field for proteins via comparison with accurate quantum chemical calculations on peptides. *The Journal of Physical Chemistry B*, *105*(28), 6474-6487.
150. Bussi, G., Donadio, D., & Parrinello, M. (2007). Canonical sampling through velocity rescaling. *The Journal of chemical physics*, *126*(1).
151. Parrinello, M., & Rahman, A. (1981). Polymorphic transitions in single crystals: A new molecular dynamics method. *Journal of Applied physics*, *52*(12), 7182-7190.
152. Essmann, U., Perera, L., Berkowitz, M. L., Darden, T., Lee, H., & Pedersen, L. G. (1995). A smooth particle mesh Ewald method. *The Journal of chemical physics*, *103*(19), 8577-8593.
153. Bannwarth, C., Caldeweyher, E., Ehlert, S., Hansen, A., Pracht, P., Seibert, J., Spicher, S., & Grimme, S. (2020). WIREs Comput. *Mol. Sci*, *10*, e01493.
154. Bannwarth, C., Ehlert, S., & Grimme, S. (2019). GFN2-xTB—An accurate and broadly parametrized self-consistent tight-binding quantum chemical method with multipole electrostatics and density-dependent dispersion contributions. *Journal of chemical theory and computation*, *15*(3), 1652-1671.
155. Neese, F., Wennmohs, F., Becker, U., & Riplinger, C. (2020). The ORCA quantum chemistry program package. *The Journal of chemical physics*, *152*(22).
156. Lu, T. (2024). A comprehensive electron wavefunction analysis toolbox for chemists, Multiwfn. *The Journal of chemical physics*, *161*(8).
157. Zhang, J., & Lu, T. (2021). Efficient evaluation of electrostatic potential with computerized optimized code. *Physical Chemistry Chemical Physics*, *23*(36), 20323-20328.
158. Neese, F., Wennmohs, F., Hansen, A., & Becker, U. (2009). Efficient, approximate and parallel Hartree–Fock and hybrid DFT calculations. A 'chain-of-spheres' algorithm for the Hartree–Fock exchange. *Chemical Physics*, *356*(1-3), 98-109.
159. Becke, A. D. (1993). Density-functional thermochemistry. III. The role of exact exchange.

The Journal of chemical physics, *98*(7), 5648-5652.
160. Zheng, J., Xu, X., & Truhlar, D. G. (2011). Minimally augmented Karlsruhe basis sets. *Theoretical Chemistry Accounts*, *128*(3), 295-305.
161. Xu, Y., Xing, L., Cao, X., Li, D., Men, Z., Li, Z., Wang, S., & Sun, C. (2023). Hydrogen bonding network dynamics of 1, 2-propanediol-water binary solutions by Raman spectroscopy and stimulated Raman scattering. *Spectrochimica Acta Part A: Molecular and Biomolecular Spectroscopy*, *284*, 121825.
162. Guan, L., Xu, H., & Huang, D. (2011). The investigation on states of water in different hydrophilic polymers by DSC and FTIR. *Journal of Polymer Research*, *18*(4), 681-689.
163. Ji, P., Jin, J., Chen, X., Wang, C., & Wang, H. (2016). Characterization of water state and distribution in fibre materials by low-field nuclear magnetic resonance. *Rsc Advances*, *6*(14), 11492-11500.
164. Elgabarty, H., & Kühne, T. D. (2020). Tumbling with a limp: local asymmetry in water's hydrogen bond network and its consequences. *Physical Chemistry Chemical Physics*, *22*(19), 10397-10411.
165. Niu, B., Li, Z., Luo, D., Ma, X., Yang, Q., Liu, Y.-E., Yu, X., He, X., Qiao, Y., & Wang, X. (2023). Nano-scaled hydrophobic confinement of aqueous electrolyte by a nonionic amphiphilic polymer for long-lasting and wide-temperature Zn-based energy storage. *Energy & Environmental Science*, *16*(4), 1662-1675.